Effect of Thermal and Chemical Treatment of Soy Flour on Soy-Polypropylene Composite Properties

by

Barbara Elisabeth Güttler

A thesis
presented to the University of Waterloo
in fulfillment of the
thesis requirement for the degree of
Doctor of Philosophy
in
Chemical Engineering

Waterloo, Ontario, Canada, 2012

Author’s Declaration

I hereby declare that I am the **sole** author of this thesis. This is a true copy of the thesis, including any required final revisions, as accepted by my examiners.

I understand that my thesis may be made electronically available to the public.

.....

Barbara Elisabeth Güttler

Abstract

Soy flour (SF), a by-product of the soybean oil extraction processing, was investigated for its application in soy-polypropylene composites for interior automotive applications. The emphasis of this work was the understanding of this new type of filler material and the contribution of its major constituents to its thermal stability and impact properties. For this reason, reference materials were selected to represent the protein (soy protein isolate (SPI)) and carbohydrate (soy hulls (SH)) constituents of the soy flour. Additional materials were also investigated: the residue obtained after the protein removal from the soy flour which was called insoluble soy (IS), and the remaining liquid solution after acid precipitation of the proteins, containing mostly sugars and minerals, which was called soluble sugar extract (SSE).

Two treatments, potassium permanganate and autoclave, were analyzed for their potential to modify the properties of the soy composite materials. An acid treatment with sulfuric acid conducted on soy flour was also considered.

The soy materials were studied by thermogravimetric analysis (TGA) under isothermal (in air) and dynamic (in nitrogen) conditions. SPI had the highest thermal stability and SSE the lowest thermal stability for the early stage of the heating process. Those two materials had the highest amount of residual mass at the end of the dynamic TGA in nitrogen. The two treatments showed minimal effect on the isothermal thermal stability of the soy materials at 200 °C. A minor improvement was observed for the autoclave treated soy materials.

Fourier transformed infrared (FTIR) spectroscopy indicated that the chemical surface composition differed according to type of the soy materials but no difference could be observed for the treatments within one type of soy material.

Contact angle analysis and surface energy estimation indicated differences of the surface hydrophobicity of the soy materials according to type of material and treatment. The initial water contact angle ranged from 57 ° for SF to 85 ° for SH. The rate of water absorption increased dramatically after the autoclave treatment for IS and SPI. Both materials showed the highest increase in the polar surface energy fraction. In general, the major change of the surface energy was associated with change of the polar fraction. After $KMnO_4$ treatment, the polar surface energy of SF, IS and SPI decreased while SH showed a slight increase after $KMnO_4$ treatment. A relationship between protein content and polar surface energy was observed and seen to be more pronounced when high protein containing soy materials were treated with $KMnO_4$ and autoclave. Based on the polar surface energy results, the most suitable soy materials for polypropylene compounding are SPI ($KMnO_4$), SH, and IS

($KMnO_4$) because their polar surface energy are the lowest which should make them more compatible with non-polar polymers such as polypropylene.

The soy materials were compounded as 30 wt-% material loading with an injection moulding grade polypropylene blend for different combinations of soy material treatment and coupling agents. Notched Izod impact and flexural strength as well as flexural modulus estimates indicated that the mechanical properties of the autoclaved SF decreased when compared to untreated soy flour while the potassium permanganate treated SF improved in impact and flexural properties. Combinations of the two treatments and two selected (maleic anhydride grafted polypropylene) coupling agents showed improved impact and flexural properties for the autoclaved soy flour but decreased properties for the potassium permanganate treated soy flour. Scanning electron microscopy of the fractured section, obtained after impact testing of the composite material, revealed different crack propagation mechanisms for the treated SF. Autoclaved SF had a poor interface with large gaps between the material and the polypropylene matrix. After the addition of a maleic anhydride coupling agent to the autoclaved SF and polypropylene formulation, the SF was fully embedded in the polymer matrix. Potassium permanganate treated SF showed partial bonding between the material and the polymer matrix but some of the material showed poor bonding to the matrix. The acid treated SF showed cracks through the dispersed phase and completely broken components that did not bind to the polypropylene matrix.

In conclusion, the two most promising soy materials in terms of impact and flexural properties improvement of soy polypropylene composites were potassium permanganate treated SF and the autoclaved SF combined with maleic anhydride coupling agent formulation.

Acknowledgements

This thesis would not have been possible without the support and guidance of many individuals that have contributed in one or another way to the completion of this thesis.

First and foremost I offer my sincerest gratitude to my supervisor, Dr. Christine Moresoli, who has supported me throughout my project with her patience and knowledge in many fields beyond my thesis. She is a great example and role model for a supervisor that acts responsibly and unselfishly based on high ethical values.

I would like to thank my supervisor Dr. Leonardo C. Simon for the opportunity to work in his laboratory and experience a very different kind of advisory environment.

I would also like to thank my committee members, Dr. Marie-Claude Heuzey, Dr. Hyock Ju Kwon, Dr. Raymond Legge, and Dr. Boxin Zhao for their comments and assistance.

I am grateful to Ralph Dickhout and Bert Habicher for their technical support in many parts throughout my project.

Furthermore, I would like to thank:

Dr. Sigrid Peldszus (University of Waterloo) for the use of the contact angle instrument.

Dr. Costas Tzoganakis (University of Waterloo) for access to the Haake Rheomex 252 single-screw extruder and pelletizer and Dr. Shuihan Zhu for his assistance with the operation.

Bunge Inc. (Hamilton, Canada) for providing soy materials; Archer Daniels Midland Company (ADM, Decatur, USA) and especially Russ Egbert for kindly providing soy materials and offering productive discussion; A. Schulman for providing polypropylene; AddComp, Arkema, Clariant, and DuPont for providing coupling agents.

Financial support from Grain Farmers of Ontario (formerly Ontario Soybean Growers), NSERC (Natural Sciences and Engineering Research Council of Canada) and Ontario Research Fund (BioCar) are gratefully recognized.

I would like to take this opportunity to thank my family for their patience, encouragement and support. My specials thanks go to my friends, without them I would never have been able to complete this thesis.

An dieser Stelle möchte ich meiner Familie danken, die mich immer wieder geduldig ermutigt und unterstützt haben. Mein besonderer Dank gilt meinen Freunden, insbesondere Katja, Saskia, Katharina, Patricia und Beate ohne deren Unterstützung und Aufmunterung diese Arbeit nicht möglich gewesen wäre.

Thanks to everyone who prayed for me.

To all engineers and doctors without formal degrees

Für alle Ingenieure und Doktoren ohne akademischen Titel

Table of Contents

List of Figures

List of Tables

List of Equations

List of Abbreviations

%	Percent
(auto)	Material subjected to autoclave treatment
($KMnO_4$)	Material subjected to potassium permanganate treatment
(single-screw)	Pre-extruded with single-screw extruder
(twin-screw)	Pre-extruded with twin-screw extruder
°	Degree
°C	Degree Celsius
µl	Microliter
µm	Micrometer
ADF	Acid detergent fiber
AOAC	Association of Official Analytical Chemists
ASTM	American society for testing and materials
cm^{-1}	Reciprocal centimeters
DI	Deionized
D-TGA	Derivative- Thermogravimetric analysis
e.g.	Exempli gratia
FESEM	Field emission scanning electron microscopy
FTIR	Fourier transform infrared spectroscopy
g/cm^3	Grams per cubic meter
H_2SO_4	Sulfuric acid
IR	Infrared
IS	Insoluble soy
J/m	Joules per meter
KBr	Potassium bromide
$KMnO_4$	Potassium permanganate
kV	Kilo Volts
M	Mole
MAH	Maleic anhydride
MAPP	Maleic anhydride grafted polypropylene
MFI	Melt flow index
min	Minutes
mm	Millimeter
mN/m	Milli-Newton per meter
MPa	Mega Pascal
mPa*s	Milli-Pascal seconds
N/A	Not available
N_2	Nitrogen
NaOH	Sodium hydroxide
NDF	Neutral detergent fiber
nm	Nanometer
Nx6.25	Total organic nitrogen factor for soy proteins
OWRK	Owens, Wendt, Rabel and Kaelble

pH	Power of hydroxide
PP	Polypropylene
RH	Relative humidity
rpm	Revolutions per minute
RT	Room temperature
s	Seconds
SD	Standard deviation
SF	Soy flour
SH	Soy hulls
SPI (c)	Soy protein isolate, commercially available
SPI (ex)	Soy protein isolate, experimentally obtained by alkaline protein extraction and acid precipitation
SSE	Soluble sugar extract
TGA	Thermogravimetric analysis
wt-%	Weight percent
σ^D	Dispersive surface energy
σ^P	Polar surface energy
σ_{Total}	Total free surface energy

1. Research Aim

Lightweight materials in automotive applications are needed to reduce the mass of vehicles and assist in reducing the fuel consumption [36-38]. The mass increase of vehicles over the past century was in response to a number of needs, safety (30 %), regulations (25 %), comfort (22 %), interior (15 %) and quality (8 %) [1] (Figure 1-1).

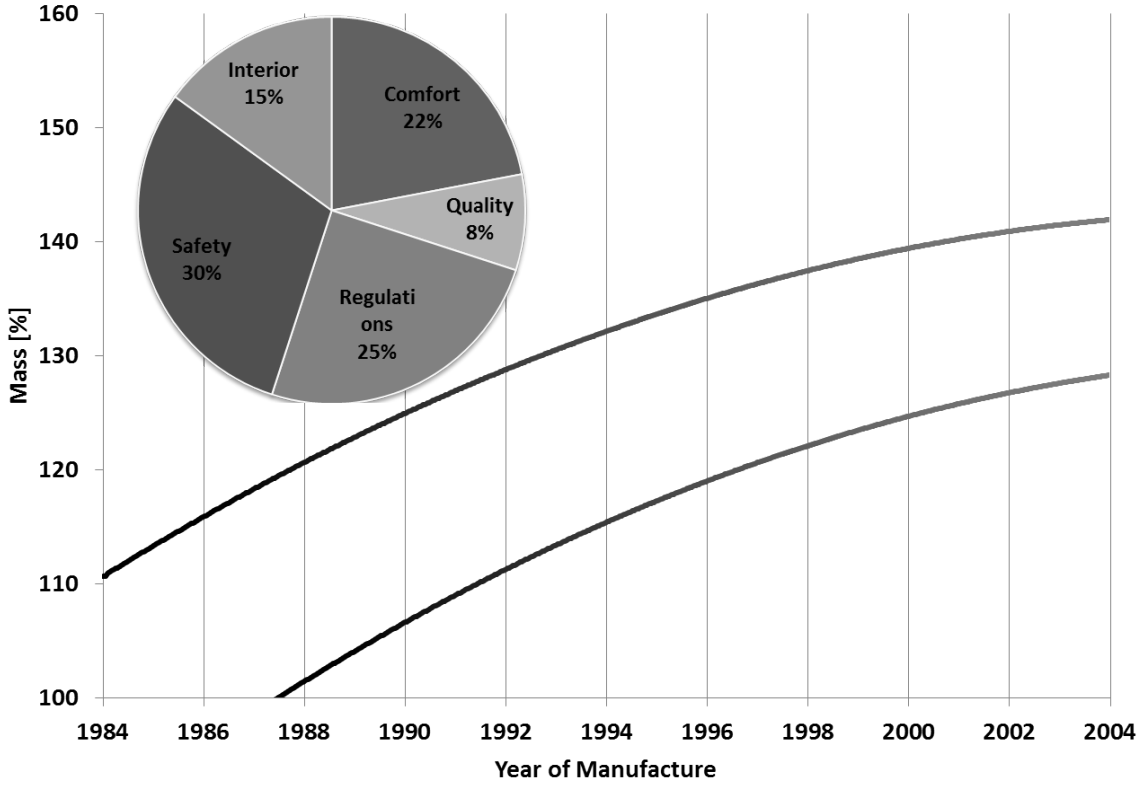

Figure 1-1 Mass development in automotive construction [1], modified

An example of the increase in vehicle mass is the BMW Dixie produced from 1927 to 1929 with a total mass of 535 kg compared to the BMW 7 series (year not specified but believed to be 2006) with a total mass of 1935 kg (depending on model and design) [1, 39]. Previously, materials in cars were steel, wood, cushion, glass and rubber. Today, cars have reduced amounts of steel and contain more specialized materials such as lightweight metals (aluminum and magnesium), thermosets and thermoplastics. Plastics and lightweight metals are increasingly replacing steel and iron [1]. Material development has moved from basic materials to composites and engineered materials with properties that can be adjusted according to their application. In addition, the “innovation focus” on the environment,

when developing new cars, has doubled from under 20 % to over 40 % from 2006 to 2009 [40].

Composites are materials from at least two phases that possess different properties than its single components. Composite materials from polypropylene and mineral and silica fillers are used in automotive applications [13, 41]. These types of fillers are characterized by their high density and the resulting heavier materials. Agricultural fillers are by-products of agricultural resources such as hemp, flax, kenaf, abaca, coir, sisal, jute, corn, wheat, cotton [23, 42-51]. In comparison to mineral fillers, agricultural fillers possess low density and can produce composite materials with equivalent mechanical properties. An additional advantage of agricultural materials is their sound absorption properties which can be a desirable feature in interior automotive applications [1]. Many automotive manufacturers use biocomposites in a wide range of applications [44]. An example of a door panel manufactured from flax biocomposites, with at least 20 % mass reduction, was discussed by Krenkel [1]. Agricultural fillers are hydrophilic and therefore highly interactive with water. Polypropylene on the other hand is a hydrophobic petroleum derived plastic with low interactions with water. Such differences need to be addressed when producing high performance biocomposites.

Soybean represented in 2009, the number one oil seed crop (53 % of world's oil seed production) and protein meal (66 % of world's protein meal consumption) in the world [52]. In 2009, the production of soybeans was almost 400 million metric tons with more than 40 % produced in North America [52]. Soy flour, a by-product resulting from the oil extraction of soybeans, possesses very different composition and structural properties when compared to typical natural fillers. Soy flour is not issued from the stem or leaves of the plant but from its seed. Its protein content is between 40 and 50 % and the carbohydrate content is between 30 and 40 % [30, 53, 54]. Therefore typical methods for analysis and testing of agricultural fillers are not applicable and need to be adapted for their use with soy flour. The applicability of soy flour as filler requires the characterization of its constituents and their thermal stability behaviour and overall performance when compounded with polypropylene. Previous studies have shown strong potential of soy flour in the development of biocomposites for automotive applications if the impact properties can be improved [20].

There is no good or inappropriate material, there is the most suitable material for its specific application and expected to fulfil a highly complex spectrum of desired attributes [1].

In the context of interior automotive materials, mechanical properties are one of the most important attributes.

2. Objectives

The main objective of this PhD project was to create soy-polypropylene biocomposites with appropriate strength and toughness properties required for interior automotive applications. A flow chart of the project is shown in Figure 2-1 and represents the main steps of this work. The first step was the characterization of soy flour and its changes when subjected to either potassium permanganate or autoclave treatment. Characterization included composition, thermal stability, and surface chemistry. The main constituents of soy flour were also investigated to better understand how thermal and mechanical properties were related to constituents of soy flour and its treatment. As there is poor compatibility between the soy flour and the polypropylene matrix, the surface properties of the selected soy materials was studied before and after their treatment. Specifically, the hydrophobicity and polar and dispersive energy components of soy materials were estimated. Characterization methods for powder-like agricultural materials were developed or modified. Intensive studies of the soy flour surface properties were carried out by evaluating the contact angle with liquids before and after specific treatments.

The second step was the preparation of soy-polypropylene composite materials for a number of soy materials, treatment and coupling agent combinations.

These composite materials were evaluated according to their mechanical properties, impact strength, flexural strength and flexural modulus.

Correlations between surface properties of the soy materials and their mechanical properties were explored. Furthermore, the compatibility of selected coupling agents was investigated with special focus on impact properties.

Morphology of the fractured composites provided information on cracks and served to formulate crack propagation mechanisms according to material formulation.

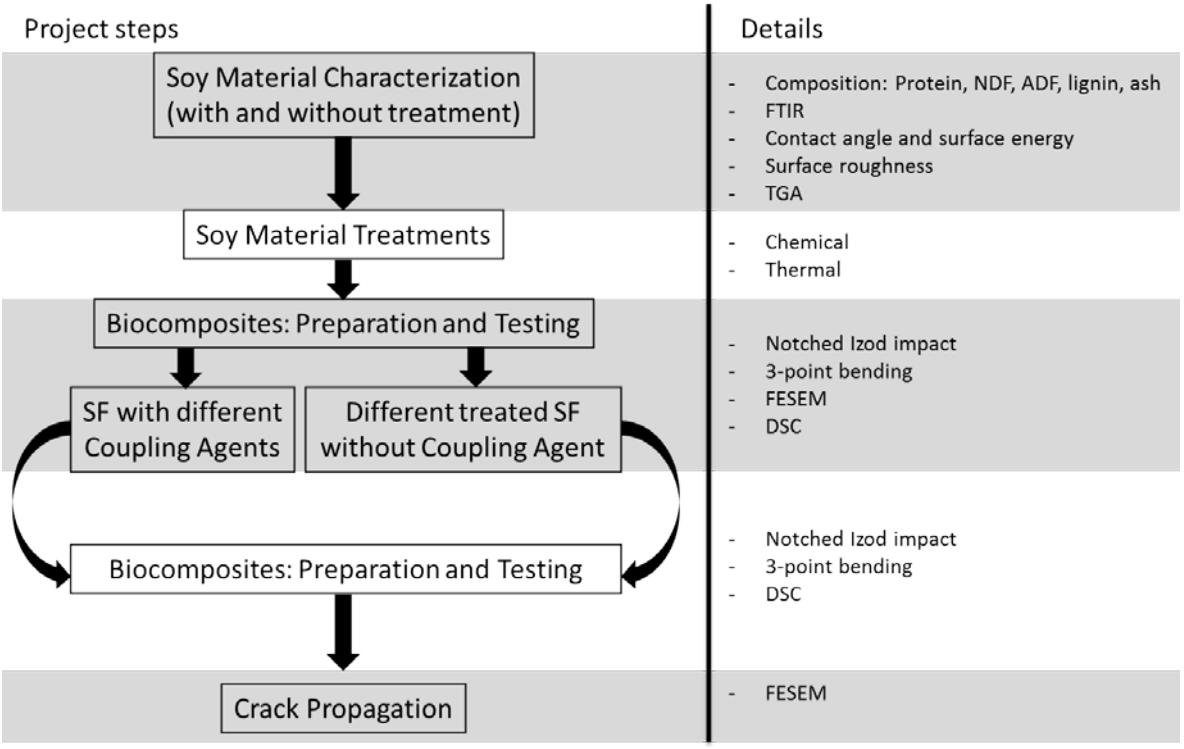

Figure 2-1 Flow chart of project with steps and associated details

3. Thesis Structure

This thesis is structured as follows. Chapter 1 discusses the research aim of the study and motivation. The objectives of the work are presented in chapter 2. Chapter 1 presents the literature review with background information on the state of the art in biocomposites and automotive applications, the production and applications of soybeans in North America, as well as details on selected methods for the characterization of agricultural filler with emphasis on methods selected for this project. Chapters 0 to 8 are presented in manuscript format. As a consequence of this format, some information will be repetitive, particularly in the introduction and materials and methods sections. The overall conclusions drawn from this work are presented in Chapter 1 together with recommendations for future work. The contents of chapters 0 to 8 are as follows:

Chapter 5

This chapter presents the chemical surface composition by FTIR and the dynamic and constant temperature thermal stability by TGA (thermogravimetric analysis) of soy materials. A number of soy materials were investigated in addition to soy flour, soy reference materials (soy protein isolate (SPI), soy hulls (SH)) and soy flour by-product materials (insoluble soy (IS), soluble sugar extract (SSE)), before and after potassium permanganate and autoclave treatment. This chapter has been prepared for submission to the Journal of Agricultural and Food Chemistry.

Chapter 6

This chapter describes the effects of potassium permanganate and autoclave treatments on the water contact angle for the characterization of the hydrophobicity of soy materials and their total surface energy and its components. This chapter has been prepared for submission to Powder Technology.

Chapter 7

This chapter presents the mechanical properties, notched Izod impact strength and flexural properties, of the composites for different soy treatment and coupling agent formulations. Correlations to the soy material properties presented in the two previous chapters are also outlined. Morphology of the composite materials and potential crack propagation mechanism are discussed. This chapter has been prepared for submission to the Journal of Applied Polymer Science.

Chapter 8

This chapter presents the surface characteristics of sulfuric acid treated SF and reports on the mechanical properties of the composites made with SF (H_2SO_4). It also shows the morphology of the dispersed phase in the composites and discusses the differences observed when compared to untreated soy flour.

4. Literature Review

4.1 Biocomposites

Biocomposites are difficult materials to define appropriately. Some information on the existing definitions will first be provided. Biomaterials (Biowerkstoffe) are materials that are fully or present in an appropriate quantity and originate from agricultural materials or wood. Typical agricultural materials – in that context also called renewable materials – include starch, vegetable oils and cellulose (wood, natural fibers, straw, grass) as well as other biomolecules such as lignin or caoutchouc (natural rubber). The fraction of the natural component present in the material shall be at least 20 %. When distinguishing between traditional biomaterial or bioproducts, like chipboards, and the more recent biocomposites, these are often called “novel” or “innovative”. Innovative bioproducts are generally produced by using novel process techniques from plastic processing like extrusion, injection moulding, or thermoforming [55].

Fowler and his colleagues define composites as: “Composites consist of two (or more) distinct constituents or *phases*, which when married together result in a material with entirely different properties from those of the individual components.” [56].

In order to call a composite “biobased” or “biocomposite”, the following definitions should be considered:

According to the ASTM standards, biobased materials are materials that contain “carbon based compound(s) in which the carbon comes from contemporary (non-fossil) biological sources.” [57].

Comparing the ASTM definition of biobased materials with the literature definition of biobased products, a “product generated by blending or assembling biobased materials, either exclusively or in combination with non-biobased materials, in which the biobased material is present as a quantifiable portion of the total product mass of the product.” [57], the biocomposite from polypropylene and soy material can be considered as biobased product, thus a *biocomposite*.

Usually, composites consist of two components, a polymeric matrix and a reinforcement component. At least one of the two components has to be biobased in order to call the final composite a biocomposite. Any polymer could function as a matrix in a biocomposite but also a blend of more than one polymer could also be used. Plastics are usually polymers of high molecular mass made from non-renewable or renewable monomers. *Renewable*

plastics are made or obtained from plants or animals or their products. *Non-renewable plastics* are made from fossil sources. Depending on the sources of the monomers and the polymerization method, the plastic can be biodegradable or recyclable. A *biodegradable plastic* implies predominantly microbial degradation by bacteria and fungi. Biodegradable plastics are used in applications such as compostable bags for grocery and gardening packaging, as well as biomedical applications. *Recyclable plastics* only imply the possibility of reuse when suitable facilities are available and also able to separate different types of plastics and process them for a new, recycled designation.

Reinforcement materials or fillers can be classified according to similar categories as for the matrices presented in the previous paragraph: biobased and non-biobased. Typical examples for non-biobased fillers in composites are talc and calcium carbonate. Typical examples for biobased and biodegradable fillers are generally particulate materials that originate from stems (e.g. wood), leaves or seeds of plants. Also, by-products during paper manufacturing and recycling can be used as filler materials.

The main constituents of plant fillers or fibers are cellulose, hemicelluloses, pectin and lignin. Different fractions are present in each part of the plant or in different species. Coir fibers for example contain high amounts of lignin and low amounts of cellulose [51]. An overview of the composition of selected agricultural fibers is presented in

Table 4-1. Differences in composition can be explained by the type of species and the stage of plant growth as well as growing or sampling locations. Some characteristics of common mineral fillers are shown in Table 4-2.

Table 4-1 Chemical composition [wt-%] of selected agricultural fillers or fibers [23], adapted.

Type of filler	Cellulose	Lignin	Pentosan	Ash	Silica
Stalk fiber					
Rice	28-48	12-16	23-28	15-20	9-14
Wheat	29-51	16-21	26-32	2.5-9	3-7
Barley	31-45	14-15	24-29	5-7	3-6
Oat	31-48	16-19	27-38	6-8	4-6.5
Rye	33-50	16-19	27-30	2-5	0.5-4
Cane fiber					
Bagasse	32-48	19-24	27-32	1.5-5	0.7-3.5
Bamboo	26-43	21-31	15-26	1.7-5	0.7
Grass fiber					
Esparto	33-38	17-19	27-32	6-8	-
Sabai	-	22	24	6	-
Reed fiber					
Phragmites communis	44-46	22-24	20	3	2
Bast fiber					
Seed flax	43-47	21-23	24-26	5	-
Kenaf	44-57	15-19	22-23	2-5	-
Jute	45-63	21-26	18-21	0.5-2	-
Hemp	57-77	9-13	14-17	0.8	-
Ramie	87-91	-	5-8	-	-
Core fiber					
Kenaf	37-49	15-21	18-24	2-4	-
Jute	41-48	21-24	18-22	0.8	-
Leaf fiber					
Abaca (Manila)	56-63	7-9	15-17	1-3	-
Sisal (agave)	43-62	7-9	21-24	0.6-1	-
Seed hull fiber					
Cotton	85-96	0.7-1.6	1-3	0.8-2	-
Wood fiber					
Coniferous	40-45	26-34	7-14	<1	-
Deciduous	38-49	23-30	19-26	<1	-

Table 4-2 Physical properties of common mineral fillers [24].

Property	Filler			
	Barite	**Talc**	**Calcium Carbonate**	**Mica (phlogopite)**
Particle shape	Orthorhombic	Platy	Orthorhombic	Platy
Specific gravity	4.5	2.8	2.7	2.8
Chemical resistance:				
Acids	Excellent	Good	Poor	Good
Alkali	Excellent	Good	Fair	Good
Thermal stability [°C]	1580	900	680	1500
pH (10 % solution)	6.5-7	9	9-9.5	9-9.5
Hardness (Mohs' scale)	2.5	1	3	2.5
Thermal conductivity [cal/cm.s.°C]	$6x10^{-3}$	$5x10^{-3}$	$5.6x10^{-3}$	$16x10^{-3}$
Specific heat [cal/g.°C]	0.11	0.208	0.205	0.206
Coefficient of thermal expansion [cm/cm/°C]	10	8	10	25
Oil absorption	6	25	10	25

4.2 Biocomposites in the Automotive Sector: State of the Art

Natural fiber reinforced plastics were first used in phenol resins in the mid nineteen twenties. In 1941, Henry Ford presented the HempCar where the body was made from hemp fiber reinforced resin. The HempCar though can only be considered as concept car since it never was in production. Until the 1980s, most thermoset plastics used in the automotive sector were reinforced by fibers from wood and cotton. Natural fiber reinforced plastics were limited to the interior parts of the cars with the exception of the Trabant produced from 1964 until 1990 in the German Democratic Republic (GDR). The Trabant model 601 was the first car produced in series with a body made completely from natural fiber reinforced plastics (Figure 4-1). The empty weight of the car was 615 kg. The motivation to build the Trabant from bio-based composites was the shortage of steel in Eastern Europe due to high cost and importation restrictions. Later, the driver cabin from trucks around the world was also made from natural fiber composites to reduce their weight. Today, many parts of the car interior are made from biocomposites [2, 58].

Recent projects in our laboratory have involved work with biocomposites from wheat straw and polypropylene which have shown to be very successful in the automotive sector [59, 60]. The material developed is used in the interior of the Ford Flex 2010 [61]. Today, the applications of biocomposites are very diverse and can be found in the automotive sector

and construction sector but also in many parts of furniture and appliances. Some examples are shown in Figure 4-2.

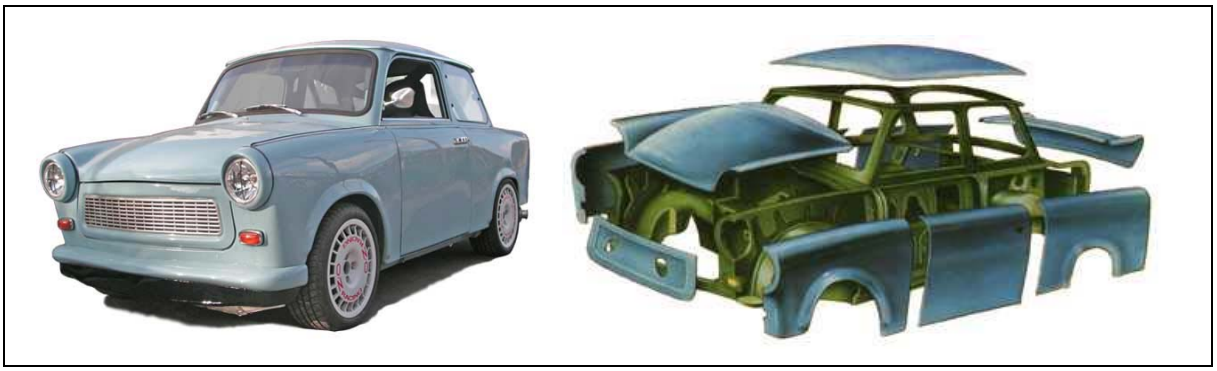

Figure 4-1 Trabant 601: Car body fully made from natural fiber reinforced plastic (phenol resin (Duroplast) and cotton) [2, 3].

Figure 4-2 Examples of biocomposites applications: car, construction, cases, dishes [4-6] modified.

4.3 Processing of Composite Materials

4.3.1 Extrusion

Extrusion is a common method for mixing plastics and filler in a process called compounding. During extrusion, the thermoplastic material is fed through a funnel into a heated chamber with one or two screws or auger propels. The plastic material melts and becomes a continuous viscous fluid. The die at the end of the extruder is open-ended and can be directly connected to other devices such as pelletizer or blower for further processing [62].

4.3.2 Injection Moulding

A variety of forming techniques for plastics can be selected and will depend on the desired properties of the plastic: thermoplastic or thermoset, plastic melting temperature (softening), plastic stability and geometry of the final product [62]. Thermoplastics are commonly obtained by injection moulding [63] where the material is fed with a plunger or ram into a cylindrical heating chamber. The melted material is then forced with the plunger or ram through a nozzle into the mould and the pressure is released once the material has solidified [62]. During injection moulding, the polymer is oriented due to shear stress and the cooling of the molten polymer in the direction of its flow through the mould [24]. The most important parameters that can affect the morphology of the material are the resin properties, such as molecular weight, and the processing conditions, such as melt temperature and mould temperature [24]. Advantage of injection moulding thermoplastics is the ability of manufacturing complex, precision parts in fast production times [63]. Limitation on the other hand can be the high processing pressure that require high quality materials equipment and tools [63].

4.4 Filler

4.4.1 Types of Filler Materials

Fillers can be classified in two major categories according to their source, organic and inorganic fillers. Organic fillers can be obtained from carbon (carbon black, graphite, ground petroleum coke), synthetic fibers (polyamide, polyester, polyacrylonitrile), lignin (ground bark, processed lignin) or cellulose (wood, cotton, stalks, leafs etc.) [25]. Fillers obtained as by-products from agricultural harvesting and processing will be referred in this study as agricultural fillers. Based on this terminology, cellulose and lignin fillers are agricultural fillers. Examples of inorganic fillers include metals and metal oxides, glass,

boron, calcium carbonates, silica and silicates including mineral fillers [25]. Common mineral fillers for automotive applications are calcium carbonate, dolomite, talc, wollastonite and kaolin [13]. In 2006, nearly 25 % of all minerals in North America were used for automobiles [41]. Talc and calcium carbonate are often used in polypropylene whereas kaolin is commonly used in combination with nylons. Wollastonite, due to its high aspect ratio, is often used in materials to balance stiffness and impact properties. Mineral fillers are characterized by their high density producing heavier composites when compared to composites with agricultural fillers.

Typical agricultural fillers are derived from plants such as wood, bamboo, wheat straw, cotton, kenaf, sisal, roselle, coir, ramie, sunhemp, hemp, flax, jute, abaca, and other plants high in cellulose content [1, 23, 64-67]. Most of these materials have fibrous structure making them reinforcements. Fillers derived from plants that are not fibers are often called flour and represent low cost by-products during processing. Examples for flours used in biocomposite applications are wood flour, rice husk flour, coconut flour [68-73].

The use of soybean stock-based nanofibers has been reviewed by Wang and Sain [74]. By chemo-mechanical treatment, cellulose nanofibers can be extracted and used as reinforcements in poly(vinyl alcohol) (PVA) and polyethylene (PE) materials. Cellulose nanofibers have a theoretical stiffness of up to 130 GPa and strength up to 7 GPa. The mechanical performance is comparable to materials such as glass fibers or carbon fibers [74].

When using agricultural materials with thermoplastics, the major challenges are the high hydrophilicity and the low thermal stability of the filler and subsequently the poor interphase due to incompatibility with hydrophobic petroleum-based polymers. High temperatures are also problematic and can lead to thermal degradation of the filler resulting in poor mechanical properties. Surface treatments have been considered for the removal of the wax components, or for the grafting of functional groups that interact with the polymer or increase the hydrophobicity by reactions on the surface [64].

4.5 Filler Characterization

The characterization of fillers should provide information on their composition, thermal behaviour, morphology, and surface chemistry which can assist with the optimization of the filler-matrix interaction [75]. Various techniques can be used to investigate filler materials regarding their reactivity with probe molecules, elemental and chemical composition, structural changes between filler and adsorbed layers, but also performance behaviour during processing [75].

Thermal behaviour is typically studied by thermogravimetric analysis (TGA) in air or nitrogen. Measurements of the thermal degradation of the filler will provide information on the different components of a material and their anticipated stability during processing and usage.

The particle size and the particle shape of the filler can affect significantly the properties of the biocomposite [75, 76]. An improved filler dispersion and distribution will lead to a more consistent biocomposite material and should result in improved interfacial interactions between the filler surface and the matrix [75]. When the small filler particles are well dispersed, the mechanical properties can be determined by the dispersed phase (its properties and interfacial interaction with the continuous phase) rather than the continuous phase alone [37]. Field emission scanning electron microscopy (FESEM) can be used for the investigation of the filler size and shape (directly on the filler) and the filler-matrix interface (on the surface of fractured composites).

The functional groups present at the surface of the filler can be characterized by Fourier-transform infrared spectroscopy (FTIR) but are generally very complex for agricultural fillers. Therefore additional techniques such as X-ray photoelectron spectroscopy (XPS) or secondary ion mass spectroscopy (SIMS) can be used [75].

For investigations on the surface characteristics, contact angle analysis can be performed which will be explained in detail in section 4.5.4.

4.5.1 Thermal Stability

The thermal stability of agricultural fillers is one of the main challenges faced when working with biocomposites. The polymer processing temperature is selected based on its crystalline melting point. Usually, the minimum processing temperature will be about 30 to 50 °C above the crystalline melting point [24]. For compounding polypropylene the lowest processing temperature is around 190 °C [24]. Therefore agricultural filler need to withstand temperatures of the processing conditions. Cellulose has a good thermal stability (~300 °C) but this depends on its crystal structure [77]. Therefore, fibers with high crystalline cellulose content such as jute and flax are preferred as agricultural fillers in biocomposite applications [46, 77].

In order to test the behaviour of a material in thermal environment, thermogravimetric analysis (TGA) can be performed. It is possible to specify conditions such as gas environment, heating range, heating rate and time allowing for experiments to be conducted in inert or air environment or in dynamic or isothermal mode. An overview of the overall thermal behaviour of a material is commonly obtained under dynamic conditions in an inert

environment. The mass loss over temperature will reveal the thermal stability of the constituents of a material.

For the processing of agricultural fillers, it is important to investigate the performance of this material at processing conditions. Therefore, processing conditions for extrusion and injection moulding can also be selected to investigate the thermal stability at isothermal (processing) temperature and air environment [24, 78] and obtain information on the mass loss of a material over time during processing.

4.5.2 Surface Chemistry with FTIR

Fourier Transform Infrared Spectroscopy (FTIR), based on infrared light, is a powerful tool for determining the structure of polymers and other molecular materials. When molecules are exposed to infrared light in a wavelength range between 4000 and 660 cm^{-1} (depending on the apparatus), the radiation will lead to stretching and vibrations of the atomic bonds in the molecule. The degrees of freedom are distributed as motions (rotation, translation, vibration) and are associated to typical band frequencies and related to the number of atoms (a chemical group) in the molecule or in the repeating units of a polymer [25]. Therefore a spectrum of an unknown polymer can be compared to a data base of spectra for known polymers and thus identify the nature of the unknown polymer. A number of common groups in polypropylene with their infrared absorption bands are presented in Table 4-3. Figure 4-3 presents the FTIR spectrum of isotactic polypropylene. An example of a FTIR reference spectrum is presented in Figure 4-4 for protein and Figure 4-5 for lignin and cellulose.

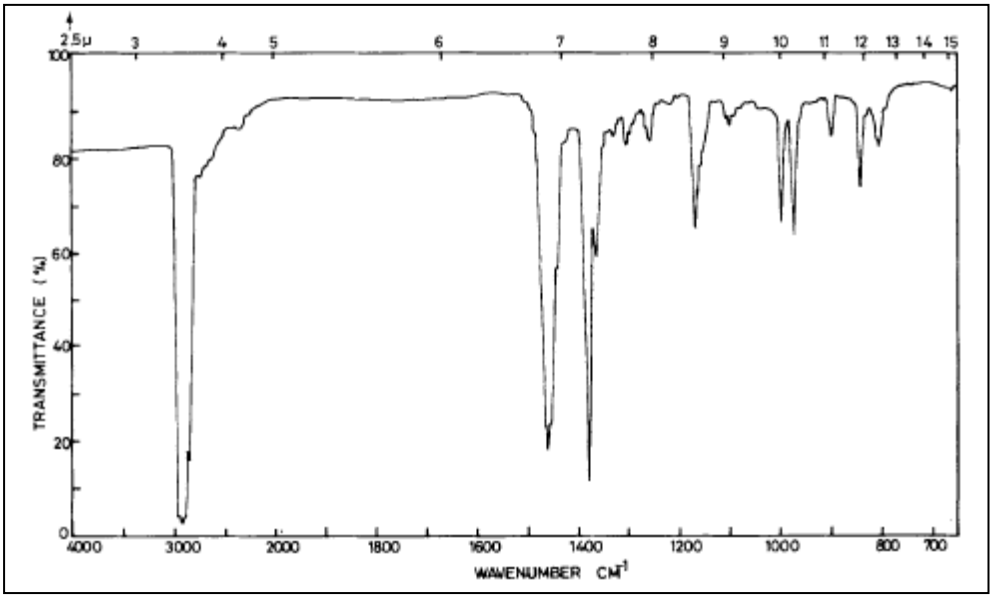

Figure 4-3 FTIR spectrum of isotactic polypropylene [7].

Table 4-3 IR absorption bands of functional groups in polypropylene [25].

Group	Type of vibration	Wavenumber [ν, cm-1]
CH_2	Stretch	2850-2960
	Bend	1465
	Rock	725-890
CH_3	Stretch	2860-2870
	Bend	1450
$H_2C=CHR$	C-H stretch	3030-3085
	C-H bend in plane	1300-1410
	C-H bend out of plane	910-990
	C-C stretch	1643
$H_2C=CR_2$	C-H stretch	3080
	C-H bend in plane	1410
	C-H bend out of plane	888
	C-C stretch	1650
OH	Stretch	3150-3700

Table 4-4 gives an overview of the plausible IR bands that can occur for protein materials. One can distinguish nine different bands, including the two predominant bands, amide I and II. Figure 4-4 shows the amide A, I, II and III bands in an FTIR spectrum. Amide IV bands are very complex due to mixtures of coordinate displacements. Also, amides V to VI bands have complex vibrational behaviour resulting from out-of-plane motions within the proteins.

Table 4-4 Characteristic bands of proteins with their corresponding wavelengths in FTIR [8].

Characteristic band of protein	**Attributive protein conformation**	**Wavelength [cm^{-1}]**
Amide A	Fermi resonance between the first overtone of amide II and the N-H stretching vibration	3500
Amide B		3100
Amide I	70-85 % from C=O stretch → backbone conformation	1600-1700
Amide II	40-60 % from N-H bending; 18-40 % from C-N stretching (conformational sensitive)	1510-1580 1610 [79]
Amide III	very complex bands resulting from a mixture of several coordinate displacements	1350 [79] 1378 [79]
Amide IV	very complex bands resulting from a mixture of several coordinate displacements	510 [79] 520 [79]
Amide V	out-of-plane motions	765 [80]
Amide VI	out-of-plane motions	537 [80]
Amide VII	out-of-plane motions	<300 [81]

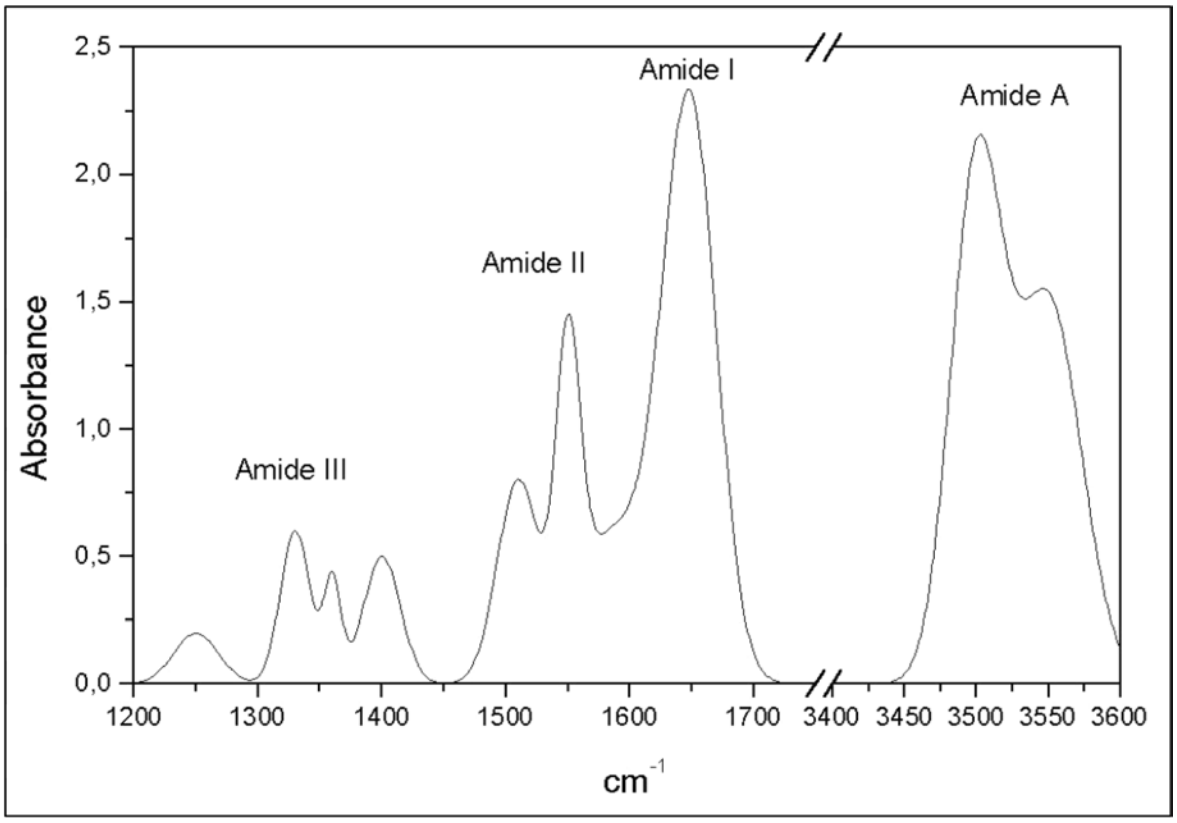

Figure 4-4 FTIR reference spectra for proteins with characteristic bands for Amide I, II, III and A [8-10]

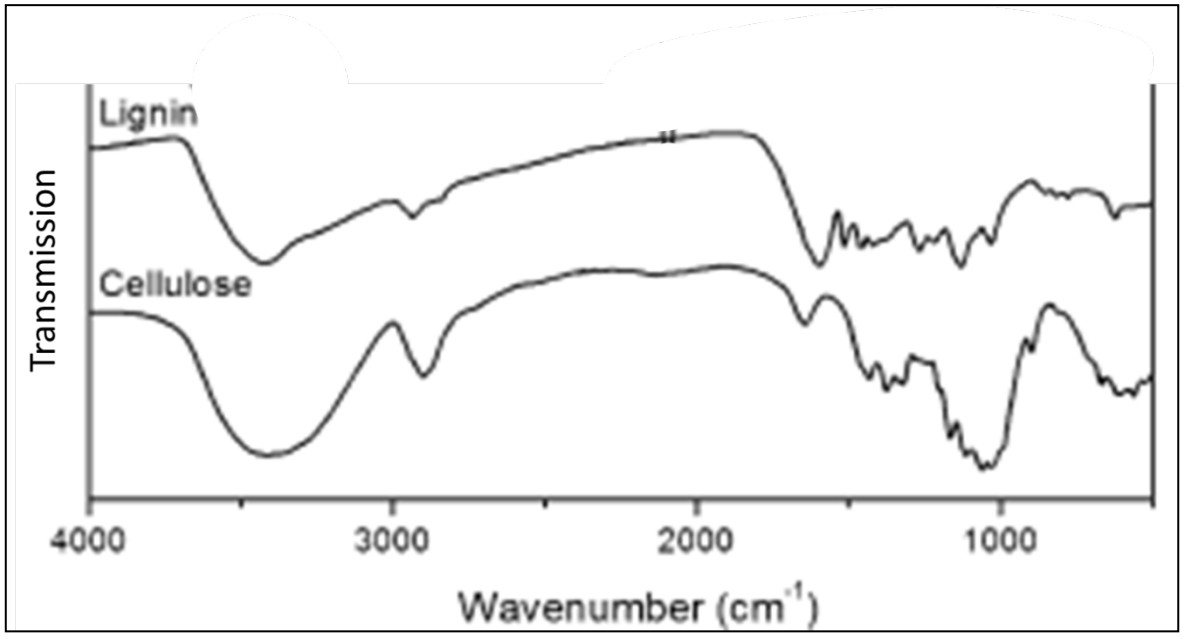

Figure 4-5 FTIR spectra of lignin and cellulose [11], modified

4.5.3 Hydrophilicity

Hydrophilicity can be reported as an index defined as the ratio of the surface abundances of hydrophilic $(HL)_i$ and hydrophobic $(HO)_j$ functional groups "i" and "j" [82]:

$$Hydrophilicity\ index = \frac{\sum k_i (HL)_i}{\sum n_j (HO)_j}$$

The factors k_i and n_j reflect the importance of the type of functional groups. Hydrophilic groups are hydroxyl and carboxyl groups and hydrophilic groups are aliphatic and aromatic CH groups [82].

Hydrophobicity is in general an anticipated feature of appropriate fillers because it can protect them from ageing [83]. It also provides better compatibility with polymer matrices that are hydrophobic resulting in improved wettability of the filler by the polymer matrix [67]. The hydrophobicity of fillers can be modified by treatments and coatings; some will be detailed in section 4.10.

A common technique to determine the hydrophobicity of a surface is the contact angle analysis which will be described in the following section.

4.5.4 Contact Angle and Surface Energy

Studies of the contact angle for a liquid drop on a solid surface can give information of the surface behaviour of solid materials. It is also possible to study surface properties of liquids but this topic will not be discussed in this work.

Contact angle can be measured with liquids that have known surface properties in static or dynamic mode. From the contact angle analysis, other properties can be determined such as surface energy and work of adhesion. There are different interactions and forces that contribute to the surface energy. The main forces are dispersive and polar interactions. Most of the theoretical concepts are based on the work of Owens and Wendt and the surface energy of polymers [84]. Krüss included this theory in their drop shape analysis system under the OWRK method (Owens, Wendt, Rabel and Kaelble) [12]. Their estimation method combines the Fowkes equation (Equation 4-1) and the Young's equation (Equation 4-2) which is arranged in a linear relationship (Equation 4-3). The resulting equation (Equation 4-4) can be plotted as shown in *Figure 4-6*. Surface energy data of selected polymer materials are listed in Table 4-5.

$$\gamma_{sl} = \sigma_s + \sigma_l - 2\left(\sqrt{\sigma_s^D * \sigma_l^D} + \sqrt{\sigma_s^P * \sigma_l^P}\right) \qquad \textit{Equation 4-1}$$

$$\sigma_s = \gamma_{sl} + \sigma_l * cos\theta$$ *Equation 4-2*

$$y = mx + b$$ *Equation 4-3*

$$\frac{(1 + cos\theta) * \sigma_l}{2\sqrt{\sigma_l^D}} = \sqrt{\sigma_s^P}\sqrt{\frac{\sigma_l^P}{\sigma_l^D}} + \sqrt{\sigma_s^D}$$ *Equation 4-4*

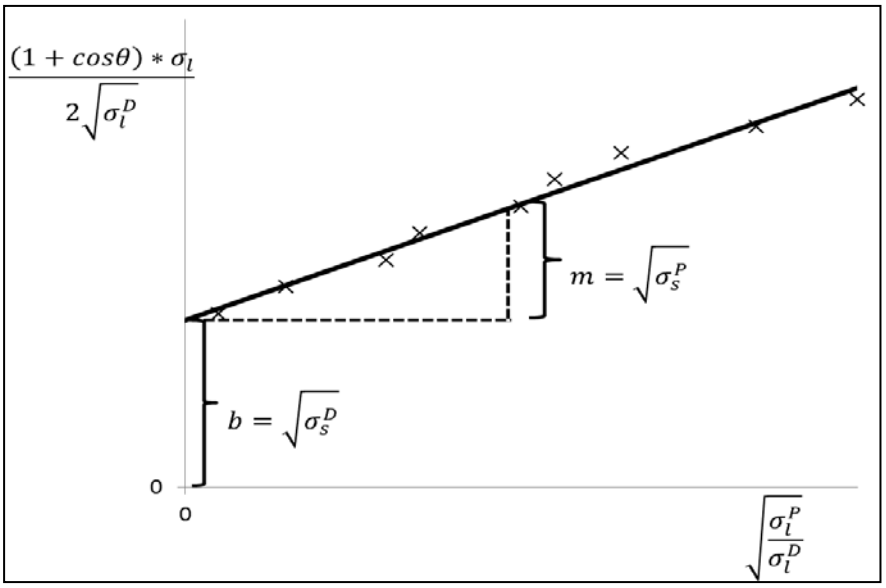

Figure 4-6 Plot of OWRK method for estimation of surface energy [12], *adapted.*

Table 4-5 Surface energy of polyethylene and polypropylene [26]

Name	Surface free energy (SFE) at 20 °C [mN/m]	Dispersive contrib. of SFE [mN/m]	Polar contrib. of SFE [mN/m]
Polyethylene-linear PE	35.7	35.7	0
Polyethylene-branched PE	35.3	35.3	0
Polypropylene-isotactic PP	30.1	30.1	0

Examples of contact angle applications are film surfaces. Dankovich investigated the surfaces of different cellulose films by studying the advancing and receding contact angles with the addition or withdrawing of liquid to a sessile drop causing changes in the volume of the drop and subsequently the contact angle [85]. For surface energy determination, water, diiodomethane and formamide are commonly selected having well-established surface tension values. Buckton developed a method for analysis of contact angle with powder materials that consists in pressing the powder in disks [86]. Roman-Gutierrez and

his colleagues studied the surface properties of wheat flour which represent highly water active materials with fast liquid absorption behaviour [87]. In order to account for this feature, time dependant studies of the contact angles were undertaken. With the new video integrated devices, it is now possible to obtain meaningful results. Alternative methods for surface studies, include the Wilhelmy method, zeta-potential analysis or inverse gas chromatography (IGC) [67, 88-90]. Closely related to surface energy and contact angle, are the work of adhesion and wettability [67].

Surface energy and surface tension are identical for liquids. For solids it describes the energy needed to overcome the van der Waals attraction of two surfaces separated to an infinite distance [91]. The surface energy of two identical materials can be seen as half the energy that is needed to "separate two flat surfaces from contact to infinity, viz. it is half the adhesion energy" [92].

Therefore, the energy needed to separate two different surfaces, the work of adhesion (W_{adh}), is described by the following equation [91] :

$$W_{adh} = \sigma_1^s + \sigma_2^s - \sigma_{12} \qquad \textit{Equation 4-5}$$

Where σ_{12} is the interfacial energy of the two materials and σ_1^s and σ_2^s are the surface energy of each material. Equation 4-6 shows the Young-Dupré equation for the estimation of the work of adhesion by using the contact angle and surface tension of the respective liquid. A linear relationship exists between the work of adhesion and mechanical properties as it can be seen in Figure 4-7.

$$W_{adh} = \sigma_l(1 + \cos\theta) \qquad \textit{Equation 4-6}$$

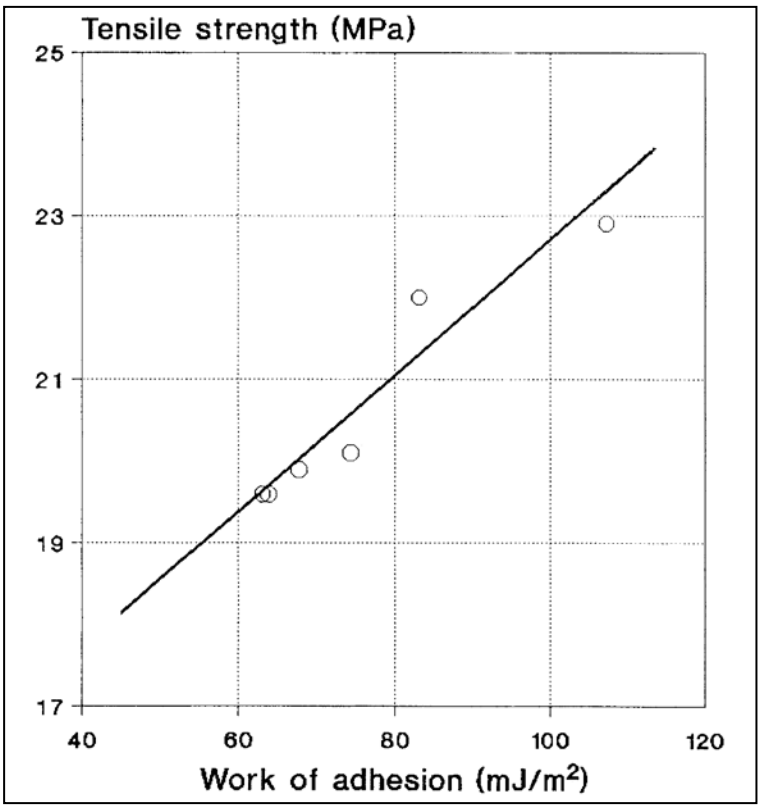

Figure 4-7 Relationship of work of adhesion and tensile strength in PP/CaCO3 composites [13]

Interfacial energy between two surfaces can be estimated according to Fowkes (Equation 4-1), who assumes that only the types of forces present in both materials will occur [12]. Therefore, for non-polar polymers, such as polypropylene, the interfacial energy can be estimated by using Equation 4-7 [12, 93].

$$\sigma_{12} = \sigma_1 + \sigma_2 - 2\sqrt{\sigma_1^D \sigma_2^D} \qquad \textit{Equation 4-7}$$

Wettability can be described as the interaction of a liquid on a solid surface which is determined by the balance of the work of cohesion and work of adhesion [27, 91]. Table 4-6 gives an overview of contact angle domains and the associated wetting behaviour.

Table 4-6 Wetting behaviour according to solid/liquid (S/L) and liquid/liquid (L/L) interactions [27]

Interactions L/L \ S/L	Weak	Strong
Weak	Wetting (0 °< θ < 90 °)	Perfect wetting (θ = 0 °)
Strong	No wetting (90 ≤ θ ≤ 180 °)	Wetting (0 °< θ < 90 °)

The contact angle analysis requires perfectly smooth surfaces for optimal results. One of the most important factors to consider is the surface roughness of the material which will be explained in the following section.

4.5.4.1 Surface Roughness

Beside chemical surface heterogeneity, surface roughness is one of the most important parameter that can affect contact angle analysis [94]. It is a term describing the topography of a surface which includes random sized and distributed elevations and cavities. Surface roughness can be the result of crystal structure, manufacturing or surface finishing [95]. Based on different models, it is believed that surface roughness decreases the contact angle when below 90 ° and increases the contact angle when above 90 ° [96]. Depending on the roughness and the contact angle, air may be trapped under the liquid drop affecting the contact angle measurements [96]. Roughness of the material is also an important parameter affecting the wetting behaviour of the material. Trapped air due to surface roughness and hydrophobic surface properties can cause the so called “Lotus effect” [97].

The surface roughness can be manipulated to modify the adhesive forces between filler and matrix [67]. The surface roughness of a composite is determined by the shape of the filler and its actual surface area [67, 98]. For experimental determination of surface roughness, optical profilers or scanning probe microscopes can be used [67, 94, 99]. In a study by Ayrilmis, the average surface roughness of wood plastic composite panels containing 50 wt- wood flour and different fire retardants was between 2.7 and 6.8 µm [100]. The surface roughness of different types of sanded wood was measured and modelled by Tan and his colleagues [101]. The average roughness between the wood surfaces was between 3.19 and 9.27 µm [101].

Moutinho and her colleagues showed that a linear relationship existed between contact angle and surface roughness for paper sheet and was not affected by processing conditions [102].

4.6 Soy Materials

Soybeans belong to the Leguminosae (legumes) family and are characterized by their high oil and protein content. During the harvest and processing of soybeans, a number of products are generated. The major products of commercial value are the soybean oil and the soy meal. The other products include the soybean stem, leaves and pods, and soy hulls. A simplified chart of the processing of soybeans is presented in Figure 4-8. After cleaning and drying, the soybeans are cracked and dehulled. During this step, the soy hulls represent a by-product high in carbohydrates and used mainly as fiber source in animal feed. The dehulled soybeans are conditioned and further processed into flakes. During this process, the oil is extracted and separated from the flakes. Heating and hexane addition, improves the oil extraction quite efficiently so that the remaining flake contains less that 1.5 % oil [103]. In order to remove the hexane, the soy flakes are toasted in a desolventizer. For human nutrition, proteins can be recovered by extraction with either alkaline solution followed by acid precipitation or by ethanol extraction. The extraction yield depends on the heat treatment prior to the extraction. Extreme pH or heat conditions will degrade the proteins resulting in lower functionalities. Therefore, lower yields will be accepted as trade-off for higher protein functionality. A large range of soy products are commercially available and differ mostly in protein and carbohydrate content as well as protein functionality, including solubility. Worldwide, there is only an average of 6 % of the soybeans used for food applications [104].

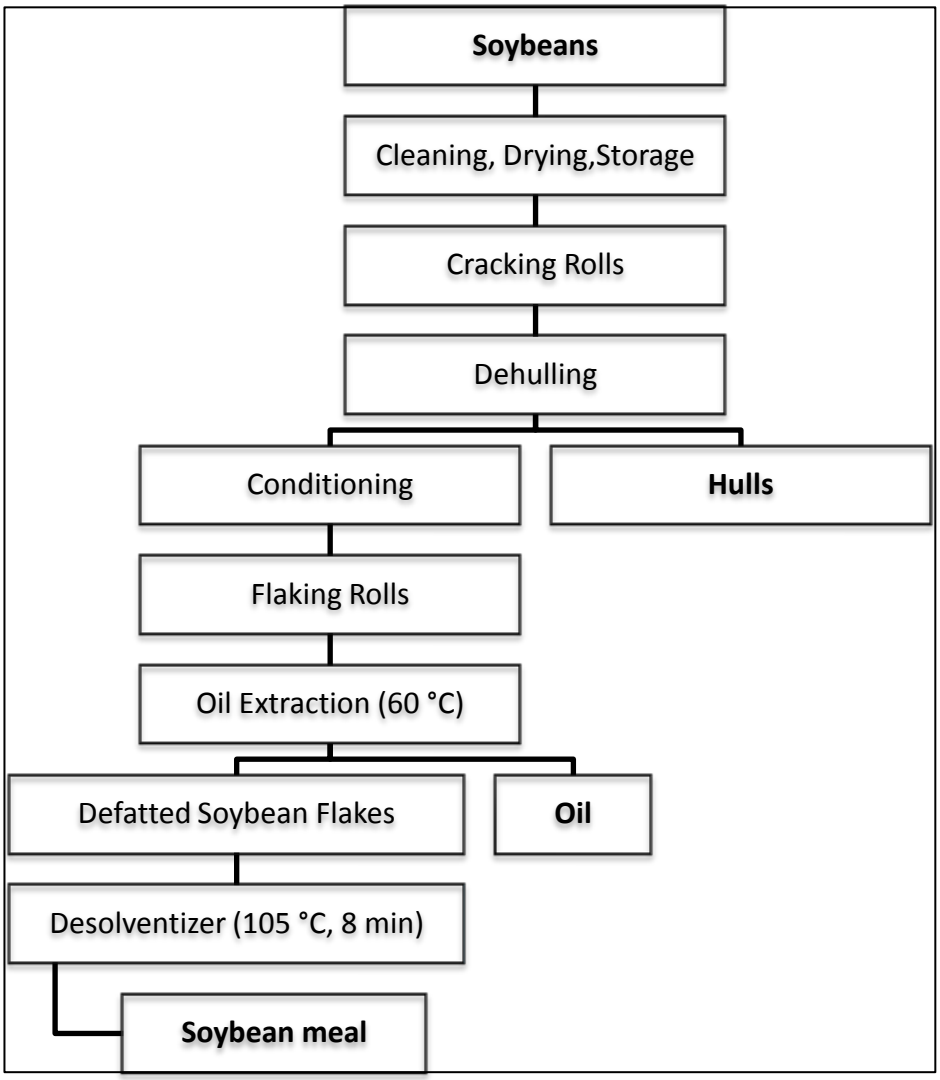

Figure 4-8 Simplified soybean processing chart.

Table 4-7 Soy flour, concentrate and isolate composition [28]

	Defatted flours and grits		Concentrates		Isolates	
Constituent	**As is**	**mfb***	**As is**	**mfb***	**As is**	**mfb***
Protein (Nx6.25)	52-54	56-59	62-69	65-72	86-87	90-92
Fat (pet. Ether)	0.5-1.0	0.5-1.1	0.5-1.0	0.5-1.0	0.5-1.0	0.5-1.0
Crude fiber	2.5-3.5	2.7-3.8	3.4-408	3.5-5.0	0.1-0.2	0.1-0.2
Soluble fiber	2	2.1-2.2	2-5	2.1-5.9	<0.2	<0.2
Insoluble fiber	16	17.0-17.6	13-18	13.5-20.2	<0.2	<0.2
Ash	5.0-6.0	5.4-6.5	3.8-6.2	4.0-6.5	3.8-4.8	4.0-5.0
Moisture	6-8	0	4-6	0	4-6	0
Carbohydrates (by difference)	30-32	32-34	19-21	20-22	3-4	3-4

*mfb = moisture-free basis

4.6.1 Soybean and Products Composition

The main constituents of soybeans are moisture, oil, proteins, carbohydrates, vitamins, phosphorus, and minerals [54]. The protein content of soybeans is around 50 %. After solvent oil extraction, the oil content is negligible. In order to remove the protein fraction, an alkaline treatment can be performed which also removes water soluble sugars and other components. Approximately 35 % of soybeans are carbohydrates which can be divided in polysaccharides and indigestible fibers [54]. A typical sugar composition of soy flour is presented in

Table 4-8. Soy protein isolates contain only about 2.27 % (±1.4) sugar [29]. Table 4-9 presents the typical mineral composition of soy meal.

Proteins represent the largest fraction of soybeans. Proteins are polypeptide chains consisting of amino acids. The polypeptides are held together by different forces such as hydrogen bonding, disulfide bridges, and electrostatic interactions. Most of these forces are very sensitive to temperature and pH extremes which may lead to protein denaturation. Since the minimal processing temperature of polypropylene is 190 °C, protein denaturation is anticipated and decomposition is also possible. The proteins in soybeans have a wide range of molecular sizes but contain about 38 % non-polar, non-reactive amino acid residues and 58 % polar and reactive amino acid residues [51]. Therefore, soybeans have a wide use as ingredient in many foods. A typical amino acid composition in soybean meal is presented in Table 4-10.

Table 4-8 Hydrolyzed carbohydrate composition of soy flour [29]

Sugar	Average content [%]	STDEV (n=19)
Rhamnose	0.56	0.171
Fucose	0.09	0.079
Ribose	0.13	0.067
Arabinose	2.37	0.194
Xylose	0.97	0.098
Pinitol	0.87	0.171
Mannose	0.94	0.331
Galactose	7.60	0.433
Glucose	8.14	0.731
TOTAL	**21.67**	**1.013**
Monosaccharides	0.47	No replication
Sucrose	7.32	No replication
Raffinose	0.88	No replication
Stachyose	4.57	No replication

Table 4-9 Mineral composition of different soy protein products [28]

Constituent	Defatted soy flour	Soy protein concentrate [%]	Soy protein isolate
Potassium	2.4-2.7	0.1-2.4	0.1-1.4
Phosphorus	0.7-0.9	0.6-0.9	0.5-0.8
Calcium	0.2-0.3	0.2-0.4	0.1-0.2
Magnesium	0.2-0.3	0.3	0.03-0.09
Chlorine	0.1-0.3	0.7	0.13
Iron	0.01	0.01-0.02	0.01-0.02
Zinc	0.005	0.005	0.004-0.009
Manganese	0.003-0.004	0.005	0.002
Sodium	0.003-0.015	0.002-1.2	0.04-1.2
Copper	0.001-0.002	0.001-0.002	0.001-0.02

Table 4-10 Amino acid characterization and composition (average) in 55 types of soy meal processed in the USA[30, 31].*

Side chain type	Amino acid (MW)	Average % dry matter*	Properties
Aliphatic	Glycine (57)	2.28	smallest amino acid no charge hydrophobic
	Alanine (71)	2.36	like glycine no charge hydrophobic
	Valine (99)	2.43	no charge hydrophobic
	Leucine (113)	4.19	no charge isomer of isoleucine hydrophobic
	Isoleucine (113)	2.33	no charge isomer of leucine hydrophobic
	Proline (97)	2.59	no charge promotes turns cyclic not hydrophobic
Aromatic	Phenylalanine (147)	2.66	no charge absorbs UV hydrophobic
	Tyrosine (163)	1.79	weak charge absorbs UV hydrogen bonding hydrophobic
	Tryptophan (186)	N/A	largest amino acid rarest amino acid no charge absorbs UV hydrogen bonding hydrophobic
Sulfur containing	Cysteine (103)	0.85	Sulfur analog of Ser weak charge forms disulfide bonds hydrophobic (0.17)

	Methionine (131)	0.79	initiator of proteins no charge hydrophobic
charged	Aspartate (115)	6.29	acidic negative charge hydrophilic
	Glutamate (129)	9.81	acidic negative charge hydrophilic
	Histidine (137)	1.41	imidizole in side chain basic reactive weak positive charge hydrophilic (-1.7)
	Lysine (128)	3.3	amine in side chain basic reactive strong positive charge hydrophilic
	Arginine (156)	3.34	guanidinium side chain basic strongest positive charge hydrophilic
Polar/uncharged	Serine (87)	3.12	no charge hydrogen bonding hydrophilic
	Threonine (101)	1.79	no charge hydrogen bonding hydrophilic
	Asparagine (114)	N/A	amide of Aspartate hydrogen bonding no charge hydrophilic
	Glutamine (128)	N/A	amide of Glutamate hydrogen bonding no charge hydrophilic

4.6.2 Polymers from Soy Proteins

From the perspective of renewable materials and for environmental benefits, soy proteins and other soybean products have been investigated as components in plastics and adhesives, and as a filler component in elastomers [105].

Soy plastics have a 50 % higher modulus than current epoxy engineered plastics [51]. Mohanty et al. showed, in their review paper, that by blending the soy protein plastic (matrix) with polyphosphate as filler, a decrease in water uptake was observed [51]. A similar observation was also reported in this review paper for a material developed from soybeans, with carbohydrate filler (not specified) and an additive for better adhesion and reduced water absorption. The final material resulted in improved biodegradable plastics having a high degree of flowability for easier processing, higher tensile strength and water resistance [51].

4.7 Polypropylene

Polypropylene (PP) belongs to a group of polymers known as polyolefins, the synthetic polymer with the largest volume of applications. One common application for polypropylene is in automotive manufacturing for various exterior and interior parts [63, 106]. Polypropylene is obtained by polymerization of propene (propylene). The most common polymerization method for manufacturing polypropylene is the Ziegler-Natta system introduced in the early 1950s'. It is most commonly processed by injection moulding. In automotive manufacturing, injection moulded parts are used for dome lights, kick panels, and car battery cases. Polypropylene compounded with fillers can be found in mounts and engine covers. When polypropylene is modified in its elastomeric behaviour (e.g. by blending with other polymers), it can be used in the automotive sector for bumpers, fascia panels, and radiator grills.

The melting temperature of polypropylene (T_m) is at about 176 °C (100 % isotactic) and the glass transition temperature (T_g) at -20 °C [107]. The density of semi-crystalline polypropylene is between $0.9 – 0.91$ g/cm^3 (homopolymer). The elastic modulus for polypropylene is between $1.05 – 2.10$ GPa (homopolymer). Polypropylene has good mechanical properties, low density, durability, resistance to X-rays, low water permeability (because of its non-polar structure), relatively good impact resistance (when modified with copolymers) and good temperature resistance up to 135 °C. It also has good properties in terms of electrical insulation.

Different behaviour can be found for each of the three stereoisomers created by changing the position of the CH_3 group during polymerization: isotactic, atactic, and syndiotactic.

Isotactic and syndiotactic polypropylene are higher in rigidity because they can pack in a regular crystalline array. Both materials are crystalline; however, syndiotactic polypropylene has a lower T_m than the isotactic polymer. Due to the presence of the methyl groups on the polymer chain, isotactic polypropylene crystallizes in a helical form. More than 90 % of the commercially available polypropylene is in the isotactic form. The amount of crystalline structure in atactic polypropylene is only 5 to 10 %. Its irregular structure results in a higher amorphous phase and produces a soft flexible material.

The crystallization of a polymer is the growth of spherulites when cooled below its melting point T_m. It starts at different points (nucleus) from where the spherulite expands and is complete when the spherulites fill completely the space.

During crystallization, the specific volume of a polymer decreases rapidly which is due to the increase in attractive forces between neighbouring molecules resulting in organization of the polymer molecules into a tight, orderly structure [107]. Crystallization in polymers is time dependant. Polymers that do not crystallize are called amorphous. The crystallization of a polymer at different times is shown in Figure 4-9.

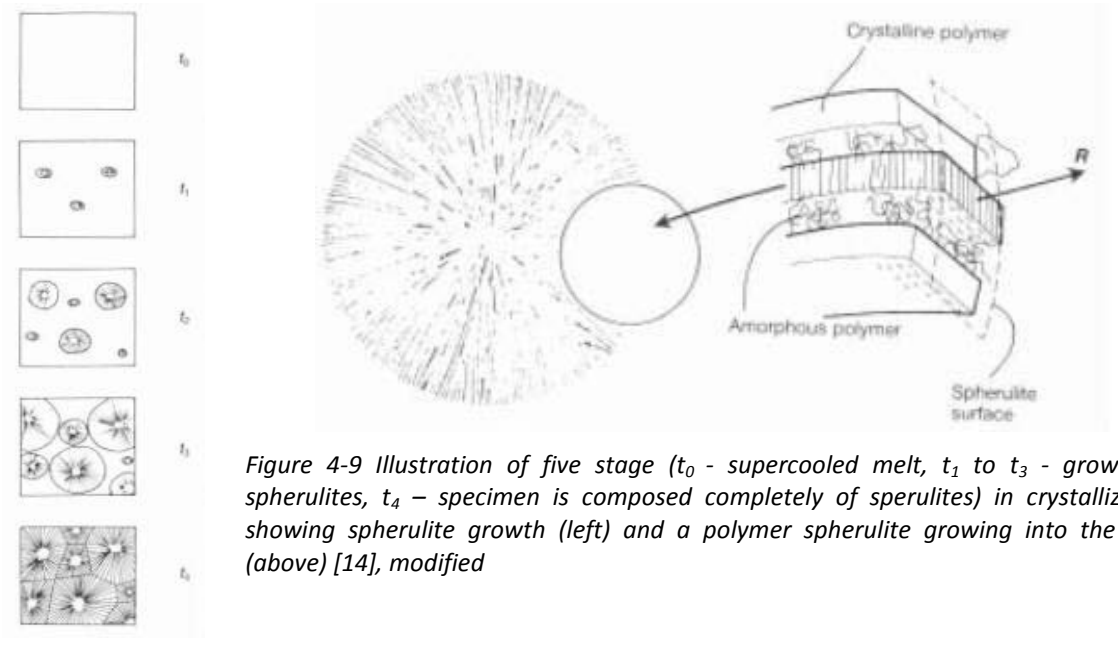

Figure 4-9 Illustration of five stage (t_0 - supercooled melt, t_1 to t_3 - growth of spherulites, t_4 – specimen is composed completely of sperulites) in crystallization showing spherulite growth (left) and a polymer spherulite growing into the melt (above) [14], modified

The morphology of a polymer depends on its tacticity and the crystallization conditions (temperature, pressure, and cooling rate) which in turn will affect its physical properties. When a nucleating agent is present, smaller crystals will be formed resulting in different properties compared to polypropylene crystallization without nucleating agent [24].

Generally, an amorphous polypropylene will be more transparent and will have greater toughness and ductility while semi-crystalline polypropylene will have high stiffness, will be chemically more resistant and can withstand higher temperatures.

The (theoretical) melting point of (perfect) isotactic polypropylene is at 171 °C. Commercially available isotactic polypropylene still contains atactic segments and thus has non-crystalline regions that result in melting points between 160 and 166 °C.

Differential scanning calorimetry (DSC) can be used for the analysis of crystallinity and glass transition of crystalline materials. When DSC is performed in the dynamic heating mode, the area under the peak represents the energy for the crystallization of the polymer fraction which gives a measure of the degree of crystallization of the polymer fraction. The total crystallinity represents the ratio between the crystalline and the amorphous region of the polymer. A typical Differential Scanning Calorimetry (DSC) diagram of the polypropylene used in this work is shown in Figure 4-10.

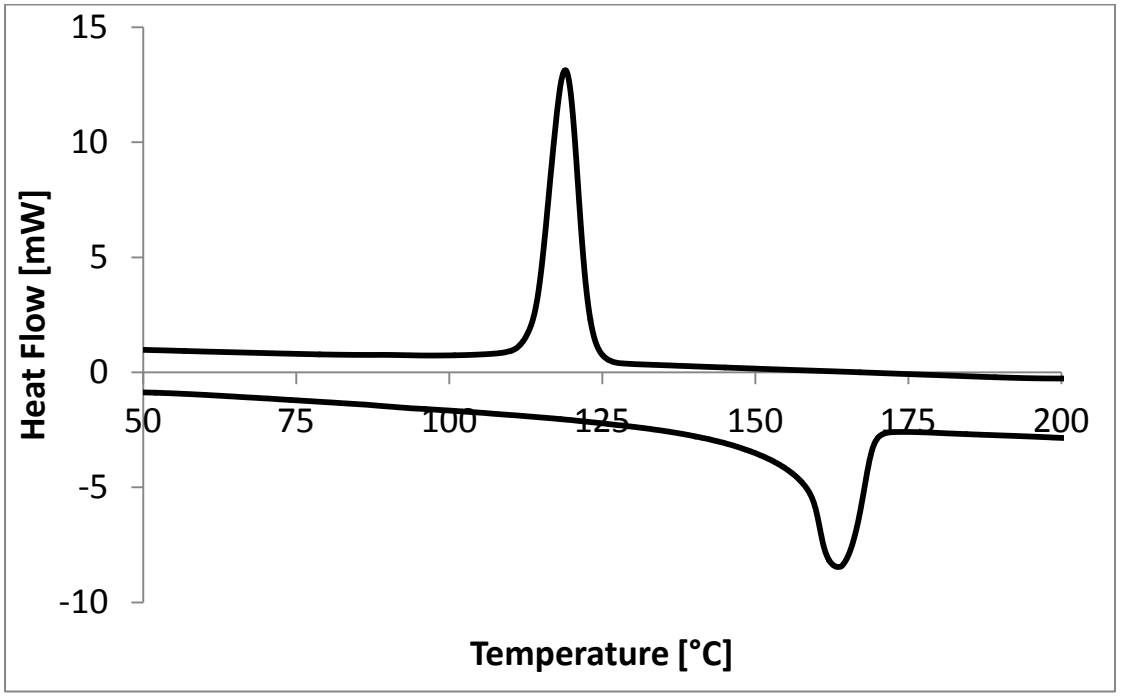

Figure 4-10 DSC graph of polypropylene blend used for composites prepared in this work.

4.8 Characterization of Composite Materials

4.8.1 Microanalysis by Field Emission Scanning Electron Microscopy (FESEM)

Field emission scanning electron microscopy (FESEM) provides information on the morphological characteristics of a material surface while Energy Dispersive X-ray

Spectroscopy (EDX or EDS) can identify and quantify the composition of materials based on the chemical elements. EDX is a microanalysis technique that requires very small amount of material (~1 μm^3).

FESEM combined with EDX provides very high magnification images of the specimen and information of the structure and elements present in the sample. In the context of composite materials, FESEM will provides information on the filler shape and size and the interface behaviour and localize the boundaries between regions of different chemical composition (measured by type of atoms).

4.8.2 Mechanical Properties

The mechanical properties of a material are the result of the polymer structure and therefore will be affected by changes in morphology. Mechanical properties of a polymer strongly depend on its crystallinity [24] and molecular weight; and thus can be engineered depending on its final application. One factor affecting polymer crystallinity is the molecular weight of the polymer but processing conditions have also a significant impact as explained in the injection moulding section. Increase in stiffness, yield stress, and flexural strength can be achieved by higher degree of crystallinity. However, the drawback of higher crystallinity is a decrease in toughness and impact strength. As an example, the flexural strength with 1 % offset lays for ultra-high crystalline polypropylene between 2067 to 2412 MPa but for polypropylene of lower crystallinity lays between 1378 and 1654 MPa. Two commercially available polypropylene materials and their mechanical properties are presented in Table 4-11.

Table 4-11 Mechanical properties for two different polypropylene homopolymers [24].

Material family		**PP homopolymer**	**PP homopolymer, flame retardant**
Supplier		BASF	Vestolen GmbH
Material Trade name		Novolen 1100L	Vestolen P 7006 S
Test Notes	**[Unit]**		
Tensile modulus (secant, 1 mm/min)	MPa	1500	1500
notched Izod impact strength (23 °C)	kJ/m^2	3.5	4

4.8.2.1 Flexural Test

The flexural properties (ability of a material to bend without visco-elastic deformation) can be measured by using the three-point-bending method as described in the ASTM standard method D 790 - 07 [108]. During this test, the specimen with dimensions 30 x 12 x 3 mm is

conditioned at constant humidity and temperature prior to testing. When a force is applied to a specimen, a typical force - displacement curve is obtained and analyzed with regard to the mechanical performance of the material.

Figure 4-11 presents different stress/strain diagrams of polymers with their respective mechanical properties. A more detailed discussion can be found elsewhere [20].

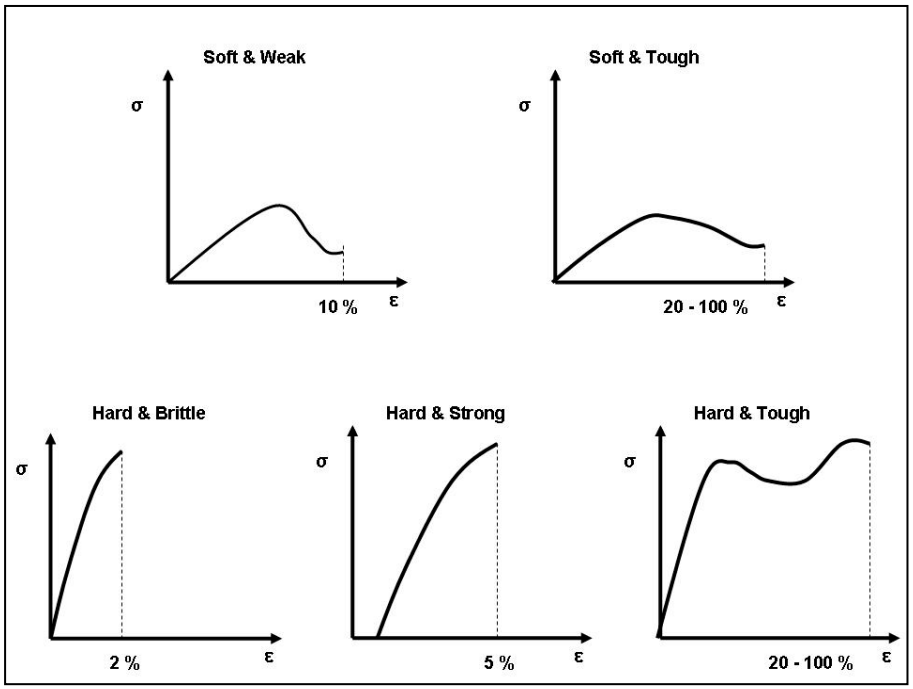

Figure 4-11 Classification of engineering stress-strain curves for polymers. σ = applied stress, ε = resulting strain (Progelhof, Throne 1993), modified.

4.8.2.2 Toughness (Impact)

The toughness of a material can be obtained with the impact test giving a measure of the impact resistance of a specimen with brittle properties. The ASTM method D 256 – 06a is commonly selected to determine the Izod impact strength of a plastic [109].

For the Izod impact test, the specimens have to be notched. After notching, the specimen will be placed in the test apparatus and fixed in such a position (180 ° in the clamping device) that the pendulum hits the specimen at a 90° angle. Constant temperature and moisture conditions are required during the test. This test is considered as a one-point test which means that even though care is taken during the preparation of the specimen; each test produces a single value for the response of the material to short-term loading.

4.9 Composite Materials and Filler-Matrix Interactions

When describing the region in a composite material where the matrix and the filler meet, two terms are used: interface and interphase. The interface illustrates the two-dimensional region between a filler and the matrix with properties intermediate between both [90]. The interphase describes an area about five µm thick with slightly different properties compared to the bulk polymer and the interface. To identify and investigate the interphase, AFM and nano-indentation devices can provide information [90].

Figure 4-12 presents the major types of mechanisms for filler-matrix bonding: (a) Micromechanical anchor (b) Permanent or induced dipole-interaction (c) Chemical bonding (d) Chain-linking (e) Trans-crystallinity [15]. Each mechanism can be enhanced by treatments of the filler which for example can increase the roughness and porosity of the filler surface or its chemistry. Figure 4-13 presents a schematic representation of a trans-crystalline interphase between a filler and a polymer matrix.

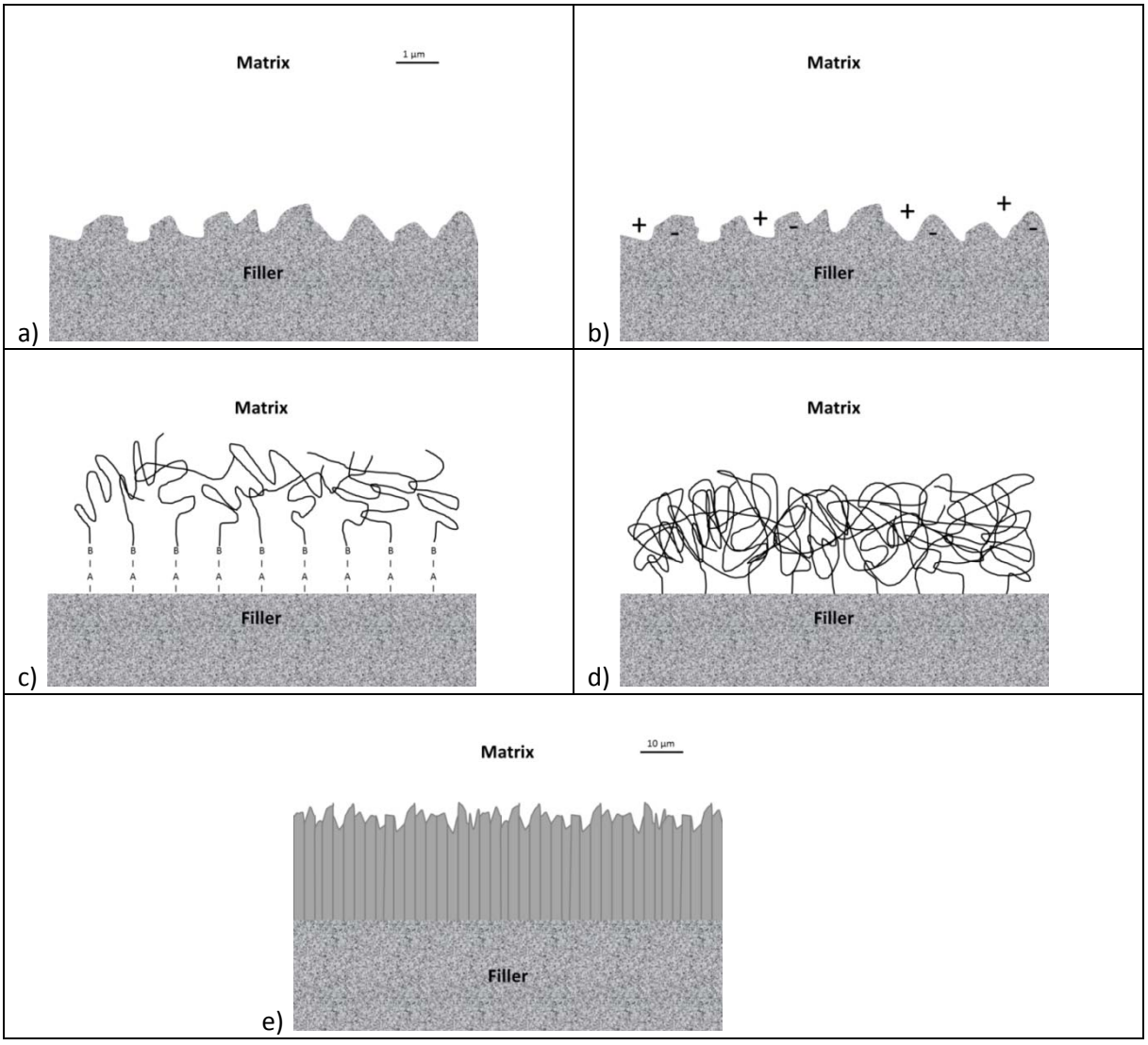

Figure 4-12 (a) Micromechanical anchor (b) Permanent or induced dipole-interaction (c) Chemical bonding (d) Chain-linking (e) Trans-crystallinity [15], adapted

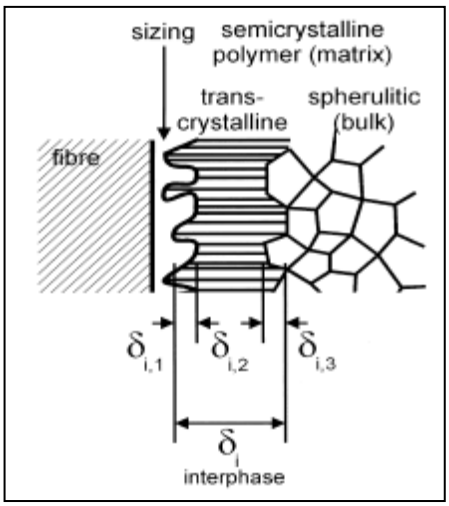

Figure 4-13 Trans-crystalline interphase in fiber/polymer composites (δ_i = thickness of interphase; $\delta_{i,1}$ = thickness of interface between fibre and transcrystalline PP, $\delta_{i,2}$ = thickness of homogeneous part of trans-crystalline layer without boundaries, $\delta_{i,3}$ = thickness of interface between trans-crystalline and spherulitic morphology) [16]

Table 4-12 shows an overview of deformation and failure mechanisms observed during SEM of composites from polypropylene and corn cob studied by Renner and colleagues [32].

Table 4-12 Deformation and failure mechanisms of PP composites [32]

Polymer	Deformation mechanism					
	Poor adhesion			Good adhesion		
	Debonding	Yielding	Fracture*	Debonding	Yielding	Fracture*
Homo-PP	+	-	-	-	-	+
Heterophase PP	+	-	-	(+)	+	-
Random PP	+	-	-	(+)	+	-

(+) possible mechanism
*Fracture of the corn cob particles

In order to obtain a composite with the desired properties for a given application, parameters of the filler such as particle size (fiber length, aspect ratio), volume fraction and orientation need to be controlled. The impregnation of the filler material by the matrix can be a complex process and needs to be well understood so that it can be controlled. Good impregnation, wetting and interaction at the interface are critical. Also, the composition of composites should be optimized in order to create a material at the lowest cost and with the best performance. The orientation of the filler can increase the tensile strain and modulus but can decrease the impact strength relative to the initial value.

During the impregnation of the filler by the polymer matrix, a good bonding will be achieved by controlling the flow of the polymer between the particles (or fibers). In this

section, fiber-like fillers will be predominantly discussed because their surface impregnation or wetting by polymers is a well-studied area in polymer composites. Therefore, the effect of aspect ratio and the particle constitute unique features that will be discussed separately. In the wetting processing of thermoset composites, the molten polymer (liquid-like resin) will be pushed through a dry fiber bed, by a pressure applied externally, allowing the liquid polymer to penetrate within the fibers. The mechanism of the surface wetting of the fibers by the molten polymer matrix is influenced by processing variables. The most important variables are polymer viscosity, the fiber content and degree of agglomeration, the fiber shape (aspect ratio, size, and diameter), the amount of shear, and the surface energy of the phases [34].

To improve the mechanical behaviour of polymer composites, interfacial bond strength is the major factor that can be influenced by chemical and/or mechanical treatments.

Shear stress is applied parallel or tangential to the surface of a material. For composites, shear stress is created in the matrix due to the difference in stress and thus difference in elongation of the fibers.

A material with high impact resistance (toughness) requires a combination of high tensile strength and high elongation at break (ductility). Impact strength depends on the characteristics of the matrix and the interface. These characteristics may be quite different from that of the isotropic matrix and may decrease or increase with dispersed phase volume fraction. In the case of a ductile polymer matrix, the presence of dispersed phase will increase the tensile strength but may decrease the ductility, thus decreasing its toughness. In the case of a brittle polymer matrix, fillers will increase the strength and act as crack stoppers by increasing the amount of energy absorbed by crack deflection. The amount of energy that can be absorbed depends on the interfacial dispersed phase-matrix bond. Therefore, if the dispersed phase-matrix bonding is weak, the stress concentration at the tip of a crack causes the dispersed phase to detach from the matrix but if the dispersed phase-matrix bonding is strong, then the dispersed phase will break before its detachment from the matrix, causing brittle failure perpendicular to the stress direction, similar to isotropic materials. Composites need to be engineered such that bond strength balances the opposite requirements for structural stiffness and strength and fracture resistance: bonding between the matrix and the dispersed phase must be neither too strong nor too weak [17, 34].

A high interfacial bond in composites is not necessarily an advantage because the stress can be localized at the tip of an advancing crack and can cause the dispersed phase to detach from the matrix [17]. As a result, the dispersed phase will act as crack arrestors and deflectors; consequently the composite can behave as a brittle material. On the other hand,

dispersed phase weakly bonded to the matrix will produce composites with higher fracture toughness. Figure 4-14 shows different crack propagation mechanisms that can occur in composite materials. There are mainly three different mechanisms representing the propagation of cracks in a composite material: a) through the matrix, b) through the dispersed phase, and c) through the interface between the dispersed phase and the matrix. Depending on the properties of matrix, dispersed phase and the interface between both, the weakest part defines the propagation of a crack.

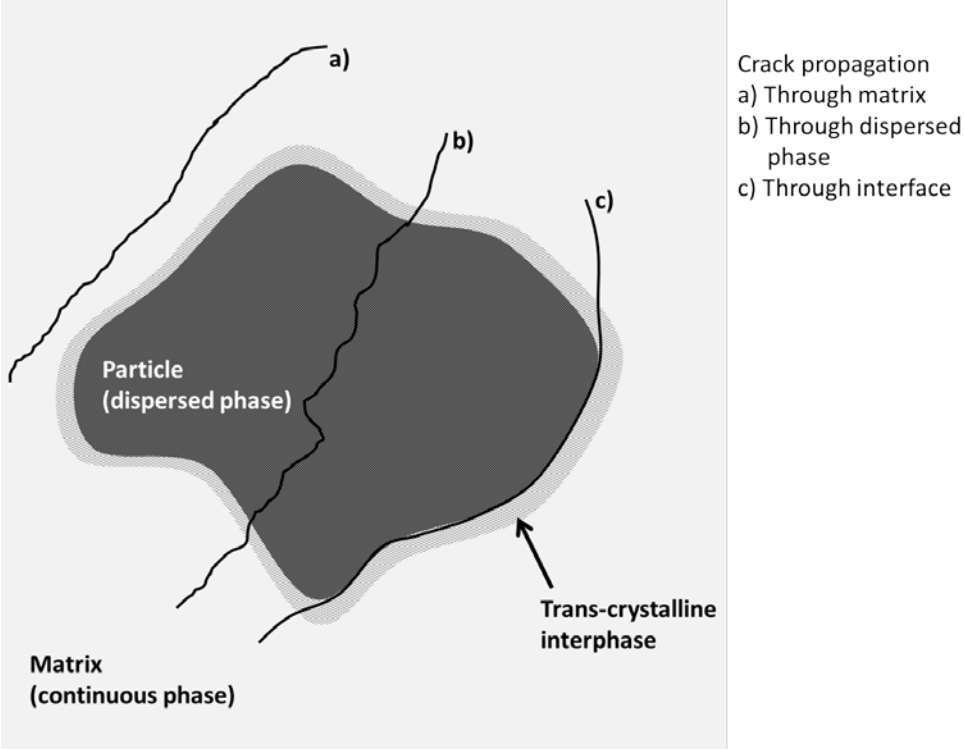

Figure 4-14 Schematic of different crack propagation theories: a) through matrix, b) through dispersed phase, c) through interface

When engineering materials, usually the toughness and strength of a material have to be a trade-off because of their relationship to each other. The conflict between toughness and strength properties was discussed by Ritchie and shows the contradiction of improving material's impact and flexural properties at the same time [17]. Often, one property can be improved by sacrificing the other because they are "generally mutually exclusive" (Figure 4-15) [17].

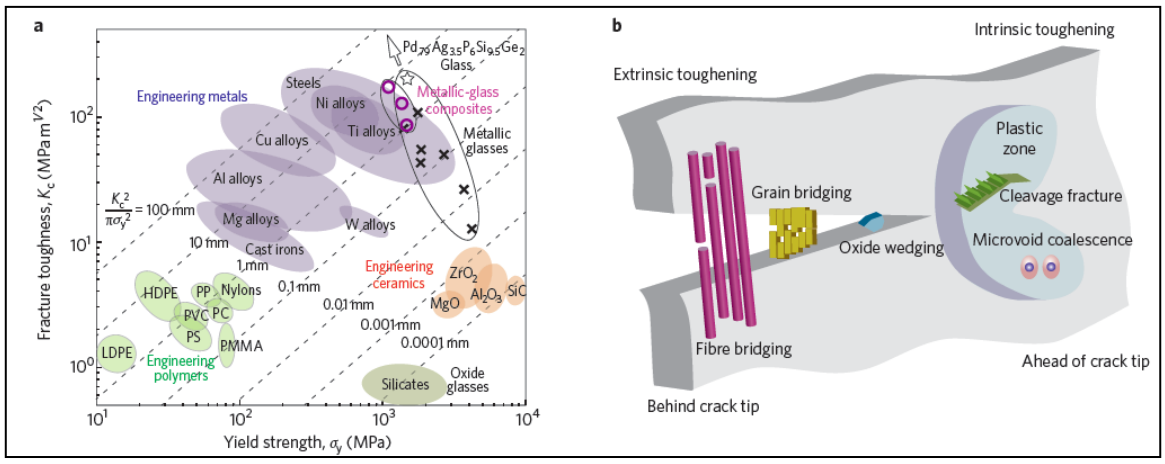

Figure 4-15 Relationship of toughness and strength for different engineering materials [17]

However, there are exceptional materials that possess the ability of high toughness and strength at the same time. The most advanced materials with this ability are found in nature and the reason for their high toughness and strength is their "hierarchical structure" [17]. Their structural assembly starts at a nano-scale and moves to the micro and macro-scale. Examples for this structural multi-scale architecture given by Ritchie are mollusc shells and bones but also wood possesses this hierarchical assembly [110]. A schematic drawing of the different levels of structure of a bone with the associated crack mechanisms is given in Figure 4-16. The relationship of Young's modulus and density of chitin fibers in a grasshopper as well as the relationship of strength and hierarchical order of a honeycomb were discussed by Degischer and Lakes [110, 111]. The complete mechanisms for these type of materials is still not fully understood but is believed to be related to their structural hierarchy levels similar to fractal model structures [110].

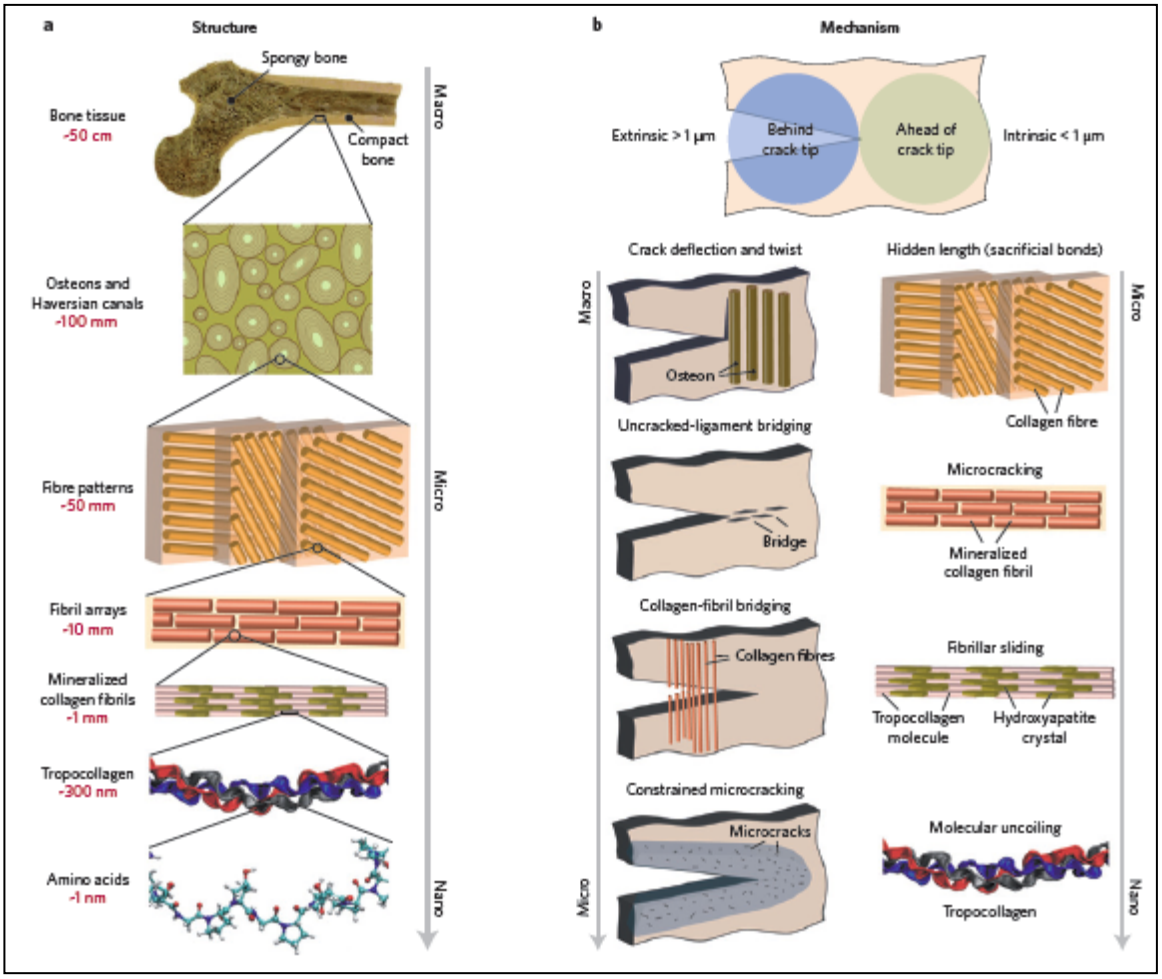

Figure 4-16 Bone composition with its "hierarchical structure" and related crack mechanisms [17]

These examples illustrate the opposing requirements for interfacial bond strength and achieve high tensile strength to the requirements for toughness. Optimal bonding conditions for both tensile strength and toughness are achieved when the bond strength causes fracture to follow a path in the polymer slightly above the dispersed phase surface. Thus, it can be said that an optimal bonded interface absorbs energy yet maintains good interfacial stress transfer (contributing to improved modulus) [17].

The dispersed phase-matrix bonding can be influenced by chemical treatment of the dispersed phase surface (covalent, ionic bonds or weak bonds like Lewis acid-base interactions and hydrogen bonding) or physically (surface etching followed by matrix shrinkage onto fibers after cure). By changing one or more of these properties, increased interfacial bonding between the matrix and the dispersed phase can be obtained, thus improving the balance among tensile strength, modulus, and toughness.

Arencón and Velasco conclude in their review paper that “fracture toughness is one of the mechanical characteristics that have more difficulty in its determination and analysis, as there are numerous factors involved: temperature, strain rate, specimen dimensions and testing geometry, mainly.“ [112]. The combination of the type of polymer (e.g. homopolymer or copolymers) and the dispersed phase with their different properties (e.g. content, size, shape, nature and surface treatment) creates a high complexity when investigating fracture mechanisms [112].

4.10 Composite Modifications

In order to improve bonding and mechanical properties, modifications of the dispersed phase and the matrix can be performed. Figure 4-17 shows a scheme of a matrix and dispersed phase and three avenues that can be explored in order to improve the dispersed phase-matrix bonding: dispersed phase treatment, matrix treatment, and addition of coupling agents or coatings. There exists a wide range of physical and chemical methods for the modification of the dispersed phase and/or the polymer. In the following section, selected methods relevant to the project will be described in more detail for a filler as dispersed phase.

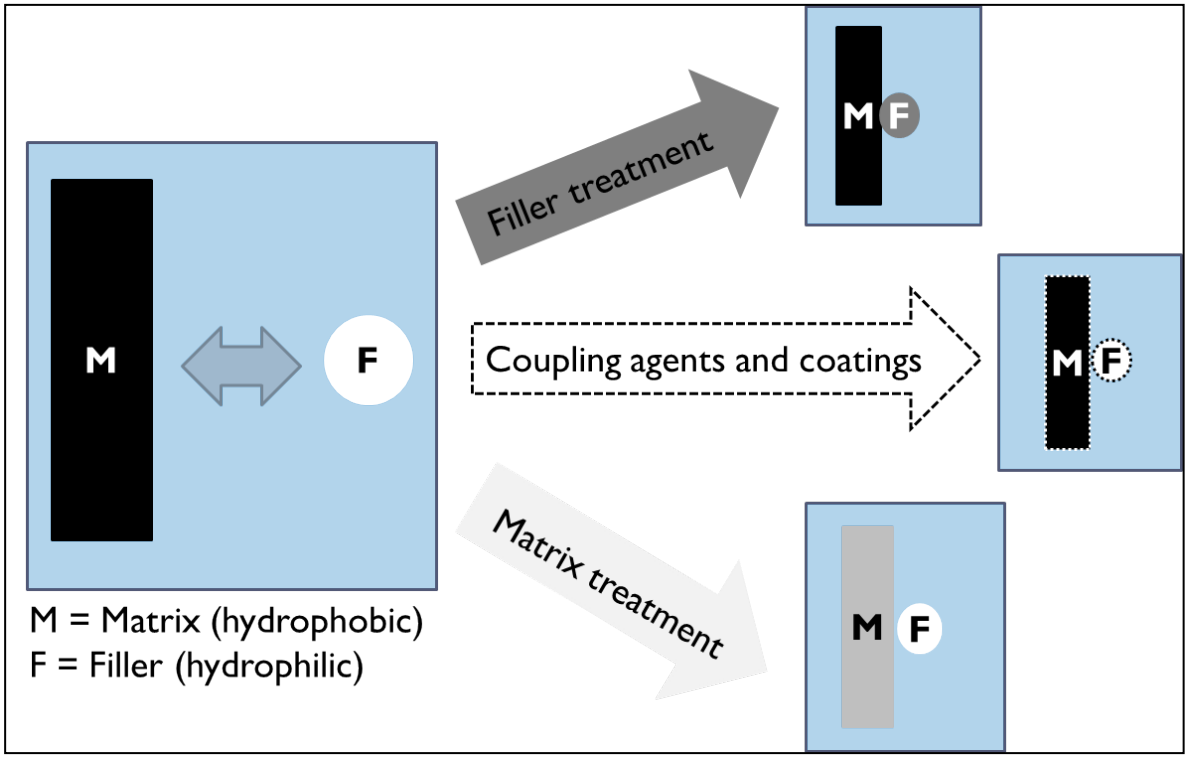

Figure 4-17 Schematic representation of possible avenues to improve filler-matrix interaction

4.10.1 Polymer Matrix Modification

Different physical methods are known to modify polymers and improve their compatibility with filler materials. Examples include plasma treatment (air, oxygen, or non-thermal), Corona discharge, and dielectric discharge [77]. Chemical treatments are also able to modify the chemical structure of polymers and combinations of chemical and physical methods can be performed. In Mallakpour's work, potassium permanganate was selected as an oxidizing agent for solid PP in combination with microwave irradiation [113]. FTIR studies showed the increase of carbonyl groups (1590–1810 cm^{-1} and 1590–1497 cm^{-1}). Therefore it was concluded that the surface of PP was oxidized.

Since the focus of this thesis was the modification of the filler component, no further details about polymer treatments will be given.

4.10.2 Coupling Agents

Coupling agents are adhesion promoters that increase the compatibility between filler and polymer (Figure 4-18). Coupling agents are used to increase the mechanical properties of composites by improving the interfacial bonding between the filler and the polymer matrix.

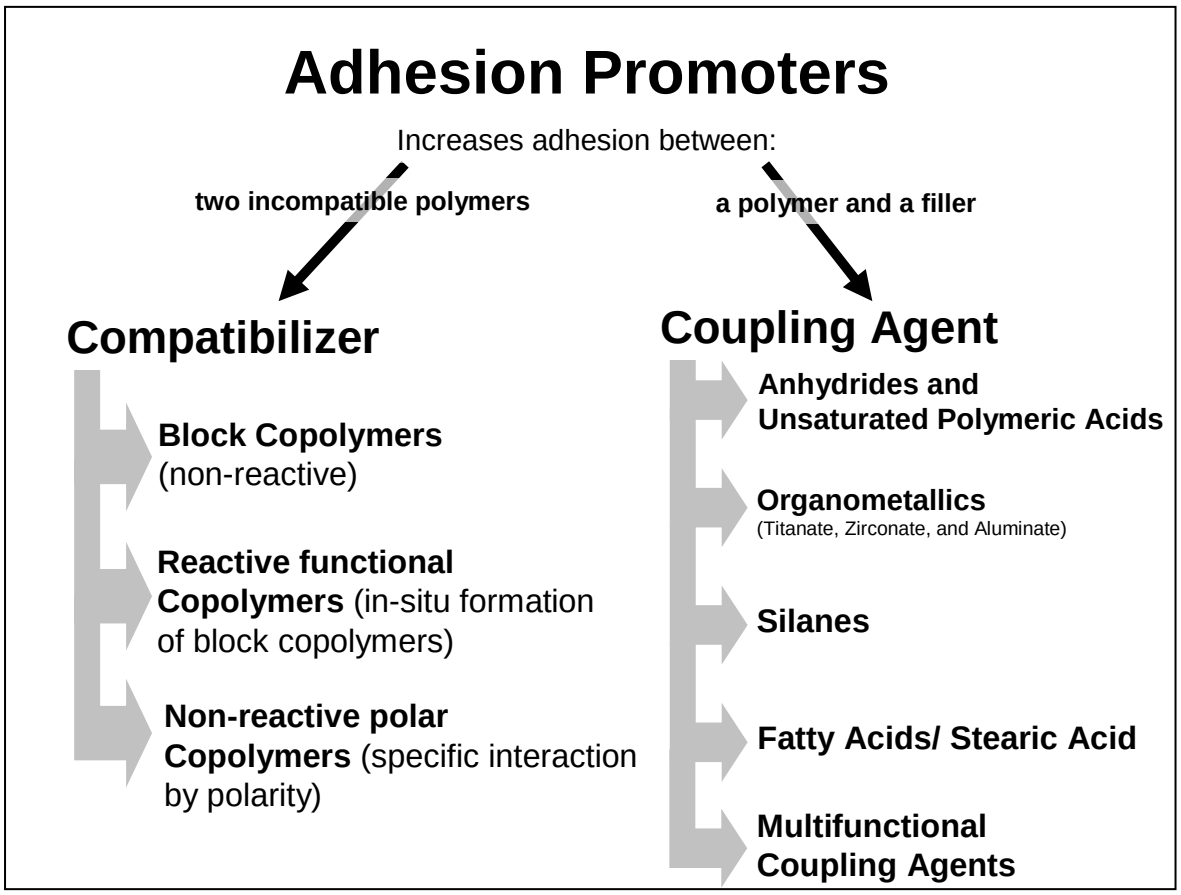

Figure 4-18 Adhesion promoters: Compatibilizer and Coupling Agents [18].

Agricultural fillers, because of their hydrophilic properties, have poor compatibility with typical hydrophobic polymer matrices such as polypropylene. To improve the compatibility, coupling agents can be used. Their role is to interact with both the matrix and the filler, thus establishing a strong chemical interface. Numerous types of coupling agents are commercially available. Their effect depends on the surface reactivity of the filler. This is an aspect that is poorly understood for agricultural fillers because most of these coupling agents were developed for mineral fillers (calcium carbonate, talc) or inorganic fibers (glass fiber). Furthermore, most of the plant natural fillers or fibers (like wood fiber, hemp, flax) developed for applications with hydrophobic polypropylene matrix, have surfaces with high hydroxyl content due to their ligno-cellulosic nature [114].

For fillers with high protein content, such as soy flour, the predominant functional groups on the material surface are hydroxyl-, amino- and carboxyl- groups. Most of the coupling mechanisms described in the literature for natural fillers are focusing on the hydroxyl groups of lignin and cellulose. When only low amounts of cellulose are present such as

fillers with high protein content, other functional groups and thus other coupling agents should be considered.

The most common treatments to improve interaction of mineral fillers with the polymer matrix surface are stearates and functionalized polymers such as maleic anhydride grafted polymers [13, 83, 115]. Silane coupling agents added to polypropylene and polyethylene are not as functional because of the non-polarity of the polymer matrices [41, 90].

Water absorption plays a very important role when the final application of the composite is a high moisture environment such as automotive parts directly exposed to precipitation, water on the road or humidity. Biological materials have the characteristic to absorb moisture from the surrounding environment because of their hydrophilic nature (hydroxyl groups) [70]. The major plant components cellulose, hemicellulose, and lignin are quite different in chemical composition and as a result possess different water uptake. The amorphous regions of cellulose have a higher water uptake than the crystalline regions because their hydroxyl groups are more easily accessible [116]. Lignin is considered as protection against hydrothermal degradation because of its hydrophobic structure and generally displays a lower water uptake then amorphous cellulose [117]. Rana et al. showed that compatibilizers could decrease the water absorption which was attributed to the ester linkage of the hydrophilic –OH groups with acid anhydrides [118]. According to Ton-That and Jungnickel, the diffusion of water in trans-crystalline layers on polypropylene is selectively passing through the amorphous phase of semi-crystalline materials [119]. Water absorption is a property often affected by the addition of coupling agent. According to the type and amount of the coupling agent, the surface properties of the filler will change and is expected to enhance interfacial interactions. The improved interactions should also reduce the content of hydrophilic groups which are responsible for the water uptake.

The following section will explain briefly the different classes of coupling agents and their binding mechanisms. The focus will be on the coupling agents used in combination with agricultural fillers and present the current knowledge for their use with biocomposites.

4.10.2.1 Anhydrides and Unsaturated Polymeric Acids

It is often reported that natural fibers based on cellulose have hydrophilic surface properties and therefore inherent incompatibilities with hydrophobic thermoplastics, such as polyolefins. This leads usually to poor interfacial adhesion when dispersing cellulose based materials in polyethylene or polypropylene [120]. Maleic anhydride grafted polyolefin is one of the most efficient coupling agents for composites with cellulose based materials (fiber or filler) and polyolefin matrixes [120]. Composites produced by melt-mixing with

maleic anhydride grafted polypropylene (MAPP) as compatibilizer resulted in improved mechanical properties. The mechanism is attributed to stronger interfacial adhesion caused by esterification between anhydride groups of MAPP and hydroxyl groups of cellulose [120] as shown in Figure 4-19.

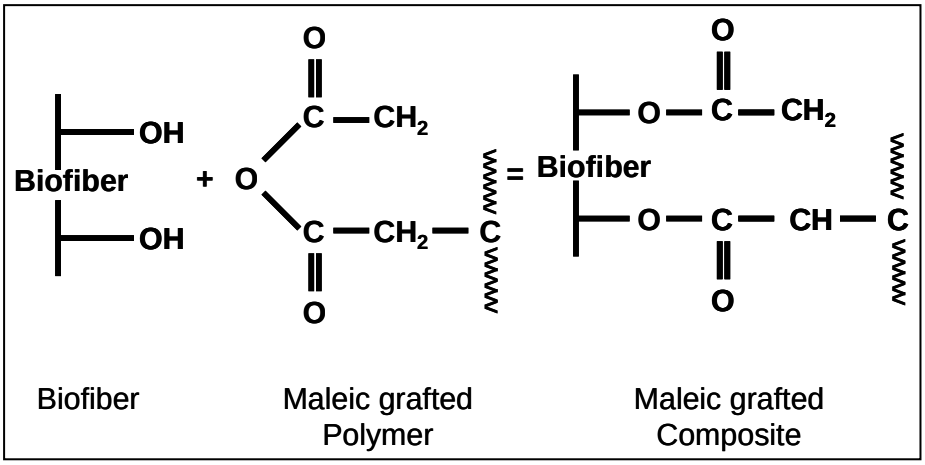

Figure 4-19 Chemical structure of maleic anhydride grafted fiber and biopolymer [19] adapted.

The preparation of biocomposites using maleic anhydride can be executed in two ways. The first method is a pre-treatment of the natural fibers with maleated polymer; then the subsequent processing steps are identical to those with untreated fibers. The second method is to combine the fibers, maleic anhydride and polymer during the extrusion with the peroxide initiator in one-step processing to get the compatibilized biocomposite product for further compression moulding/injection moulding [19].

A visual comparison from previous studies [20] is presented in Figure 4-20 and Figure 4-21 where a soy-polypropylene biocomposite material with similar composition was used except for the presence of a maleic anhydride coupling agent (Figure 4-21).

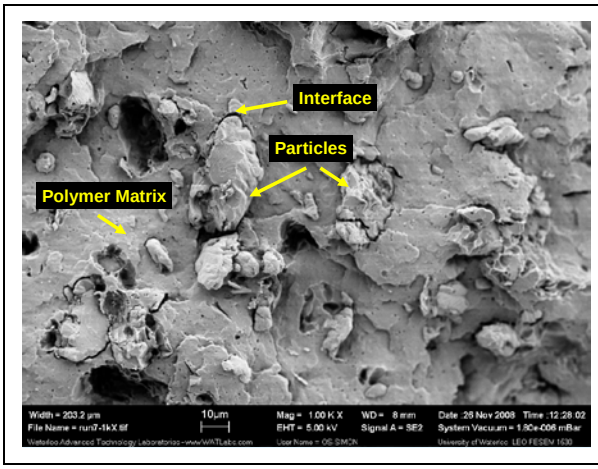

Figure 4-20 Biocomposite from 30 % soy flour and 70 % polypropylene with no coupling agent [20].

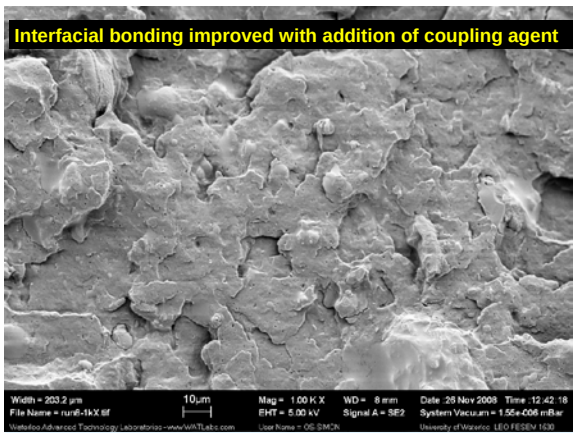

Figure 4-21 Biocomposite from 30 % soy flour and 67 % polypropylene with 3 % coupling agent (maleic anhydride polypropylene) [20].

Five different types of MAPP were investigated in biocomposites with wood flour and biocomposites with rice husk flour by Kim and colleagues [73]. All types of MAPP could increase the tensile, impact, and flexural strengths as well as crystallinity, and thermal stability. MAPP with very low and very high molecular weight showed lower mechanical properties which were attributed to insufficient entanglement with the PP matrix for low molecular weight MAPP and did not provide satisfactory interaction between the coupling agent and the filler. The interactions of the high molecular weight MAPP with the particles led probably to lower amounts of coupling agent remaining at the interface as well as distances too close to the hydrophilic surface resulting in insufficient interactions with the polypropylene matrix. A concentration of around 3 % MAPP gave the best results [73].

4.10.2.2 Silanes

Silanes are the most well-known coupling agents. Their general structure is X-$(CH_2)_n$-Si $(OR)_3$ where X represents the organofunctional group (e.g. amino, vinyl, epoxy, methacryl) which will bind to the resin, and Si $(OR)_3$ is the component that will react with the inorganic filler (e.g. glass fiber, metal hydroxides, silica, silicates). The component (OR) is often a methoxy or ethoxy group which binds via condensation or hydrogen bonds to the surface of the filler [121]. The general binding principle is presented in Figure 4-22. The efficiency of silane coupling is high for reactive polymers such as thermosets, rubbers, and polar thermoplastics. However, unreactive polymers such as polyolefins (PP, PE) do not bind to silanes. Nevertheless, silanes are used with polyolefins to improve the dispersion of the filler and to decrease the water absorption. Silanes have shown to decrease the moisture sensitivity of biocomposites [46].

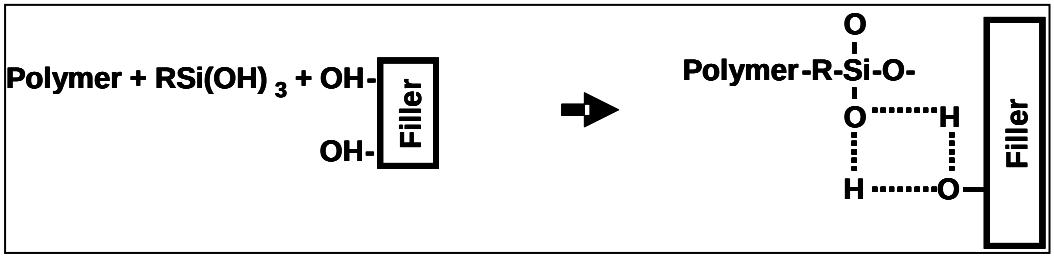

Figure 4-22 Coupling reaction of silane with natural filler.

Biocomposites prepared with silane coupling agents (PROSIL 2020, PROSIL 9234 [$C_{14}H_{32}O_3Si$]), rice husk ash (high in silica) and polypropylene showed the highest improvement in tensile strength for PROSIL 2020 and the highest impact improvement for PROSIL 9234 [122].

The aminofunctional silane coupling agent γ-aminopropyltriethoxysilane and its analogues were studied in aqueous solution and in films by Ishida et al. [123]. In their work, no mechanical tests on composites were performed but this type of coupling agent could be an interesting additive for biocomposites with amino group (protein) rich filler. Bledzki reported on studies by Bisanda et al. and Gassan et al. with γ-aminopropyltriethoxysilane in natural fiber – epoxy composites that resulted in a "remarkable" reduction of the water absorption and a significant increase in compression strength. The flexural strength, however, was not affected by the coupling agent. Nevertheless, a review paper by Bledzki reports on work by Gassan et al. that showed an increase in flexural strength and flexural modulus with the addition of γ-aminopropyltriethoxysilane as coupling agent in different concentrations and modified conditions for the treatment [46].

4.10.2.3 Multifunctional Coupling Agents

Most coupling agents are bifunctional molecules as described in 4.10.2. The application of such molecules is restricted to reactions with two functional groups and requires a very homogeneous polymer or composite containing mainly these two functional groups (one on matrix and one on filler). This means e.g. for polyesters, such as nylon, the carboxylic groups would react with bis-2-oxazolines and the hydroxyl and amino groups would react preferably with bis-2-oxazinones or bislactamates [124].

The synthesis of multifunctional coupling agents with different types of reactive groups was studied intensively by a research group of the Leibniz Institute of Polymer Research. Böhme, Jakesch, and Komber created different types of molecules that have multifunctional binding sites with different reactive groups [124-126]. According to this group, it is possible to create "taylor-made polymer modificators and coupling agents" [127].

A summary of typical examples for “multifunctional polymer modifiers and coupling agents with high reactivity and selectivity for amino-, carboxy-, and hydroxy groups” [127] published by Böhme and Jakisch indicates that coupling agents containing 2-oxazoline-, 2-oxazinone-, and caprolactamate groups are potential candidates. These groups “can be used in the compatibilization of polymer blends, the synthesis of segmented block copolymers, the functionalization of polymers (side and terminal groups), and the covalent bonding of polymer on surfaces” [127].

4.10.3 Filler Modifications

This section will give an overview of modifications that can alter the shape or the surface chemistry of fillers and fibers resulting in enhanced interfacial interactions. The focus will be on modifications for agricultural filler.

4.10.3.1 Particle Size

The particle size of the filler plays an important role in the balance of mechanical properties but also affects the dispersion of the filler in the matrix [75]. Brechet et al. published in 2001 a study on the behaviour of nanoparticles (cellulose) in a polymer matrix with focus on the effect of size and shape, the volume fraction, as well as the effect of processing on filler-filler and matrix-filler interactions. Mathematical models were also used by those authors to describe the observed behaviour in the nanocomposites [128]. Their study indicates that the size and shape of the filler material has a significant impact. The addition of nanoparticles gives an extremely high interfacial area and very short distance between the surfaces of the filler particles.

Another important parameter is the particle shape because many particles, especially the ones from natural sources, are irregular shaped which can introduce a complexity to processes and mechanisms [75]. Therefore, reports on natural fillers can vary quite significantly not only according to size (or size range) but also according to shape, porosity, heterogeneity and others [112].

The effects of particle size on various mechanical properties of different composites are presented in Figure 4-23 and Figure 4-25. Figure 4-23 and Figure 4-24 clearly show the effect of the particle size on the material properties whereas Figure 4-25 shows no change in properties with increase in particle size.

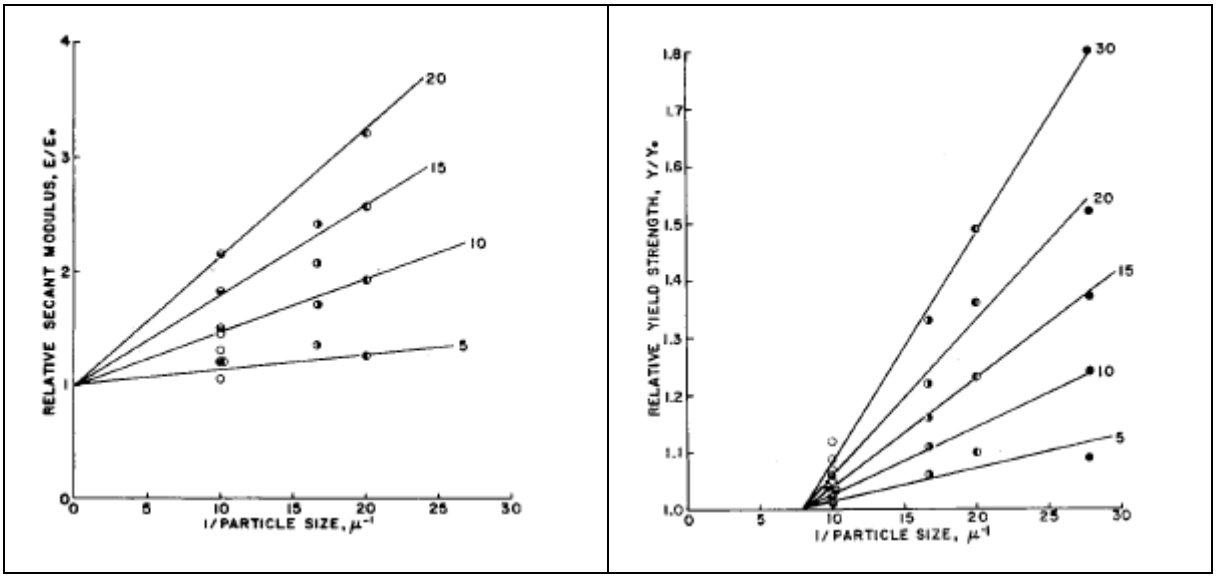

Figure 4-23 Effect of particle size on relative secant modulus and relative yield strength of polyethylene filled with different particles [21]

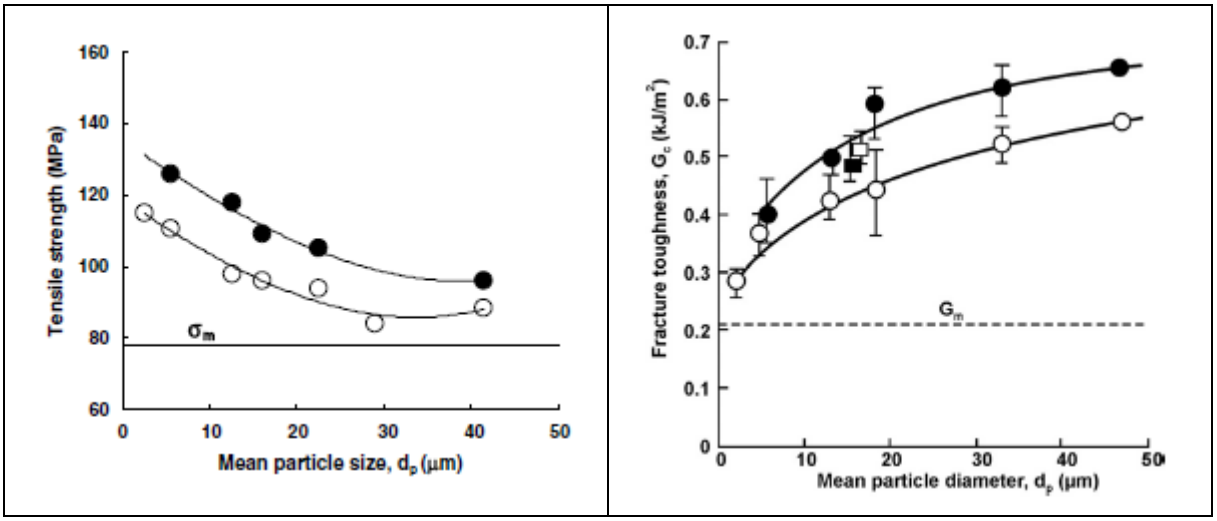

Figure 4-24 Effect of particle size on tensile strength and fracture toughness of epoxy composites filled with silica particles [22]

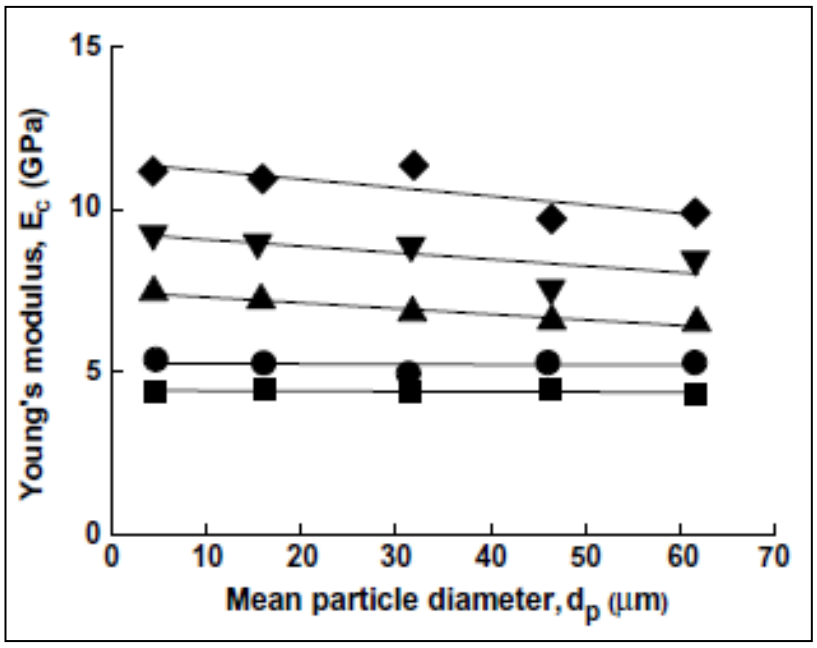

Figure 4-25 Effect of particle size on Young's modulus in glass bead filled epoxy composites [22]

4.10.3.2 Chemical Treatments

Chemical treatments of fillers are conducted predominantly to improve the filler-matrix interactions and obtain a reinforcing effect [67]. There are two major approaches when modifying filler surfaces: increasing the number of active sites or changing the chemical surface by reactions on existing sites [67]. This section will give some examples of possible chemical treatments with a brief explanation of their principles.

4.10.3.2.1 Potassium Permanganate ($KMnO_4$)

Potassium permanganate ($KMnO_4$) oxidizes aldehydes to carboxylic acids [129]. The addition of permanganate groups (MnO^-_4) to cellulose leads to the development of radicals on the cellulose which can initiate the graft polymerization [130]. A review paper on chemical treatments of natural fibers reports that the treatment with potassium permanganate in acetone can reduce the hydrophilicity of the fiber surface which results in reduced water absorption [130]. Often permanganate treatments are conducted with potassium permanganate ($KMnO_4$) solution in different concentrations with soaking duration from 1 to 3 min after alkaline pre-treatment [113, 130-132]. Paul et al. [132] dipped alkaline treated sisal fibers in potassium permanganate solution at concentrations of 0.033, 0.0625 and 0.125 % (unit not specified but believed to be wt-%) in acetone for 1 min. As a result of the permanganate treatment, the hydrophilic tendency of the fibers was reduced, and thus, the water absorption of fiber-reinforced composite decreased. The

hydrophilic tendency of fiber decreased as the $KMnO_4$ concentration increased. Potassium permanganate concentration higher than 1 % (unit not specified but believed to be wt-%) lead to the degradation of the cellulose [130]. De Rosa also reported that potassium permanganate treatment damaged cellulose in okra [133].

Potassium permanganate is able to degrade lignin but also polysaccharides due to its strong oxidizing and electrophilic character [131]. Garves found that the oxidizing effect of potassium permanganate was quite mild when comparing CO and COOH numbers but a stronger effect was observed regarding cellulose degradation [131].

4.10.3.2.2 pH Treatments with H_2SO_4 and NaOH

Treatments in the alkali pH range, also called mercerization, are widely used in filler modifications for the removal of impurities and modifications of the filler surface [134, 135]. For the treatment of soy flour, other aspects should be considered. It is known that proteins and especially their conformation are affected significantly by pH changes which subsequently alter their interaction with other molecules. Modifications can be observed for example in hydrophobicity and solubility [136, 137]. Important properties of the native protein to be considered include their isoelectric point (pI) and amino acid composition. Soy proteins have their isoelectric point at around pH 4. Changing the pH of the solution for soy proteins below their pI will result in positively charged proteins. Adjusting the pH above their pI will result in negatively charged proteins. At pH 10, soy proteins should have maximum unfolding [138].

Acids are common catalysts for hydrolysis or pyrolysis methods which lead to partial or complete breakdown of materials into their single components. Examples include protein hydrolysis into their amino acid components or sugar hydrolysis [139, 140]. One derivative of the sugar hydrolysis is furfural which can also act as cross-linking agent in protein films [141, 142].

Treatments with NaOH will modify components of the cell wall such as hemicellulose, lignin, and wax that support the wall structure and thus will depolymerize the primary cellulosic configuration [46, 49]. One effect is the removal of the “cementing substances” between the cellulose fibers and their fibrillation which produces long fibers with a small diameter and thus high aspect ratio. Therefore, removing these components results in lower density, lower rigidity, and higher surface roughness which can all contribute to increased filler-matrix interaction and thus higher modulus and tensile strength [68]. Treating fibers with NaOH changes the chemical composition of the fiber which subsequently changes the mechanical behaviour (especially strength and stiffness) due to modifications in the degree

of polymerization and molecular orientation of the cellulose crystallites. Furthermore, an alkali treatment increases the amount of amorphous cellulose by simultaneously reducing the amount of crystalline cellulose and eliminating the hydrogen bonds in the network structure [143].

4.10.3.2.3 Acrylation

When cellulose is exposed to high energy radiation, free radicals and chain scission are generated that can initiate the acrylation reaction [130]. Acrylic acid (CH_2=CHCOOH) can be graft polymerized which is usually done to modify glass fibers. When this treatment was carried out on oil palm fibers, the tensile strength was not affected. Gaveva et al. reported an increase in flexural behaviour after the acrylation which points towards an increase in elasticity [143].

Acrylonitrile can be used to modify fibers by reacting with their hydroxyl groups present on the fiber surface.

4.10.3.2.4 Other treatment types

Isocyanate

The functional group of isocyanate (-N=C=O) is susceptible to react with the OH-groups of the fiber surface. Depending on the R-group of the isocyanate, the fiber can be modified to react with the polymer matrix [130, 135, 144].

Peroxide

The peroxide induced adhesion is an easy and inexpensive method. Peroxides dissociate into free radicals which react with the OH groups present on the fiber surface [130]. The addition of low quantities of benzoyl peroxide or dicumyl peroxide can lead to further enhancements of the fiber-matrix interface resulting in improved mechanical properties [143].

Sorbitol and Glycerol

Sorbitol and glycerol are types of sugars and can be used in filler treatments. Derivatives of sorbitol are known to act as nucleating agent for polypropylene [145-147]. Glycerol is commonly used as plasticizer in protein films [148-152]. Glycerol treated mica in composites was reported by Juskey and glycerol treated soy flour was investigated by Sailaja [153, 154].

4.10.3.3 Physical Modifications

Physical methods do not change the chemical composition but will change the structural and surface properties of the fiber. Examples are stretching, calendering, thermo-treatment, electric discharge, and production of hybrid yarns [46]. Electric discharge treatments are corona and cold plasma treatment which are used for surface oxidation activation to change the energy of the fiber surfaces. Using the corona technique on wood fibers increases the quantity of aldehyde groups [46]. Cold plasma treatments can create different surface modifications, which are for example modifications in surface energy, cross-linking, and free radicals.

Electron beam irradiation is another physical process that is dry, clean and can be conducted at room temperature. Electron beam irradiation removes pectin and waxes and thereby creates small pores which increases the surface area of the filler [155].

4.10.3.4 Thermal Treatments

Heat is known to change the conformation of proteins, polysaccharides and other components. Depending on the level of heat and environment (air, acid), reactions can be catalyzed resulting in partial or complete degradation of chemical groups or compounds.

In wood, heat pre-treatment in combination with acid are used to hydrolyze the sugars [156, 157]. When sugars are exposed to heat, the colour of the material can be affected due to Maillard reaction [158]. Proteins can break down due to deamidation and dephosphorylation [159, 160]. Rong et al. investigated heat treated sisal exposed for 4 hours to 150 °C in an air-circulating oven. They could not detect any chemical modifications of the fiber surface nor changes in mechanical properties [161]. Pietak and his colleagues explored a steam treatment, in an autoclave at 170 °C, and found changes in the hemp fiber structure and an increase polarity after the treatment [162]. Steam treated (100 °C, 45 min) defatted peanut flour showed significant changes in their functionality [163].

5. Characterization of the Chemical Composition and Thermal Stability of Soy Materials Subjected to Chemical and Thermal Treatment

5.1 Outline

The characterization of soy materials according to their thermal stability under isothermal and dynamic conditions and their chemical surface composition was carried out to understand the contribution of the different constituents of soy flour and their modification when subjected to autoclave and chemical treatment. The soy materials were soy flour and reference samples for its protein (soy protein isolate) and carbohydrate fraction (soy hulls), and the residue after protein removal (insoluble soy, IS)).

Thermal degradation studies in the dynamic mode, included analysis of the soluble sugar extract (SSE) obtained after acid precipitation of protein. Dynamic TGA between 40 and 800 °C conducted in nitrogen environment showed two degradation peaks for SF that were assigned to the soluble sugar and protein fraction of the reference materials. Isothermal degradation studies conducted at 200 °C in air environment revealed the degradation behaviour to be expected during a typical composite processing with polypropylene. SPI had the most stable behaviour with the lowest mass loss. The autoclave or potassium permanganate treatment had little effect on the isothermal degradation behaviours.

The chemical surface analysis by FTIR showed very complex spectra with overlapping peaks where differences between the soy materials were assigned to the protein and carbohydrate fractions.

5.2 Introduction

The use of agricultural materials as filler in polymeric matrices has received considerable interest for developing lightweight composite materials. When designing composites with agricultural materials, the advantages of agricultural materials are their abundance, renewable source and low density. The polymeric matrices of thermoplastic composites are generally polyolefins either derived from fossil or renewable resources [164, 165]. Their processing temperature is usually between 190 °C and 210 °C. The exposure of agricultural materials to such temperatures can result in thermal degradation and the development of volatile components leading to poor mechanical properties of the composite materials [23,

65, 133, 166]. Another important issue arising from agricultural materials is the incompatibility of these hydrophilic materials with the hydrophobic polymer matrix.

Soybean, the world number one oilseed (53 % in 2009) and protein meal (67 % in 2009) had a production, in 2009, near 400 million metric tons with 41 % in North America [52, 53]. The soybeans are used primarily for their oil. After oil removal, the remaining soy meal (high in protein and carbohydrate) is used primarily as animal feed. Only 6 % of the world's soybeans are used in food applications [104]

The objective of this work was to investigate the thermal stability and chemical surface composition of a number of soy materials subjected to $KMnO_4$ and autoclave treatments. Four materials were selected to represent the major constituents of soy flour (SF): soy protein isolate (SPI) containing predominantly proteins (at least 90 %), soy hulls (high carbohydrate content), insoluble soy (IS), the solid residue obtained after alkaline protein extraction, and the soluble sugar extract (SSE), produced during the acid precipitation of the aqueous extract generated during the alkaline treatment of soy flour. Fourier transform infrared spectroscopy (FTIR) was considered to study the chemical surface composition before and after treatment. Thermogravimetric analysis was selected to study the thermal stability of the material after treatment.

5.3 Materials and Methods

5.3.1 Materials

Defatted soy meal and soy hulls (SH) were obtained from Bunge Inc. (Hamilton, Canada). Soy protein isolate (SPI (c)) ProFam 974 was obtained from Archer Daniels Midland (ADM) Company (Decatur, USA).

5.3.2 Preparation of Soy Materials

5.3.2.1 Soy Flour Processing

Soy flour (SF) was obtained by milling soy meal, with an ultracentrifugal mill ZM200 (Retsch GmbH, Germany) and 0.08 mm sieve with trapezoid shaped holes (part # 03.647.0231).

Figure 5-1 shows a diagram of the soy flour processing with the corresponding intermediate products. After milling of the soy meal, an aqueous mixture was prepared with soy flour and milli-Q water and pH adjusted to 9.0 with 1M NaOH. The mixture was heated to 50 °C under stirring on a magnetic stirrer for one hour. The mixture was centrifuged at

10 000 rpm (RCF_{max} = 11 200) for 20 minutes (Sorvall WX 100 with A-621 rotor, Thermo Scientific, USA) and the solid residue (insoluble fraction (IS)) was dried at room temperature in a fume hood (RH<20 %). The supernatant, containing mostly proteins, sugars and minerals, was adjusted with 1M H_2SO_4 (95-98 %, GR ACS, Fisher Scientific, Canada) to pH 4, just below the isoelectric point of the major soy proteins (glycinin and conglycinin) and centrifuged at 10 000 rpm. The resulting precipitate is referred to as soy protein isolate (SPI (ex)). The remaining liquid solution, containing mostly sugars and minerals, was called soluble sugar extract (SSE).

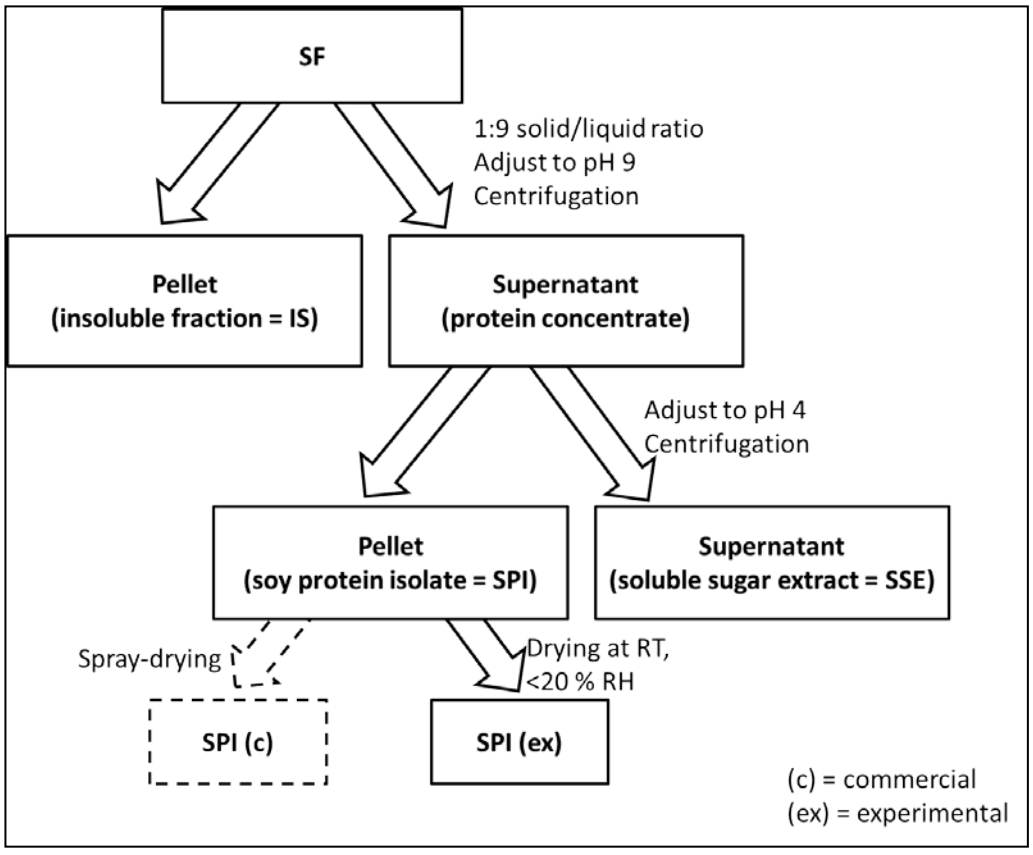

Figure 5-1 Diagram of soy flour (SF) processing for fractionation of the water insoluble fraction (IS), acid precipitated soy protein isolate (SPI) and the water soluble sugars (SSE).

Prior to their use or treatment and after treatment, the soy materials were milled with a ZM 200 ultracentrifugal mill (Retsch GmbH) and sieved with trapezoid shaped 0.08 mm holes (part # 03.647.0231) with the exception of SPI (c) that did not require milling because its particle size was already below 0.08 mm and therefore was used as received. After treatment, the soy materials were dried in a fume hood (RH<20 %) at room temperature (RT) until their moisture content was below 5 %.

5.3.2.2 Autoclave Treatment

The soy material (~500 g), placed on a glass tray resulting in a material height less than one centimeter, was put in a direct steam heated sterilizer-autoclave for sterilization of biological materials (Consolidated Stills & Sterilizers, USA) and subjected to 125 °C and steam for 25 minutes. The treated soy material was then dried and milled as described previously.

5.3.2.3 Potassium Permanganate ($KMnO_4$) Chemical Treatment

An aqueous solution containing potassium permanganate ($KMnO_4$, GR ACS, EMD, USA) was prepared with a $KMnO_4$ to soy material 1:2 mass ratio. The volume of water added was adjusted until it was possible to fully mix the water-filler blend. The mass ratios are summarized in Table 5-1. The soy material was soaked at room temperature in the $KMnO_4$ aqueous solution and stirred manually with a spatula until the mixture was homogenous (at least 5 minutes). The mixture was then dried at room temperature and <20 % RH and milled as described previously.

The $KMnO_4$ was not removed due to cost reasons for the process upscale and potential positive interactions of $KMnO_4$ with polypropylene. At this point, consequences of this decision were possible since interaction with the polypropylene and coupling agent could occur but remained to be tested.

Table 5-1 Mass ratios of water, soy material and $KMnO_4$ for treatment.

Soy material	Parts water	Parts soy material	Parts $KMnO_4$
SF	6	2	1
IS	12	2	1
SPI	20	2	1
SH	6	2	1

5.3.2.4 Thermal Characterization

All thermogravimetric analysis (TGA) was conducted with thermogravimetric analyzer (TGA Q500, TA Instruments, USA). Two modes were considered: (1) dynamic TGA mode in a nitrogen environment with temperature increase from 40 to 800 °C and heating rate of 10 °C/min; (2) isothermal TGA in air, to simulate processing conditions of biocomposites manufacture as described previously for flax and wood [64, 78]. These conditions were air at 110 °C for 5 minutes followed with 60 minutes at 200 °C.

The analysis of the dynamic TGA in nitrogen was obtained by plotting the temperature against the relative mass. Due to different exposure times of the samples in the air prior to

TGA, the relative mass of the sample was adjusted to the mass recorded at 110 °C. It is assumed that at 110 °C, all water is evaporated and changes in mass can only be due to the degradation of the material [167].

The isothermal TGA data were plotted as the mass change over time. The reported values are the residual mass after 60 minutes exposure to 200 °C in an air environment.

5.3.2.5 Fourier Transform Infrared Spectroscopy (FTIR)

The soy materials were prepared with potassium bromide (KBr, IR grade CAS 7758-02-3, Fisher Scientific) and pressed into pellets with an evacuable KBr pellet die (International Crystal Laboratories, USA) in a press (model #3925, Carver, Inc., USA). The FTIR measurements were performed with a Tensor27 (Bruker Optik GmbH, Germany) and the spectra were analyzed with the software OPUS Version 4.2 (Bruker Optik GmbH, Germany). The background spectrum was recorded and 32 scans were performed per sample in a range between 4000 and 400 cm^{-1} with a resolution of 4 cm^{-1}.

Since the spectra consist of numerous overlapping peaks associated with the many constituents of the soy materials, the analysis of the spectra was performed by integrating the area under the spectra for specific regions of wavenumber (Table 5-2). The changes in the ratio of specific area were also investigated. An example of a FTIR absorbance spectrum and its analyzed wavelength regions is presented in Figure 5-2. The analysis was conducted with OPUS 4.2 software (Bruker Optik GmbH, Germany) using the integration method A.

Table 5-2 Wavenumber regions with corresponding vibration and functional groups [33].

Area	Wavenumber region [cm^{-1}]	Vibration	Functional Groups
1	3800-3000	O-H stretch N-H stretch	Alcohols, phenols Amines Carboxylic acids
2	3000-2850	C-H stretch	Alkanes Carboxylic acids
3	1900-1482	C=O, C=C double bonds	Alkenes, ketones, aldehydes, ester, carboxylic acids
4	1195-875	N-H wag C-N stretch C-O stretch O-H bend	Amines, amides, carboxylic acids

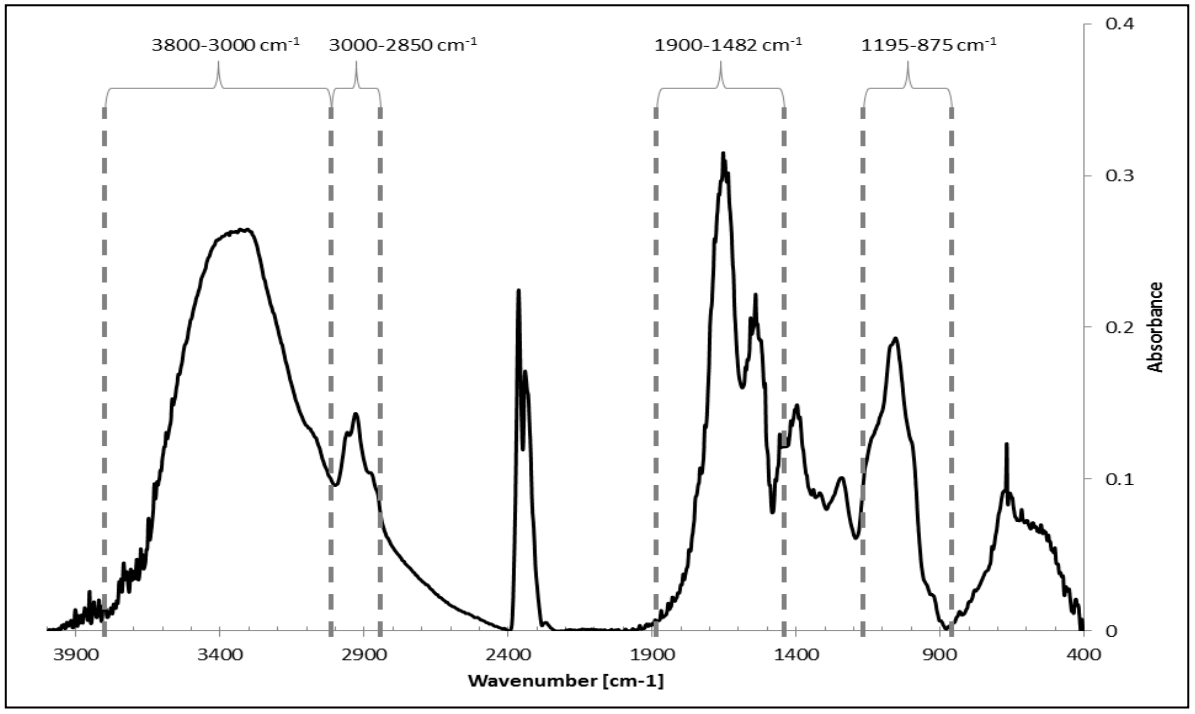

Figure 5-2 Example of FTIR spectra of SF with analyzed wavelength regions

5.3.2.6 Chemical Composition

The ash, cellulose, hemicellulose, lignin and fat content analysis of the soy materials were carried out according to AOAC methods and performed by Agri-Food Laboratories, Guelph, Canada. The ash content was determined by the AOAC 942.05 method, lignin by the ANKOM filter bag modified method of AOAC 973.18, protein content by the combustion method AOAC 990.03 and oil content by the AOAC 920.39 method.

Cellulose content was obtained by subtracting the lignin content from acid detergent fiber (ADF) content. The hemicellulose content was obtained by subtracting the ADF content from the neutral detergent fiber (NDF) content.

Protein was also estimated by the Kjeldahl method according to the method described by Lang [168] but modified for 96-well plates as previously described [20]. The digestion solution contained H_2SO_4, potassium sulphate (K_2SO_4, GR ACS, J.T.Baker) and selenium oxychloride ($SeOCl_2$, 97 %, Sigma-Aldrich). The samples were boiled in 30 ml Kjeldahl flasks (VWR International LLC) on heating units (Kjeldahl heating units, Labconco). The photometric measurement was carried out at 420 nm for Nessler's reagent (Ammonia – Nitrogen (water, 10 wt-% mercuric iodide, 16 wt-% sodium hydroxide, potassium iodide, VWR International) with a Synergy 4 plate reader (BioTek Instruments, Inc.) and with an

ammonium sulfate standard prepared and measured accordingly. The spectrophotometer absorbance readings were first converted to nitrogen and then to protein content using the conversion factor of 6.25 for soy proteins [169].

5.3.2.7 Statistical Analysis

The t-test was used for data analysis of significances between mean values of set of samples. The confidence interval was determined at a significance level of $\alpha = 0.05$.

5.4 Results and Discussion

5.4.1 Composition of Soy Materials

The composition of SF, SH, and SPI is presented in Table 5-3 (before treatment) and the protein content before and after treatment is presented in Table 5-4. As expected, the protein content of SF, SPI and SH are significantly different. The major constituent of SF and SPI is protein with nearly 48 wt-% and 90 wt-% respectively whereas the major constituents of SH are lignin, hemicellulose and cellulose with a combined total mass of at least 63 wt-%. IS has a similar protein content to SF (~50 wt-%) but significantly higher hemicellulose and lignin content. SH had the lowest protein content (12.1 wt-%).

Table 5-3 Chemical composition of soy materials before treatment.

Material	Protein (Nx6.25) [wt-%]	Ash [wt-%]	Cellulose [wt-%]	Hemicellulose [wt-%]	Lignin [wt-%]	Fat [wt-%]	Other* [%]
SF	47.6	6.2	6.9	1.5	0.03	1.5	36.3
IS	45.9	N/A	10.4	10.2	6.0	N/A	27.5
SPI (c)**	<90.0	<5.0	N/A	N/A	N/A	4.0	1.0
SH	12.6	4.5	32.1	23.7	7.5	N/A	19.7

*Other are mainly sugars other than cellulose and hemicellulose (e.g. pectin, starch)
**reported values obtained from ADM [170]

The protein content after treatment remained the same for a given type of soy material (Table 5-4).

Table 5-4 Protein content determined with Kjeldahl total nitrogen analysis for soy materials before and after treatment (±SD, n=2).

Soy material (treatment)	Protein [wt-%]
SF	48.3 ±0.39
SF (auto)	50.5 ±1.45
SF ($KMnO_4$)	50.0 ±1.12
IS	47.9 ±0.03
IS (auto)	48.3 ±0.19
IS ($KMnO_4$)	43.9 ±2.84
SPI	85.0 ±3.28
SPI (auto)	89.1 ±1.25
SPI ($KMnO_4$)	88.5 ±0.40
SH	12.1 ±2.68
SH (auto)	15.7 ±0.06
SH ($KMnO_4$)	15.3 ±0.59

auto = autoclave treatment
$KMnO_4$ = potassium permanganate treatment

5.4.2 Spectroscopy Analysis

A large number of functional groups were expected from the FTIR analysis of the soy materials as a result of their complex composition and the overlap between chemical spectra is illustrated in Figure 5-3 (appendix I., Table 10-1 and Table 10-2). Cellulose and hemicellulose have relatively well defined FTIR spectra [171, 172]. Lignin, on the other hand, has a very complex structure not yet fully elucidated [173]. Proteins present a different challenge since they can take on many conformations. Surewicz in his critical assessment of the applicability of FTIR for the determination of protein structure [174] explains how the spectrum can be affected and lead to shifts in peaks. He also indicates that quantitative analysis is limited to relative analysis [174]. Proniewicz stated in his work on groundwood, that one cannot expect to elucidate all spectral features of macromolecules consisting of glucose units when one of the glucose anomer can be expected to have at least eighteen normal modes in the 1200-1500 cm^{-1} spectral region [175]. With this in mind, the analysis of the FTIR spectra will be discussed according to four regions of wavenumber listed previously in Table 5-2 and shown in Figure 5-2. Quantitative analysis was obtained by calculating the area under the spectra and normalized for a given sample (Table 5-5) and as ratio between the areas for two wavenumber regions (Table 5-7). Carboxylic acid vibrations are present in all selected wavenumber regions. Therefore, differences between the spectra for two wavenumber region can only be attributed to other functional groups.

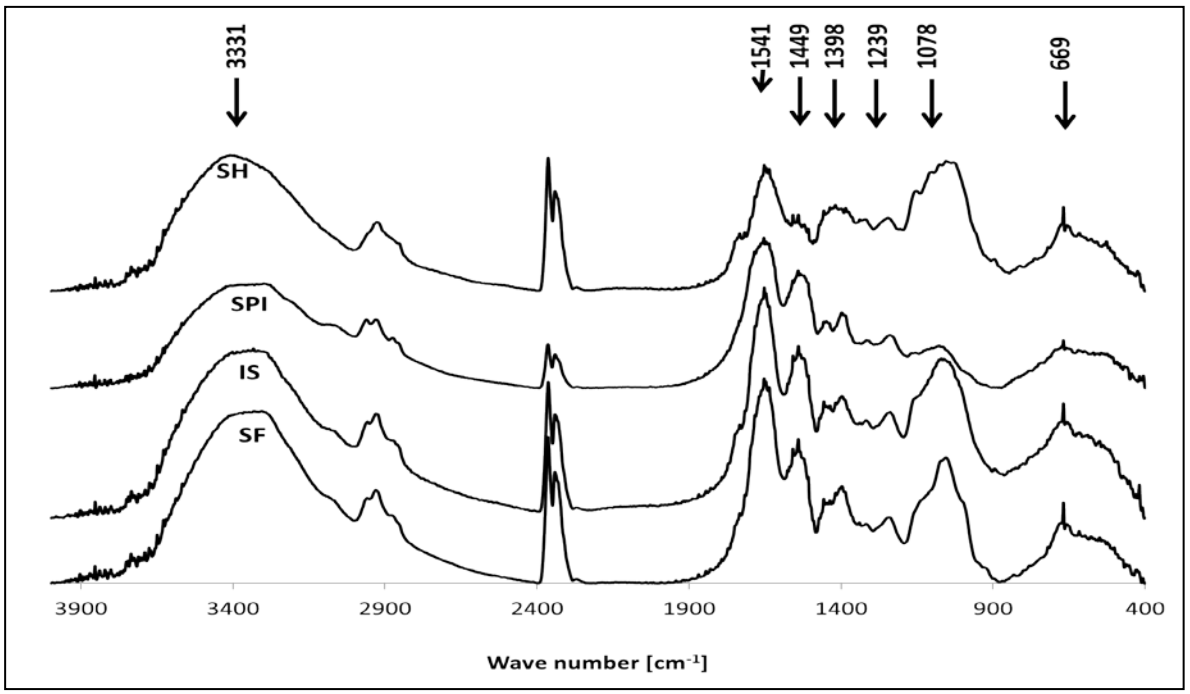

Figure 5-3 Staked FTIR spectra of SF, IS, SH, SPI with peak positions.

Table 5-5 Normalized area for FTIR wavenumber region.

	Normalized Area [%]			
Soy material (treatment)	**3800-3000 cm^{-1} (1)**	**3000-2850 cm^{-1} (2)**	**1900-1482 cm^{-1} (3)**	**1195-875 cm^{-1} (4)**
SF	56.0*	2.5	26.5	15.0
SF (auto)	57.0	2.6	25.2	14.5
SF ($KMnO_4$)	56.0*	2.5	26.6	14.9
IS	54.9*	2.7*	26.1	16.3
IS (auto)	53.8*	2.4	27.7	16.1
IS ($KMnO_4$)	57.3	2.0	26.7	14.0
SPI	57.6	3.0*	35.2*	4.1*
SPI (auto)	58.1	2.5	35.7*	3.6*
SPI ($KMnO_4$)	59.6*	2.6	34.0*	3.9*
SH	61.0*	2.5	16.5*	20.0
SH (auto)	60.4*	2.6	15.7*	21.3*
SH ($KMnO_4$)	60.6*	2.1*	19.4*	18.0*

*Statistical significance $\alpha = 0.05$

Table 5-6 Peak picking of FTIR transmission spectra with 5 % sensitivity

SF	IS	SPI	SH	SF (auto)	SF ($KMnO_4$)	Assigned group
			3410			Free bounded –OH and –NH (proteins, cellulose, hemicellulose, acids)
3331	3337	3299		3314	3346	Free bounded –OH and –NH (proteins, cellulose, hemicellulose, acids)
		2961				C-H stretch
2930	2930		2927	2928	2931	-NH (amide I and II)
1653	1653	1654	1653	1653	1654	C=O stretch of proteins (amide I), random coils and α-helix (proteins)
			1559			
1541	1541	1541	1541	1540	1541	N-H (protein, amide II)
	1457	1449				O-H bend of cellulose, C=C stretch of aromatic groups
			1419			
1397	1398	1398		1399	1399	C-H bend of cellulose, O-H bend of acids
1241	1245	1239	1246	1241	1242	Proteins (amide III), acetyl groups (lignin, hemicellulose)
	1075	1078				C-O-P potassium phytate, saccharides
1055			1055	1054	1052	Saccharides (soy), C-O stretch of cellulose, out-of-plane C-H bend of aromatic groups
669	669	669	669	668	669	700-900 Aromatic hydrogen

The FTIR spectra of the untreated soy materials with identified peaks, listed in

Table 5-6, are shown in Figure 5-3. For all soy materials, the dominant wavenumber region (at least 50 %) was between 3800 and 3000 cm^{-1}, corresponding to stretching vibrations of O-H and N-H. Soy hulls (SH), with the highest cellulose content (32 %), had the highest (61 %) contribution of this wavenumber region to the total area. The wavenumber region between 3000 and 2850 cm^{-1}, corresponding to C-H stretch, had the lowest relative contribution to the total area (2.5-3.0 %). The relative contribution to the total area for the wavenumber region between 1900 and 1482 cm^{-1}, corresponding to C=O and C=C double bonds, differed according to soy material type and treatment. The soy protein isolate, predominantly proteins, had the highest relative contribution to the total area (35 %) while the soy hulls, with the highest cellulose content, had the lowest relative contribution to the total area (15-19 %). The potassium permanganate treatment was quite unusual where the relative contribution to the total area decreased for SPI but increased for SH compared to the respective untreated soy material.

The relative contribution to the total area for the wavenumber region between 1195 and 875 cm^{-1}, corresponding to amines, amides, and carboxylic acids, also differed according to type of soy material and treatment. The lowest contribution to the total area was observed for SPI (highest protein content) and the highest contribution for SH (highest cellulose content).

The intensity of the amide I (1600-1700 cm^{-1}) and amide II (1510-1580 cm^{-1}) bands seemed to reflect the differences in protein content of the various soy materials investigated in this study. These two bands did not seem to be affected by the autoclave treatment.

Table 5-7 Ratio of relative FTIR spectra areass for wavenumber regions reported in Table 5-2 of soy materials.

	Normalized Area [%]					
Soy Material (Treatment)	**1/3**	**Change [%]#**	**1/4**	**Change [%]#**	**3/4**	**Change [%]#**
SF	2.11	0	3.73	0	1.77	0
SF (auto)	2.29	0.1	3.99	0.1	1.74	0.0
SF ($KMnO_4$)	2.11	0.0	3.76	0.0	1.78	0.0
IS	2.10	0	3.36	0	1.60	0
IS (auto)	1.94	-0.1	3.33	0.0	1.72	0.1
IS ($KMnO_4$)	2.14	0.0	4.10	0.2	1.91	0.2
SPI	1.64*	0	13.89*	0	8.49*	0
SPI (auto)	1.63*	0.0	16.09*	0.2	9.89*	0.2
SPI ($KMnO_4$)	1.75*	0.1	15.29*	0.1	8.73*	0.0
SH	3.70*	0	3.05*	0	0.82*	0
SH (auto)	3.84*	0.0	2.84*	-0.1	0.74*	-0.1
SH ($KMnO_4$)	3.13*	-0.2	3.36	0.1	1.07*	0.3

#Change compared to respective untreated soy material
*Statistical significance $\alpha = 0.05$

The relative changes between two wavenumber regions (not reported for region 2 (minimal overall contribution) reported in Table 5-7, indicate also differences according to soy material and treatment. Soy materials differed according to the ratios between regions. SF and IS had similar ratios while SPI and SH had unique and opposite area ratios. SPI overall had lower area ratios 1/3 and higher 1/4 and 3/4 area ratios when compared to SF and SH. SH had overall higher 1/3 area ratios and lower 1/4 and 3/4 area ratios when compared to SF and SPI.

The autoclave treatment of SF (SF (auto)) increased the area ratio 1/3 whereas a decrease of the 1/3 ratio was observed for IS and SH. Overall the changes in area ratios, compared to

the other soy materials, were relatively low which indicates that the autoclave treatment affected the major constituents to a similar extent.

The potassium permanganate treatment for SPI increased by 7 % the 1/3 area ratio while the SPI (auto) area ratio remained similar to the untreated SPI. The area ratio 1/4 also increased for both treatments with a more significant increase for SPI (auto) (16 %). The area ratio 3/4 decreased for both treatments when compared to SPI, with a more pronounced increase for SPI (auto), 16.5 %. These observations suggest that the treatments decreased the amines and amides content.

The changes of the treatments on SH were opposite. While SH (auto) showed increased area ratios for 1/3 a decrease was observed for SH ($KMnO_4$). This suggests an increase of ketones, aldehydes and esters content after autoclave. In contrast, amines and amides content decreased when SH was treated with $KMnO_4$.

In a previously published thermal study of soy protein films at 100 °C by Tian, amide I and amide II bands at 1650 and 1550 cm^{-1} respectively were reported to decrease with time while bands at 1700 and 1500 cm^{-1} increased [176]. Previous thermal stability studies of films prepared with soy protein isolate performed at 200 °C reported decrease in the absorbance bands associated with C-H and C=O stretching of CH_2, CH_3 and ester moieties [177] but not for the amide bands of the proteins.

5.4.3 Thermal Stability at Dynamic Conditions

Dynamic thermogravimetric analysis in nitrogen is presented as mass loss over temperature and as the change of the mass loss over temperature (D-TGA) in Figure 5-4. The D-TGA of untreated SF showed two peaks overlapping with a 1 wt-% onset of degradation at 185 °C and a residual mass at 793 °C of 24.4 wt-%. The D-TGA of IS showed only a shoulder for the same temperature range while no peak was observed for SPI (c) as well as SPI (ex) (data not shown). In contrast, the soluble sugar extract (SSE) exhibited a very early 1 wt- % onset of degradation at 119 °C and two peaks overlapping. This suggests that the most thermal sensitive fraction of soy flour is the soluble sugar fraction (SSE). Table 5-8 presents the degradation temperatures at 1 and 5 % mass loss as well as the residual mass at 793 °C for the soy materials.

Table 5-8 Degradation temperature at 1 wt-% and 5 wt-% mass loss and residual mass at 793 °C of SF, SPI (ex), SSE, SH and IS during dynamic TGA in N_2 environment.

Soy material	1 wt-% Degradation [°C]	Change [%]#	5 wt-% Degradation [°C]	Change [%]#	Residual Mass at 793 °C [wt-%]	Change [%]#
SF	177	0	213	0	24	0
IS	186	4.9	226	6.2	25	3.9
SPI (c)	223*	26.0	250	17.1	34*	41.6
SPI (ex)	182	2.9	231	8.3	23	-5.9
SH	172	-3.1	228	6.9	21	-14.3
SSE	119*	-32.9	135*	-36.7	35*	45.8

#Compared to SF
*Significant at α = 0.05

Remarkable is the relatively high thermal stability of the commercially available SPI (c). The SPI (ex) also showed a good thermal stability with a 1 wt-% onset of degradation at 182 °C. The IS had a 1 wt-% onset of degradation at 186 °C which is more than 8 % higher when compared to SH (1 wt-% onset of degradation at 172 °C).

Since the focus of this study was mainly on the temperature region between 100 and 200 °C, the residual mass at the end of the runs was not of a high importance in this study. Overall, that the residual mass represents the oxidizable fraction and minerals. SF, IS, SPI (ex) and SH had similar residual mass ranging between 21 and 25 wt-%. The sugar extract showed the highest increase (45 %) in residual mass when compared to SF but also SPI (c) had a high residual mass (34 %) which could be due to stabilizing additives present in this commercial product.

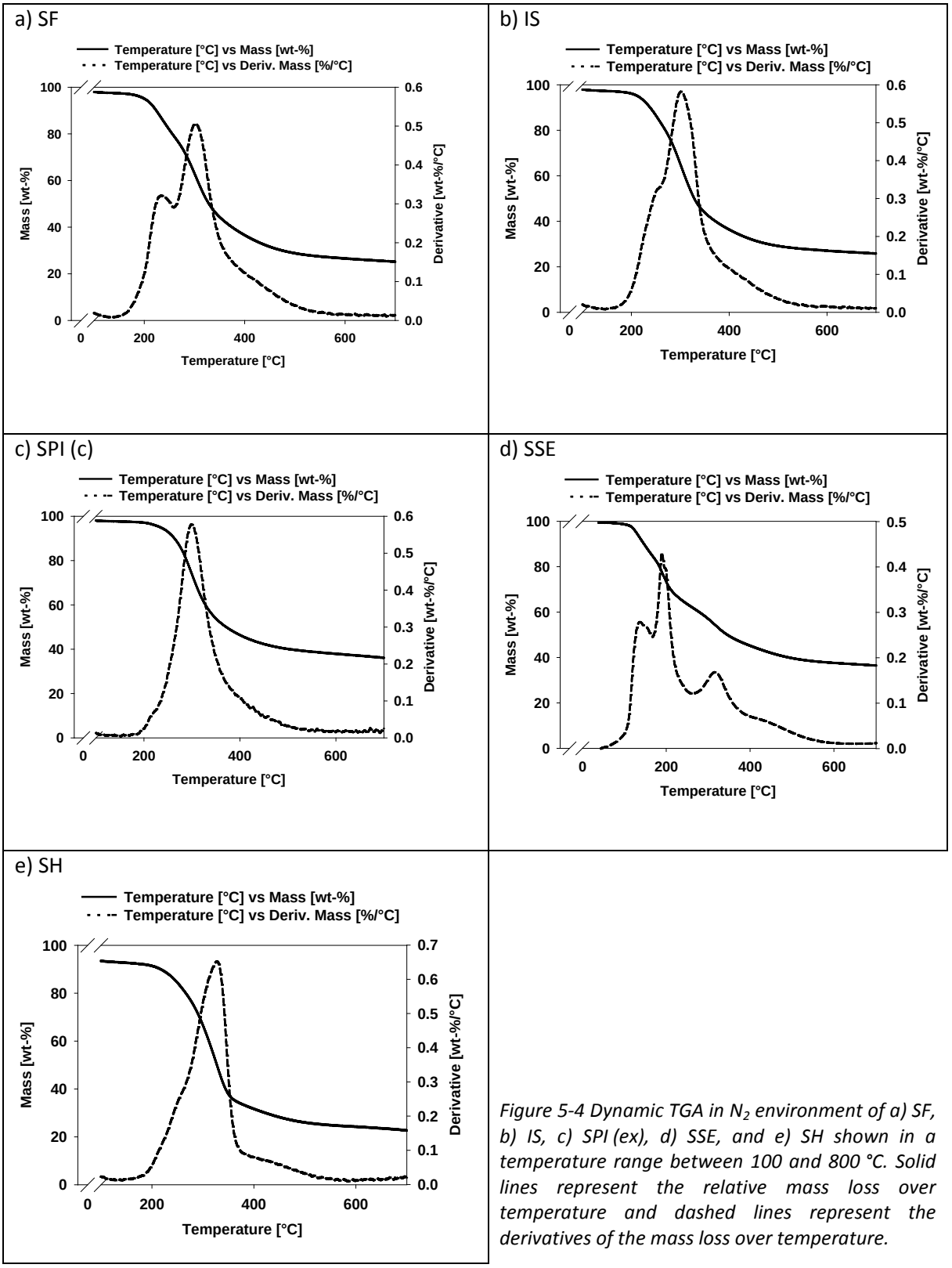

Figure 5-4 Dynamic TGA in N_2 environment of a) SF, b) IS, c) SPI (ex), d) SSE, and e) SH shown in a temperature range between 100 and 800 °C. Solid lines represent the relative mass loss over temperature and dashed lines represent the derivatives of the mass loss over temperature.

The thermal properties of the soy materials and the effect of autoclave and potassium permanganate treatment are presented in Table 5-9 to Table 5-12. When comparing the degradation behaviour of SF after treatment, the autoclave treatment stands out. The SF (auto) compared to SF had a 36 % higher residual mass at 793 °C. Volatile compounds released by the untreated SF at the beginning of the thermal degradation were not observed in SF (auto) leading to a more thermally stable material.

Overall SPI (c) with the highest thermal stability (highest temperature for the 1 wt-% onset of degradation during dynamic TGA) was affected by the treatments. Both, potassium permanganate and autoclave treatments, decreased its thermal stability (temperature for 1 wt-% onset of degradation). This may be due to the industrial processing of SPI by spray-drying. This drying technique is known to affect the protein conformation leading to an increase in solubility [136].

The other soy materials, SF, SH and IS, showed an increase 1 wt-% onset of thermal degradation, between 0.5 and 6.4 % when subjected to the autoclave treatment. The most significant effect translated in 36 % increase in residual mass for SF (auto) at 793 °C. The $KMnO_4$ treatment, on the other hand, showed a slight decrease in thermal stability for all of these soy materials.

Table 5-9 Degradation temperature at 1 wt-% and 5 wt-% mass loss and residual mass at 793 °C of SF and different treatment conditions obtained during dynamic TGA in N_2 environment.

Soy material	Temperature at 1 wt-% mass loss [°C]	Change [%]#	Temperature at 5 wt-% mass loss [°C]	Change [%]#	Residual mass at 793 °C [wt-%]	Change [%]#
SF	177	0	213	0	24	0
SF (auto)	178	0.5	215	0.7	33	36.7
SF ($KMnO_4$)	165	-7.1	211	-0.8	23	-5.9

#Compared to untreated material

Table 5-10 Degradation temperature at 1 wt-% and 5 wt-% mass loss and residual mass at 793 °C of IS and different treatment conditions obtained during dynamic TGA in N_2 environment.

Soy material	Temperature at 1 wt-% mass loss [°C]	Change [%]#	Temperature at 5 wt-% mass loss [°C]	Change [%]#	Residual mass at 793 °C [wt-%]	Change [%]#
IS	186	0	226	0	25	0
IS (auto)	193	3.9	228	0.7	24	-4.3
IS ($KMnO_4$)	188	1.0	226	-0.4	26	2.6

#Compared to untreated material

Table 5-11 Degradation temperature at 1 wt-% and 5 wt-% mass loss and residual mass at 793 °C of SPI (c) and different treatment conditions obtained during dynamic TGA in N_2 environment.

Soy material	Temperature at 1 wt-% mass loss [°C]	Change [%]#	Temperature at 5 wt-% mass loss [°C]	Change [%]#	Residual mass at 793 °C [wt-%]	Change [%]#
SPI	223	0	250	0	34	0
SPI (auto)	209	-6.3	248	-0.7	24	-30.3
SPI ($KMnO_4$)	205	-8.4	245	-1.6	25	-26.4

#Compared to untreated material

Table 5-12 Degradation temperature at 1 wt-% and 5wt- % mass loss and residual mass at 793 °C of SH and different treatment conditions obtained during dynamic TGA in N_2 environment.

Soy material	Temperature at 1 wt-% mass loss [°C]	Change [%]#	Temperature at 5 wt-% mass loss [°C]	Change [%]#	Residual mass at 793 °C [%]	Change [%]#
SH	172	0	228	0	21	0
SH (auto)	183	6.4	233	2.4	23	8.4
SH ($KMnO_4$)	165	-3.8	227	-0.5	25	18.7

#Compared to untreated material

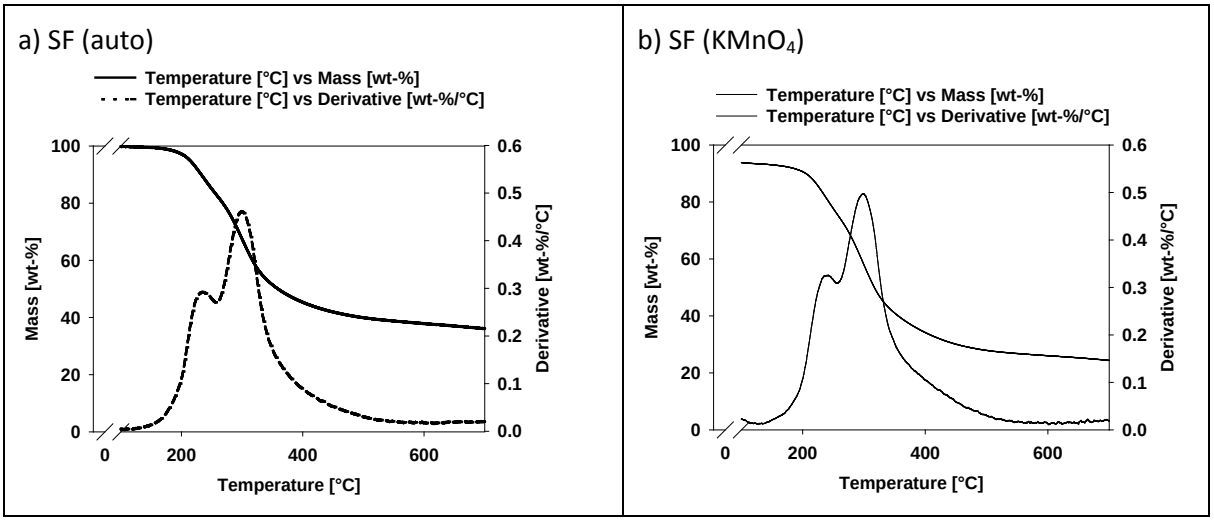

Figure 5-5 Dynamic TGA in N_2 environment for SF treatments a) SF (auto) and b) SF ($KMnO_4$). Continuous lines represent mass change over temperature. Dashed lines are the first derivatives of the respective straight line (D-TGA) which represent the fraction of weight loss over temperature.

5.4.4 Thermal Stability at Isothermal Conditions

An estimate of the mass loss of the soy materials occuring during biocomposite manufacturing was obtained by simulating the processing conditions in the TGA system. The operations of the TGA were isothermal conditions, 200 °C and air for 60 minutes. Prior to these isothermal conditions, the moisture was removed from the samples with an initial phase, 5 minutes at 110 °C (data not shown). The isothermal mass loss over time at 200 °C is presented in Figure 5-6. SPI (c) had the lowest mass loss resulting in the highest thermal stability (about 10 wt-% mass loss). As seen previously, treating SPI (c) with $KMnO_4$ or autoclave decreased its thermal stability which is believed to be due to the spray-drying process that can alter the protein configuration (e.g. due to disulfide-bond breakage) and subsequently its properties e.g. solubility. SF showed the lowest thermal stability with about 20 wt-% mass loss. Autoclaving SH and SF increased moderately their thermal stability whereas IS behaviour was not affected by this treatment. The $KMnO_4$ treatment decreased the thermal stability for SPI (c) and IS whereas SH behaviour was not affected. SF showed improvements in thermal stability for both treatments. Since SH has a high cellulose content and IS has a much higher protein content, one can assume that the autoclave treatment affected mainly the cellulose content whereas the $KMnO_4$ treatment affected mainly the protein content of the soy materials.

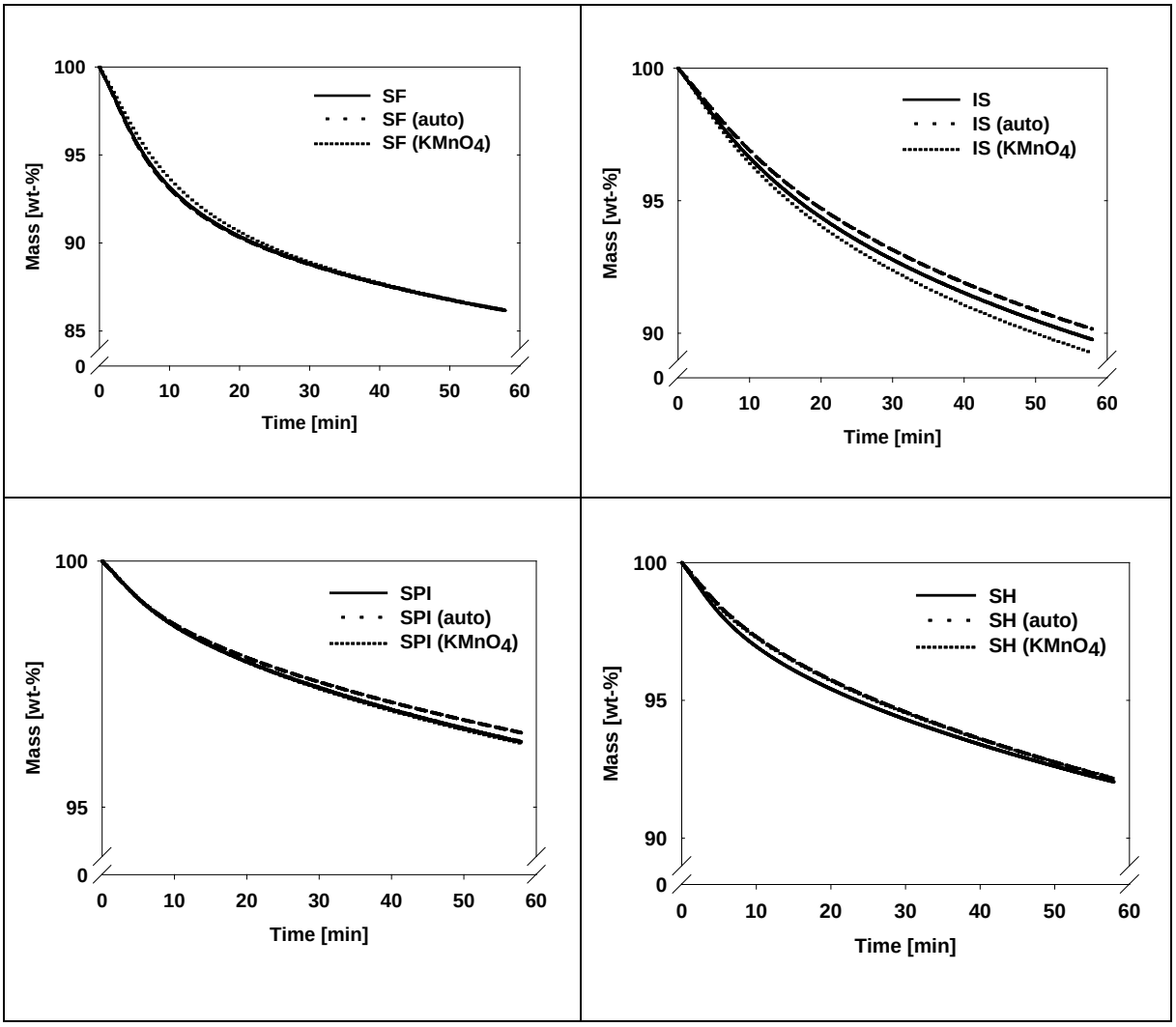

Figure 5-6 Isothermal TGA in air environment of SF, SPI (c), SH and IS (no treatment; $KMnO_4$ treatment; autoclave treatment). Samples were subjected to 110 °C during 5 minutes (water removal) and 60 minutes at 200 °C.

Table 5-13 Residual mass of soy materials after isothermal TGA for 60 minutes at 200 °C in air.

Soy material	Residual mass [%]*
SF	86
SF (auto)	86
SF ($KMnO_4$)	86
IS	90
IS (auto)	90
IS ($KMnO_4$)	89
SPI (c)	96
SPI (c) (auto)	97
SPI (c) ($KMnO_4$)	96
SH	92
SH (auto)	92
SH ($KMnO_4$)	92

*Residual mass with time = 0 min at Temperature = 200 °C (values are excluding moisture)

5.5 Conclusions

Soy flour, its two major constituents, proteins (soy protein isolate (SPI)) and carbohydrates (soy hulls (SH)), and by-products from its alkaline and acidic treatment (soluble sugar extracts (SSE) and insoluble soy (IS)) were investigated for their chemical composition and thermal stability. The interpretation of the FTIR spectra of the soy materials was challenging due to the presence of protein, cellulose, hemicelluloses and lignin. In spite of these challenges, clear differences between the area ratios for specific regions of wavenumber were identified. SH and SPI had unique and distinct FTIR spectra for two regions (1900 to 1482 and 1195 to 875 cm^{-1}), agreeing with differences in protein and cellulose content. The autoclave treatment of all soy materials did not affect the contribution of the four wavenumber regions and their respective ratios for a given soy material. In contrast, the $KMnO_4$ treatment affected the relative contribution of the wavenumber region between 1900 to 1482 cm^{-1} for SPI (decreased) and SH (increased) while remained constant for SF and IS. The $KMnO_4$ and autoclave treated SF showed no significant differences in FTIR spectra possibly due to the opposing effects of the treatment and the two constituents, protein and cellulose, present in SF.

Thermogravimetric analysis in the dynamic mode (D-TGA), from 40 °C until 800 °C and nitrogen environment, showed that SPI was the most thermally stable material with the highest 1 wt-% onset of degradation at 223 °C. The SSE was the least thermally stable material with the lowest 1 wt-% onset of degradation (119 °C). SPI and SSE had similar residual mass at 793 °C, 34 % and 35 % respectively, which was at least 40 % higher when

compared to SF. The analysis of the isothermal thermal behaviour at 200 °C showed that SPI (91 % residual mass) had the highest thermal stability compared to IS and SH with residual masses of 82 % and 84 % respectively. The lowest thermal stability was observed for SF with a residual mass of 78 %. SF and SH improved in thermal stability when subjected to the autoclave treatment whereas the thermal stability of IS remained constant and decreased for SPI. $KMnO_4$ treatment showed no change in thermal stability for SF and SH but a 1 and 2 wt-% decrease in residual mass for IS and SPI respectively.

5.6 Acknowledgements

The authors would like to thank Bunge Inc. (Hamilton, Canada) for providing soy materials, and Archer Daniels Midland Company (ADM, Decatur, USA) and especially Russ Egbert for kindly providing soy materials and productive discussions. Financial support from Grain Farmers of Ontario (formerly Ontario Soybean Growers), NSERC (Natural Sciences and Engineering Research Council of Canada) and Ontario Research Fund (BioCar) are gratefully recognized.

6. Contact Angle and Surface Energy Analysis of Soy Materials Subjected to Potassium Permanganate and Autoclave Treatment

6.1 Outline

Initial water contact angle, apparent rate of water absorption and dispersive and polar surface energy were investigated for compacts of soy flour, two reference materials, soy protein isolate (protein reference material) and soy hulls (carbohydrate reference material), and an additional by-product, the residue obtained after alkaline treatment of soy flour (insoluble soy). Untreated soy flour compacts had an initial water contact angle (57 °) similar to soy protein isolate compacts (64 °) but significantly lower than insoluble soy compacts (74 °) and soy hulls compacts (85 °). Potassium permanganate oxidation treatment increased the initial water contact angle of soy flour compacts (70 °), soy protein isolate compacts and insoluble soy residue compacts (81 °) but did not increase for soy hulls compacts. The apparent rate of water absorption after potassium permanganate treatment, decreased for all types of soy compacts except for insoluble soy compacts. Autoclave treatment did not affect the initial water contact angle of soy flour and soy hulls compacts but increased significantly for soy protein isolates and insoluble soy compacts. The effect of autoclave treatment was reflected by the apparent rate of water absorption observed during contact angle study. A significant increase was measured according to the type of soy material. The total surface energy and the dispersive and polar components, estimated from water and diiodomethane contact angle, indicated similar dispersive surface energy for soy flour, soy protein isolate and insoluble soy compacts (30 mN/m) but higher for soy hulls (36 mN/m). Significant differences of the polar surface energy component compared to compacts of the untreated materials were measured, 18.4 mN/m (soy flour), 13.6 mN/m (soy protein isolate), 8.2 mN/m (insoluble soy) and 2.7 mN/m (soy hulls). The potassium permanganate oxidation treatment reduced significantly the polar surface energy component of soy materials compacts except soy hulls which increased. In contrast, autoclave treatment did not affect the polar surface component of soy flour but increased for all other soy materials compacts. The most appropriate surface properties, based on the contact angle analysis for compatibility with hydrophobic polymeric materials, appear to be soy flour or insoluble soy subjected to potassium permanganate treatment.

6.2 Introduction

The interest in lightweight materials for automotive and construction applications has significantly increased over the past years. The petroleum supply has become less secure resulting in price volatility. In addition, environmental concerns are becoming more pronounced. The increase in weight for improved safety and comfort can be reduced by employing lightweight composite materials. Composite materials for automotive interior parts commonly contain minerals or glass materials which possess high density (compared to agricultural fillers) and result in somewhat heavy composite materials. Agricultural fillers represent a promising alternative that can deliver similar performance materials for reduced weight.

Agricultural fillers can be taken from by- or waste products during the harvesting and the processing of products such as corn, wheat, rice, hemp, palm, soybean, cotton and other plants cultivated predominantly for their seeds and fruits. Soybeans are the number one (53 %, 2009) oil seed crop and protein meal (66 %, 2009) in the world [52]. The production of soybeans in 2009 represented nearly 400 million metric tons with at least 40 % of the production in North America [52]. Intense research on chemical and thermal treatments of natural materials has been on-going for the development of high performance materials or for biorefineries. For example, oxidation by potassium permanganate is a well-established treatment in the paper industry that increases carbonyl and carboxyl groups [131]. Heat treatment has been evaluated for the improvement of the nutritional value of soy products, e. g. soy flours, grits and proteins [28].

However, when developing composites from agricultural fillers and polyolefins, the major challenge remains their incompatibility due to differences in surface properties. Fillers derived from agricultural resources are hydrophilic in nature because of their composition (cellulose, hemicellulose, lignin, protein) and their water content. Polyolefins on the other hand, are mainly derived from petroleum and are hydrophobic. As a result of such differences, the two materials are difficult to mix and have little interaction resulting in poor mechanical properties [121, 162, 178]. Surface modification and the addition of coupling agents are known to improve the interaction between the surface of the two materials by introducing chemical bonds [43, 46, 90, 121]. Surface modifications that alter the properties of the materials can be chemical or physical and can target the filler or the polymer matrix [43, 46, 179-182]. Combinations of two or more treatments are also possible [75, 121, 130].

The surface characteristics of inert solid materials with smooth surfaces, such as films, sheets, plastics and composites, are well established and obtained by contact angle analysis and surface energy study [84, 85, 183, 184]. In contrast, powder-like materials, such as milled agricultural materials, need special attention because of their interaction with liquids, their particles size and shape and their heterogeneous surface characteristics. Several studies, by Buckton and his colleagues, on methods for contact angle and surface energy analysis of powder-like materials have been published mainly for pharmaceutical applications [86, 185, 186]. Sample preparation initially developed for powder materials [86] have recently been reported by Roman-Gutierrez and his colleagues for wheat flour and its constituents [87]. Sample preparation consists of a preliminary stage of compaction at high pressure and equilibration of the materials under controlled humidity conditions. Roman-Gutierrez and his colleagues showed that wheat flour and its constituents possess significantly different initial water contact angle characteristics. The initial water contact angle for two types of wheat flour, hard and soft wheat, was 68 ° while the initial water contact angle for the two major wheat flour constituents was 85 ° for gluten (protein rich fraction) and between 38 and 41 ° for starch and pentosans [87].

The total free surface energy can generate information on specific forces. Owens and Wendt developed a method for the estimation of surface free energy of polymers based on the theories of Young's equation and Fowkes [84]. The two main contributing forces were identified as the dispersive and hydrogen (polar) forces. The surface free energy of polypropylene is around 30 mN/m mainly contributing to dispersive forces [187]. The grafting of maleic anhydride onto polypropylene will modify primarily the polar component of its surface free energy [182, 183]. Agricultural materials have significant polar surface energy component due to their significant carbohydrate content [23]. Surface free energy analysis for natural materials is based on the Wilhelmy method for wood plates [188] or the receding and advancing contact angle method for cellulose films [85].

The motivation for this study was to evaluate and compare the effects of thermal and chemical treatment on the surface properties of soy flour with the ultimate goal of matching its surface properties to those of polypropylene for the development of quality composite materials. Four types of soy materials, soy flour, soy protein isolate (protein reference constituent), soy hulls (carbohydrate reference constituent) and insoluble soy (by-product) were considered to better understand the contribution of proteins and carbohydrates, the two major constituents of soy flour. To our knowledge, this is the first study reporting the surface properties of soy flour and its constituents. The potential of contact angle analysis as a screening tool for the relative assessment of the effect of chemical and autoclave treatment on soy flour will also be discussed.

6.3 Materials and Methods

6.3.1 Materials

Defatted soy meal and soy hulls (SH) were obtained from Bunge Inc. (Hamilton, Canada). Soy protein isolate (SPI (c)) ProFam 974 was obtained from Archer Daniels Midland (ADM) Company (Decatur, USA).

6.3.2 Preparation of Soy Materials

6.3.2.1 Soy Flour Processing

Soy flour (SF) was obtained by milling soy meal, with an ultracentrifugal mill ZM200 (Retsch GmbH, Germany) and 0.08 mm sieve with trapezoid shaped holes (part # 03.647.0231).

Figure 6-1 shows a diagram of the soy flour processing with the corresponding intermediate products. After milling of the soy meal, an aqueous mixture was prepared with soy flour and milli-Q water and pH adjusted to 9.0 with 1M NaOH. The mixture was heated to 50 °C under stirring on a magnetic stirrer for one hour. The mixture was centrifuged at 10 000 rpm (RCF_{max} = 11 200) for 20 minutes (Sorvall WX 100 with A-621 rotor, Thermo Scientific, USA) and the solid residue (insoluble fraction (IS)) was dried at room temperature in a fume hood (relative humidity (RH)<20 %). The supernatant, containing mostly proteins, sugars and minerals, was adjusted with 1M H_2SO_4 (95-98 %, GR ACS, Fisher Scientific, Canada) to pH 4, just below the isoelectric point of the major soy proteins (glycinin and conglycinin) to change their total charge to a positive value and centrifuged at 10 000 rpm. The resulting precipitate is referred to as soy protein isolate (SPI (ex)). The remaining liquid solution, containing mostly sugars and minerals, was called soluble sugar extract (SSE).

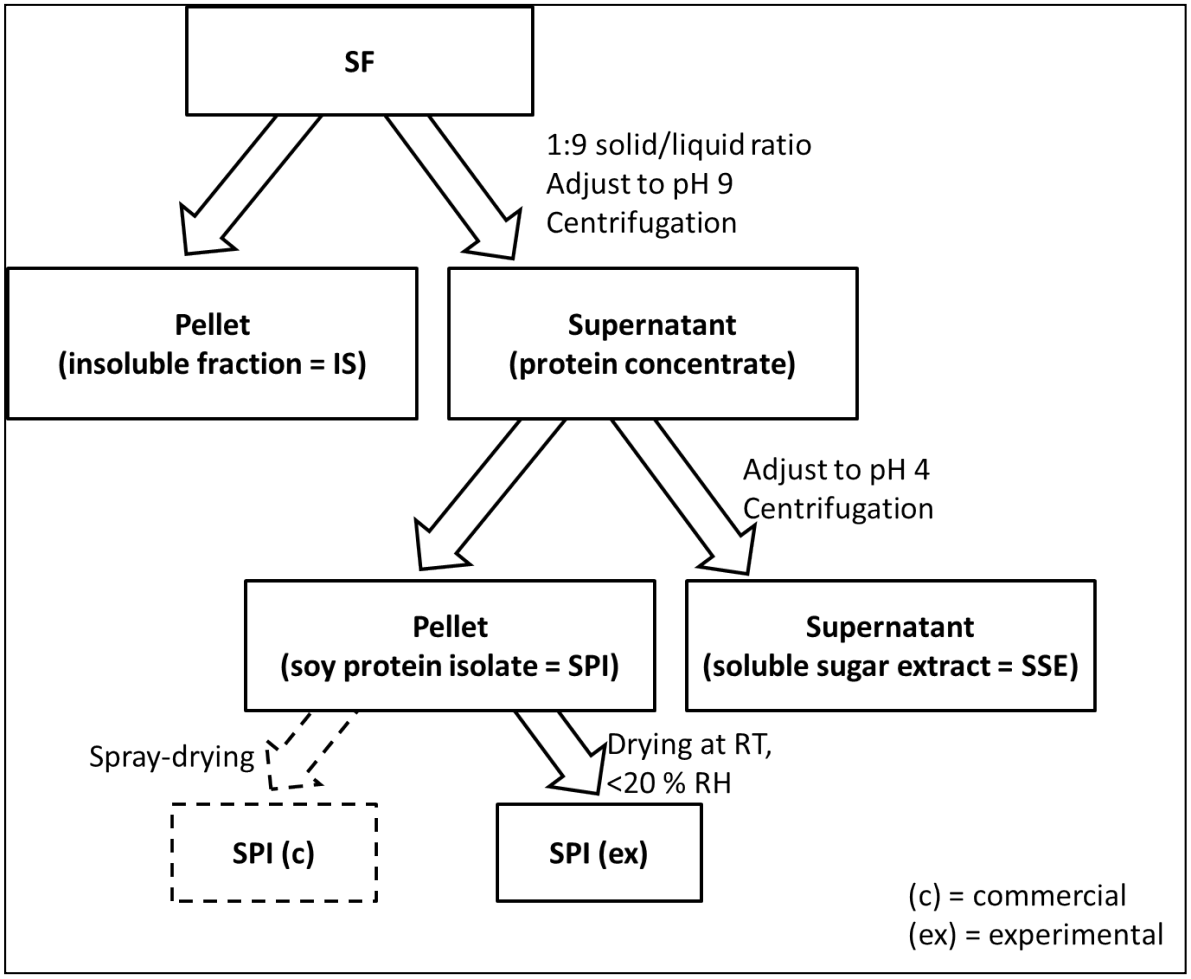

Figure 6-1 Diagram of soy flour (SF) processing for fractionation of the water insoluble fraction (IS), acid precipitated soy protein isolate (SPI) and the water soluble sugars (SSE).

Prior to their use or treatment and after treatment, the soy materials were milled with a ZM 200 ultracentrifugal mill (Retsch GmbH) and sieved with trapezoid shaped 0.08 mm holes (part # 03.647.0231) with the exception of SPI (c) that did not require milling because its particle size was already below 0.08 mm and therefore was used as received. After treatment, the soy materials were dried in a fume hood (RH<20 %) at room temperature (RT) until their moisture content was below 5 %.

6.3.2.2 Autoclave Treatment

The soy material (~500 g), placed on a glass tray resulting in a material height less than one centimeter, was put in a direct steam heated sterilizer-autoclave for sterilization of biological materials (Consolidated Stills & Sterilizers, USA) and subjected to 125 °C and steam for 25 minutes. The treated soy material was then dried and milled as described previously.

6.3.2.3 Potassium Permanganate ($KMnO_4$) Chemical Treatment

An aqueous solution containing potassium permanganate ($KMnO_4$, GR ACS, EMD, USA) was prepared with a $KMnO_4$ to soy material 1:2 mass ratio. The volume of water added was adjusted until it was possible to fully mix the water-filler blend. The mass ratios are summarized in Table 6-1. The soy material was soaked at room temperature in the $KMnO_4$ aqueous solution and stirred manually with a spatula until the mixture was homogenous (at least 5 minutes). The mixture was then dried at room temperature and <20 % RH and milled as described previously.

Table 6-1 Mass ratios of water, soy material and $KMnO_4$ for treatment.

Soy material	Parts water	Parts soy material	Parts $KMnO_4$
SF	6	2	1
IS	12	2	1
SPI (c)	20	2	1
SH	6	2	1

6.3.2.4 Chemical Composition

The composition of SF, SH, and SPI is presented in Table 6-2 (before treatment). The ash, cellulose, hemicellulose, lignin and fat content analysis of the soy materials was carried out according to AOAC methods and performed by Agri-Food Laboratories, Guelph, Canada. The ash content was determined by the AOAC 942.05 method, lignin by the ANKOM filter bag modified method of AOAC 973.18, protein content by the combustion method AOAC 990.03 and oil content by the AOAC 920.39 method.

Cellulose was obtained by subtracting lignin from acid detergent fiber (ADF). Hemicellulose was obtained by subtracting ADF from neutral detergent fiber (NDF).

Table 6-2 Chemical composition of soy materials before treatment.

Material	Protein (Nx6.25) [wt-%]	Ash [wt-%]	Cellulose [wt-%]	Hemicellulose [wt-%]	Lignin [wt-%]	Fat [wt-%]	Other* [%]
SF	47.6	6.2	6.9	1.5	0.03	1.5	36.3
IS	45.9	N/A	10.4	10.2	6.0	N/A	27.5
SPI (c)**	<90.0	<5.0	N/A	N/A	N/A	4.0	1.0
SH	12.6	4.5	32.1	23.7	7.5	N/A	19.7

*Other are mainly sugars other than cellulose and hemicellulose (e.g. pectin, starch)
**reported values obtained from ADM [170]

6.3.2.5 Sample Preparation for Contact Angle Analysis

For contact angle analysis, soy materials were pressed in compacts with evacuable KBr pellet die (International Crystal Laboratories, USA) at room temperature as suggested for pigment specimens in ASTM D7490 – 08 [189]. The KBr mould was 13 mm in diameter and a 7 t (7000 kg/132.73 mm^2 = 517.19 MPa) load applied during at least 60 seconds in a press Model #3925 (Carver Inc., USA). The pellets were then fixed onto a microscope object slide (Pearl 7101,T & Q Industries, China) with double sided tape (137-2C, Scotch, Canada (part of 3M)) and stored in a desiccator (Nalgene, Sybron Corporation, USA) until testing.

6.3.2.6 Surface Roughness Measurement

For measurements of the surface roughness, the soy materials were prepared as compacts for the contact angle analysis. The optical profiler WYKO NT100 (Veeco Instruments Inc., Plainview, NY, USA) was used in VSI mode with a magnification of 5.1x (set-up parameter: size 736 x 480; sampling 1.65 µm). Each material sample was measured at least three times and the average surface roughness (R_a) and peak-to-valley difference (R_t) over the entire profile was calculated by the Wyko Vision® analysis software (Veeco Instruments Inc., Plainview, NY, USA) based on Equation 6-1 and Equation 6-2.

$$R_a = \frac{1}{N}\sum_{i=1}^{N}|Z_i| \qquad \textit{Equation 6-1}$$

N = Number of peak spacings
Z_i = height of each pixel after the zero mean is removed

$$R_t = R_p - R_v \qquad \textit{Equation 6-2}$$

R_p = maximum peak hight
R_v = minimum valley height

6.3.3 Contact Angle Measurement

Contact angle analysis was conducted with the Drop shape analyzer DSA100 (Krüss GmbH, Germany) at room temperature in a static mode with at least six liquid drops per specimen. The measurement was digitally recorded and the videos were analyzed with the software DSA1 V1.9-03 9 (Krüss GmbH, Germany). Two analysis methods were considered for low contact angle values: Tangent method 1 and Young-Laplace method (sessile drop) [12]. The initial contact angle and the change over time (at least ten seconds) were recorded for a drop of liquid deposited on a compact of a given soy material. The apparent absorption rate of the liquid drop was calculated by linear regression as the slope of contact angle measurements versus time curves during the first five seconds [85, 87].

6.3.4 Surface Energy

The total surface energy, the dispersive surface energy and the polar surface energy were estimated according to the method of Owens, Wendt, Rabel and Kaelble (OWRK)[12]. Milli Q water and diiodomethane (99 % CAS# 75-11-6, Alfa Aesar, USA) were selected as liquids with surface energy properties presented in Table 6-3.

Table 6-3 Reported surface energy components of water and diiodomethane [12].

Liquid	Total Surface Energy [σ_{Total}, mN/m]	Dispersive Surface Energy Component [σ^D, mN/m]	Polar Surface Energy Component [σ^P, mN/m]
Water (W)	72.8	21.8	51.0
Diiodomethane (D)	50.8	50.8	0.0

6.3.4.1 Statistical Analysis

The t-test was used for data analysis of significances between mean values of set of samples. The confidence interval was determined at a significance level of $\alpha = 0.05$.

6.4 Results and Discussion

Soy flour (SF) is a mixture that contains nearly equal amounts of protein and carbohydrate making difficult the identification of which constituent can be affected by a given treatment. Thus soy materials with high protein content, soy protein isolate (SPI), and high carbohydrate content, soy hulls (SH), were investigated as reference materials for the soy flour constituents. The insoluble residue (IS) after aqueous alkaline treatment of soy flour was also considered for its potential as low cost filler material in the manufacture of composite materials.

6.4.1 Surface Roughness

The roughness of the compact surfaces was determined to evaluate its effect during contact angle analysis. Figure 6-2 shows examples of the surface scans for compacts of the soy materials and Table 6-4 presents the surface roughness estimates. Overall the surface roughness for all soy material compacts ranged between 1.15 and 3.05 µm which differs by 1.9 µm. The lowest average surface roughness was found to be 1.15 µm for SF (auto) and 1.17 µm for SPI (auto). The soy material with the highest surface roughness was IS (auto) with 3.05 µm. The autoclave and $KMnO_4$ treatment increased the surface roughness of IS and SH but decreased the surface roughness of SF and SPI except for $KMnO_4$ treated SF which increased. The opposite effect of the treatments could be due to structural differences resulting from the different composition of the soy materials. SPI and SF have the highest protein content whereas IS and SH have higher carbohydrate content.

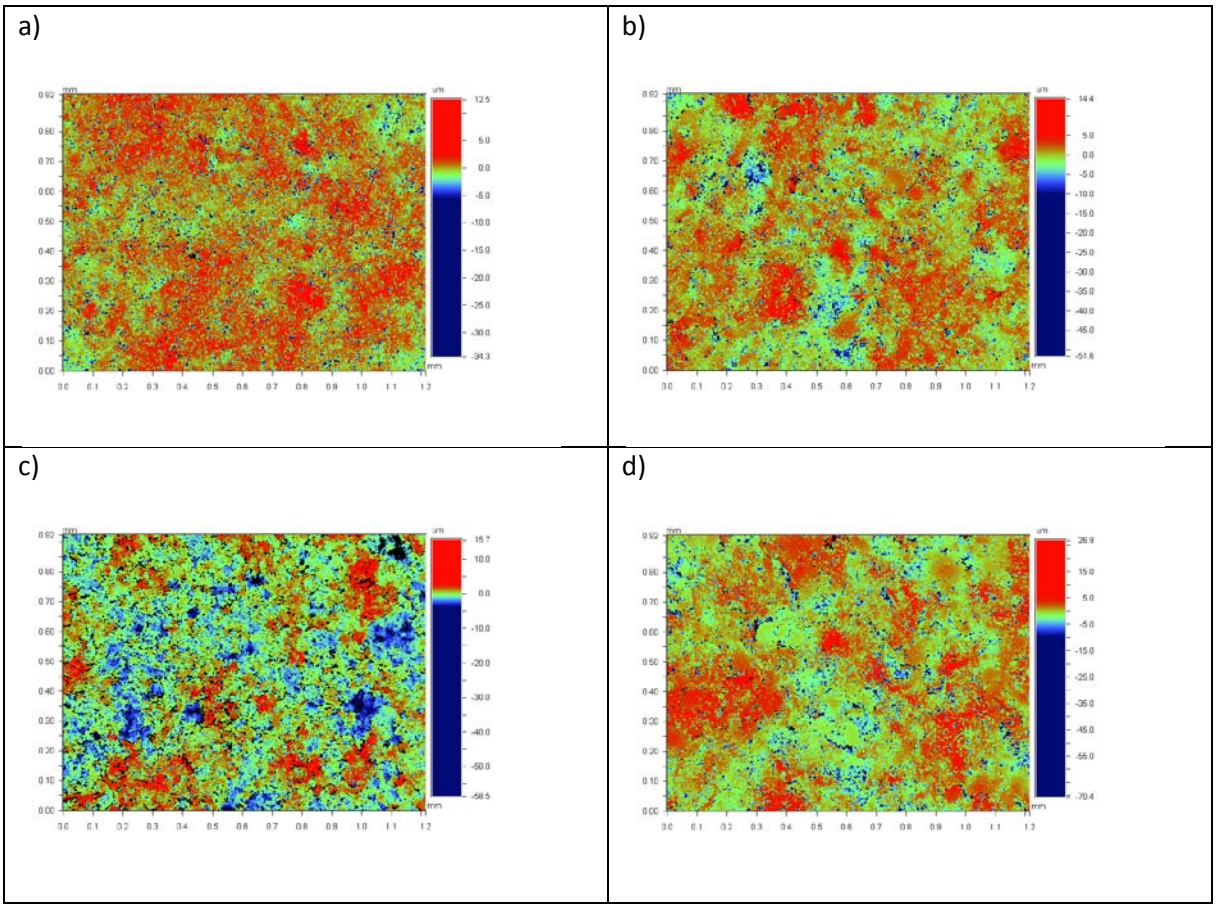

Figure 6-2 Surface scans of soy material compacts: a) SF, b) IS, c) SPI, and d) SH

The peak-to-valley difference is presented in Table 6-4. SPI shows the largest peak-to-valley difference with slight increase when subjected to the treatments. SF shows the

smallest peak-to-valley difference that increases nearly up to 20 µm when subjected to $KMnO_4$ treatment. IS shows an increase of 15 µm when subjected to both treatments. An opposite behaviour was observed for SH which showed a decrease in peak-to-valley difference when treated. A direct relationship between the trends of the peak-to-valley difference and surface roughness as well as contact angle could not be seen.

Table 6-4 Surface roughness estimates and peak-to-valley differences of soy material compacts (±SD, n≥3)

Soy material	Roughness, R_a [µm]	Peak-to-valley difference, R_t [µm]
SF	1.32 ±0.11*	48.74 ±3.66*
SF (auto)	1.15 ±0.10*	58.47 ±3.82*
SF ($KMnO_4$)	1.61 ±0.08	66.63 ±3.28
IS	2.36 ±0.20	68.49 ±2.01
IS (auto)	3.05 ±0.10*	83.56 ±6.10*
IS ($KMnO_4$)	2.89 ±0.21*	83.96 ±5.95*
SPI	1.24 ±0.14*	83.14 ±6.36*
SPI (auto)	1.17 ±0.13*	93.21 ±3.85*
SPI ($KMnO_4$)	1.21 ±0.05*	91.54 ±2.28*
SH	2.34 ±0.11	78.77 ±14.08
SH (auto)	2.49 ±0.11*	64.18 ±4.74*
SH ($KMnO_4$)	2.36 ±0.16	68.75 ±4.44

*Statistical significance $\alpha = 0.05$

6.4.2 Initial and Evolution with Time of Contact Angle of Soy Materials

A typical initial and change over time of liquid contact angle and drop volume for soy materials is presented in Figure 6-3. The liquid contact angle and the drop volume have similar evolution over time for water but minor differences for diiodomethane. The evolution over time of the contact angle gives a measure of the rate of liquid absorption of soy materials. The situation for SPI compact, illustrated in Figure 6-3, shows a very stable water contact angle. The change in water contact angle, even over a 20 s period, showed negligible absorption (-0.1 °/s). In contrast, the change over time of the diiodomethane, a non-polar liquid, over the SPI compact showed significantly different behaviour with very fast liquid absorption resulting in a very high absorption rate (-26.7 °/s). The contact angle over time for the three other soy materials, SF, SH and IS, will be discussed in the next sections when evaluating the effect of potassium permanganate treatment and autoclave treatment.

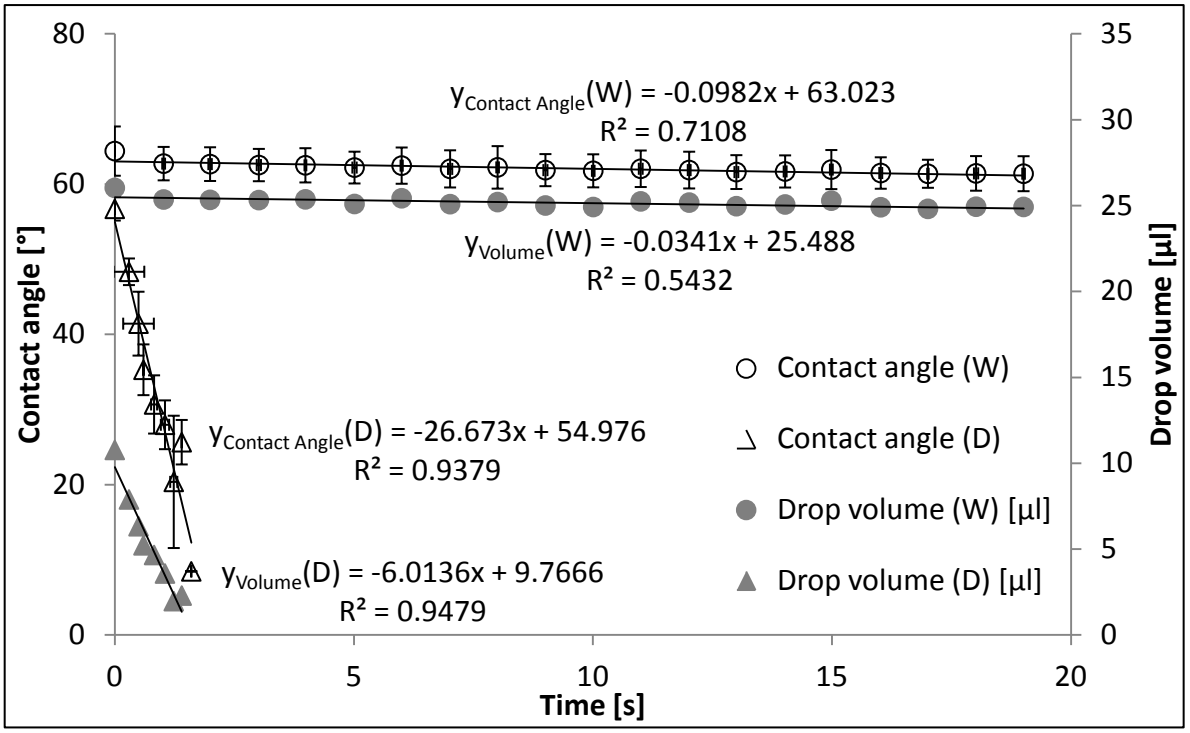

Figure 6-3 Typical contact angle and drop volume behaviour. SPI with water (W) and diiodomethane (D) (error bars represent SD (n≥6) and lines represent linear relationship).

6.4.3 Water Contact Angle Analysis

6.4.3.1 Effect of Treatment on the Water Contact Angle of Soy Materials

The initial water contact angle for all soy materials and treatments is summarized in Table 6-5. Hydrophilic surface properties (contact angle < 90 °) were observed for all soy materials irrespective of the treatment. In contrast, literature values reported for the contact angle of polypropylene (PP), a potential polymeric matrix of composite materials, has hydrophobic characteristics with contact angle ranging between 87.5 ° and 117 ° according to the PP type and the method for estimation [187]. Untreated soy materials possess different initial water contact angle. Statistically significantly higher initial water contact angle was obtained for the reference materials, SPI and SH, when compared to soy flour suggesting that soy flour has unique initial water contact angle that does not represent the contribution of its two major components, proteins and carbohydrates. IS also had a statistically significantly higher initial water contact angle when compared to soy flour.

The effects of the treatments were different according to the type of soy material. The autoclave treatment had negligible effect on the initial water contact angle of soy flour and soy hulls compacts but caused the most dramatic decrease for SPI (23 % decrease). The autoclave treatment may have led to protein denaturation such that the relative content of

carboxyl groups increased [190]. Alternatively, deamidation could have occurred resulting in increased carboxyl groups due to the substitution of the side chains in the asparagine and glutamine amino acid constituents of proteins with carboxyl groups [159, 160]. Potassium permanganate treatment of SF and SPI showed significant increase in initial water contact angle compared to untreated SF, 22 % increase for SF and 33 % increase for SPI. A moderate increase was observed for IS. In contrast, potassium permanganate treatment decreased the initial contact angle for soy hulls. The increase in initial contact angle for potassium permanganate treated materials could be due to redox-reactions that reduce the number of hydroxyl groups [132].

These results indicate that the effect of the treatments investigated in this study appear to be related to the protein content of the soy material. As the protein content increases, the potassium permanganate treatment resulted in higher initial water contact angle. The opposite effect was observed for the autoclave treatment: with increasing protein content, the autoclave treatment resulted in lower initial water contact angle.

Table 6-5 Protein content, water contact angle and relative change of initial water contact angle according to soy material and treatment (±SD, n≥6).

Soy material (treatment)	Protein [wt-%]	Contact angle [°]	Change [%]#
SF	48.3 ±0.39	57.1 ±2.2*	0
SF (auto)	50.5 ±1.45	54.1 ±3.3*	-5.3
SF ($KMnO_4$)	50.0 ±1.12	69.6 ±3.7	21.9
IS	47.9 ±0.03	74.3 ±1.0	0
IS (auto)	48.3 ±0.19	62.1 ±2.4	-16.4
IS ($KMnO_4$)	43.9 ±2.84	80.8 ±1.7*	8.8
SPI	85.0 ±3.28	64.4 ±3.3	0
SPI (auto)	89.1 ±1.25	49.4 ±4.1*	-23.3
SPI ($KMnO_4$)	88.5 ±0.40	85.7 ±2.1*	33.2
SH	12.1 ±2.68	84.7 ±1.1*	0
SH (auto)	15.7 ±0.06	76.4 ±6.7	-9.8
SH ($KMnO_4$)	15.3 ±0.59	80.3 ±4.9*	-5.2

*Statistically different compared to corresponding material and no treatment (α=0.05)
#Estimated as % difference compared to untreated soy material. Negative values indicate decrease in contact angle and positive values indicate increase in contact angle when compared to respective untreated soy material

The apparent rate of water absorption, obtained from the linear portion of the evolution with time of contact angle during the first five seconds (Table 6-6), also differed according to soy material and treatment. SF displayed a moderate apparent rate of water absorption

(-1.04 °/s) comparable to IS (-1.29 °/s). SH had a significantly high apparent rate of water absorption (-5.76 °/s) while SPI had a low apparent rate of water absorption (-0.40 °/s).

The apparent rate of water absorption for the autoclave treated soy materials increased for SF, SPI and IS while decreased for SH, the cellulose containing soy material. Autoclaving SPI altered significantly the water-material interactions, with the highest apparent rate of water absorption (-46.53 °/s) representing 115 times the rate of water absorption for the non-treated SPI. This suggests that the protein component is sensitive to the autoclave treatment and results in increased water interaction after the treatment.

The potassium permanganate treatment decreased the apparent rate of water absorption for all materials indicating a decrease in water-material interactions. Potassium permanganate treatment did not show a direct correlation with either the protein or the cellulose components present in soy flour. One possible reason could be the oxidation of functional groups due to potassium permanganate treatment. This behaviour is quite surprising since potassium permanganate is known to be a mild oxidizing reagent and is able to degrade cellulose [131, 191, 192]. A possible explanation could be the limited accessibility to the cellulose contained in the soy material by the potassium permanganate.

Table 6-6 Protein content, apparent rate of water absorption and relative change of apparent rate of water absorption (±SD)

Soy material (treatment)	**Protein [wt-%] (n=2)**	**Apparent rate of water absorption [°/s] (n≥6)**	**Change [%]#**
SF	48.3 ±0.39	-1.04 ±0.1	0
SF (auto)	50.5 ±1.45	-2.04 ±0.9	95.6
SF ($KMnO_4$)	50.0 ±1.12	-0.17 ±0.1	-83.7
IS	47.9 ±0.03	-1.29 ±0.8	0
IS (auto)	48.3 ±0.19	-64.41 ±12.3*	4897.2
IS ($KMnO_4$)	43.9 ±2.84	-1.40 ±0.7	8.5
SPI	85.0 ±3.28	-0.40 ±0.3	0
SPI (auto)	89.1 ±1.25	-46.53 ±9.7*	11529.7
SPI ($KMnO_4$)	88.5 ±0.40	-0.28 ±0.2	-30.9
SH	12.1 ±2.68	-5.76 ±1.4	0
SH (auto)	15.7 ±0.06	-3.12 ±0.8	-62.7
SH ($KMnO_4$)	15.3 ±0.59	-3.80 ±0.7	-54.5

*Statistical different compared to corresponding material and no treatment ($\alpha = 0.05$)

#Estimated as % difference compared to untreated soy material. Negative values indicate decrease in contact angle and positive values indicate increase in contact angle when compared to respective untreated soy material

6.4.4 Surface Energy of Soy Materials

The surface energy of treated soy materials was estimated from the contact angle measurements of the material pressed in compacts. Two liquids were selected, water and diiodomethane, such that estimation of the material interactions with each liquid could be obtained. It has to be pointed out that the surface energy values for powder materials are relative estimates as these measures are affected by the preparation procedure (e.g. pressure used for pressing compacts). Moreover, since soy materials are very hydrophilic, absorption of the liquids was quick and occurred over a very short time which was much more pronounced for diiodomethane.

The surface energy and its changes due to $KMnO_4$ and autoclaving treatments for soy materials, SF, SPI, SH, IS, is summarized in Table 6-7. The total surface energy remained relatively constant after the autoclave treatment (52 mN/m) but decreased for the $KMnO_4$ treatment (42.7 mN/m). The dispersive energy component remained relatively constant (30 mN/m), for all soy materials and treatments. In contrast, differences were obtained for the polar surface energy component. SPI treated with potassium permanganate had the lowest polar surface energy component (2.5 mN/m) while the autoclaved SPI showed the highest polar surface energy (23.6 mN/m). This difference indicates that the heat-treatment of soy protein due to autoclaving increased the polar surface energy component while the potassium permanganate treatment decreased the polar surface energy component. SF subjected to the potassium permanganate treatment showed a decrease in the polar surface energy by half while the autoclave treatment showed negligible effect. Autoclaving soy flour seemed to have no significant effect on the total surface energy and the dispersive and polar surface energy components. A possible explanation could be that the two major components (protein and cellulose) produce opposite effects during the autoclave treatment resulting in no net change of the chemical groups affecting the surface energy.

Table 6-7 Total, dispersive and polar surface energy for SF, SPI, SH and IS before and after potassium permanganate or autoclave treatment.

Soy material (treatment)	Initial contact angle (D) [°]	Initial contact angle (W) [°]	Dispersive surface energy [mN/m]	Polar surface energy [mN/m]	Total surface energy [mN/m]
SF	57.7 ±3.8*	57.1 ±2.2*	29.9*	18.4*	48.3*
SF (auto)	52.7 ±2.4	54.1 ±3.3*	32.8	18.9*	51.7*
SF ($KMnO_4$)	52.3 ±5.5	69.6 ±3.7	33.0	9.7	42.7
IS	56.4 ±1.4	74.3 ±1.0	30.7*	8.2	38.8*
IS (auto)	52.7 ±3.7	62.1 ±2.4	32.7	14.0	46.8
IS ($KMnO_4$)	44.6 ±5.7*	80.8 ±1.7*	37.2*	3.7*	40.9
SPI	56.7 ±1.6*	64.4 ±3.3	30.5*	13.6	44.1
SPI (auto)	58.1 ±2.8*	49.4 ±4.1*	29.7*	23.6*	53.2*
SPI ($KMnO_4$)	47.6 ±3.7	85.7 ±2.1*	35.6*	2.5*	38.1*
SH	46.3 ±0.9	84.7 ±1.1*	36.3*	2.7*	39.0*
SH (auto)	50.1 ±3.9	76.4 ±6.7	34.2	6.1	40.3
SH ($KMnO_4$)	53.0 ±2.4	80.3 ±4.9*	32.6	4.9*	37.5*

*Statistical significant $\alpha = 0.05$

A correlation was observed between the protein content of the soy materials and the polar surface energy component (Figure 6-4) showing increasing polar component of the surface energy with increasing protein content for the autoclave treatment ($R^2 = 0.9101$). No such correlation was observed for the potassium permanganate treatment ($R^2 = 0.0908$).

As the total surface energy of PP reported in literature range between 25.7 and 38.1 mN/m, with the polar surface energy as the main contributing fraction (up to 100 %)[187], the soy materials and treatments that best match the PP surface energy characteristics are soy flour and insoluble soy subjected to potassium permanganate treatment.

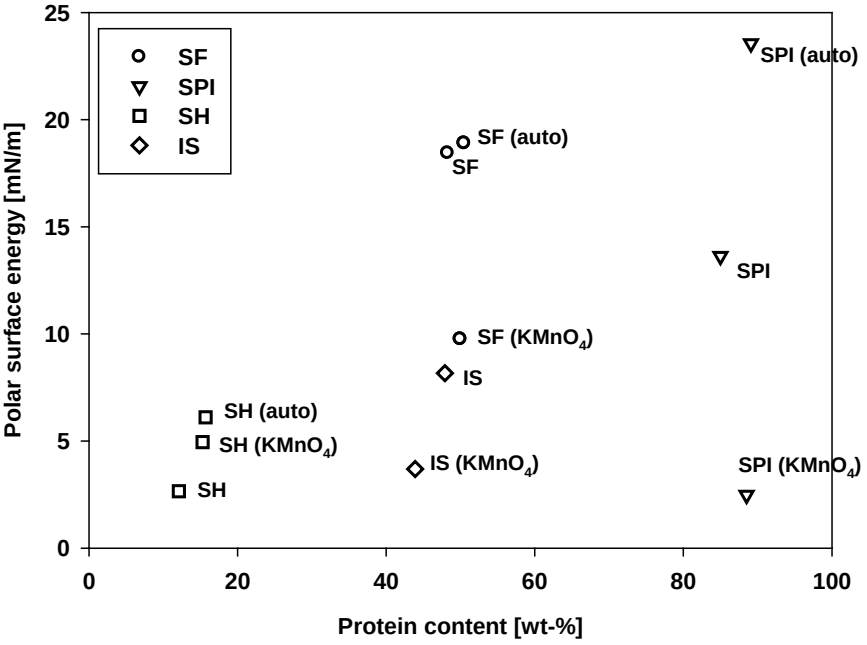

Figure 6-4 Polar surface energy vs. protein content of soy materials (SF, SPI, SH and IS) before and after potassium permanganate or autoclave treatment.

6.4.5 Interfacial Energy and Work of Adhesion

The interfacial energy (Equation 4-7) as well as the work of adhesion (Equation 4-6) were calculated using the initial water contact angle values and the surface energy value found in literature for polypropylene (30.1 mN/m (non-polar)) [187] as presented in Table 6-8. The behaviour and the effect of the treatments on the interfacial energy were identical to the surface energy. The autoclave treatment increased the interfacial energy of the soy materials while the potassium permanganate treatment decreased. The degree of change is the lowest for SH and the highest for SPI. The initial work of adhesion follows the same trend as the interfacial energy.

Table 6-8 Initial work of adhesion and interfacial energy of soy materials

Soy Material	Initial Work of Adhesion [mN/m]	Change [%]*	Interfacial energy [mN/m]	Change [%]*
SF	112.4	0.0	18.4	0.0
SF (auto)	115.5	2.8	19.0	2.8
SF ($KMnO_4$)	98.2	-12.6	9.8	-46.8
IS	92.5	0.0	8.2	0.0
IS (auto)	106.9	15.5	14.1	72.2
IS ($KMnO_4$)	84.4	-8.8	4.1	-50.2
SPI	104.3	0.0	13.6	0.0
SPI (auto)	120.2	15.2	23.6	72.8
SPI ($KMnO_4$)	78.2	-25.0	2.7	-80.1
SH	79.5	0.0	2.9	0.0
SH (auto)	89.9	13.0	6.2	111.6
SH ($KMnO_4$)	85.1	7.0	5.0	69.5

***Estimated as % difference compared to untreated soy material**

6.5 Conclusions

Extensive contact angle analysis and surface energy characterization were conducted for compacts of soy flour, two reference soy materials, soy protein isolate (protein reference material) and soy hulls (carbohydrate reference material), and insoluble soy, the residue obtained after alkaline treatment of soy flour and subjected to potassium permanganate and autoclave treatments. Significant differences were observed for the initial water contact angle, apparent rate of water absorption and dispersive and polar surface energy. Untreated soy flour compacts had an initial water contact angle similar to soy protein isolate compacts (57 °) but significantly lower than insoluble soy compacts (74 °) and soy hulls compacts (85 °). The potassium permanganate oxidation treatment increased the initial water contact angle of soy flour compacts (70 °), soy protein isolate compacts and insoluble soy residue compacts (81 °) but not for soy hulls compacts. The apparent rate of water absorption, after potassium permanganate treatment, decreased for three types of soy compacts but remained constant for insoluble soy. Autoclave treatment did not affect the initial water contact angle of soy flour and soy hulls compacts but increased significantly for soy protein isolates and insoluble soy compacts.

The effect of autoclave treatment was related to the apparent rate of water absorption where significant increase, but with different magnitude, was measured according to the type of compact. Total surface energy and the dispersive and polar constituents, estimated from water and diiodomethane contact angle, indicated that the dispersive surface energy was

similar for soy flour, soy protein isolate and insoluble soy compacts (30 mN/m) and higher for soy hulls (36 mN/m). Significant differences of the polar surface energy according to compacts was obtained, 18.4 mN/m (soy flour), 13.6 mN/m (soy protein isolate), 8.2 mN/m (insoluble soy) and 2.7 mN/m (soy hulls). Potassium permanganate oxidation treatment reduced significantly the polar surface energy of all soy materials compacts except soy hulls which increased. In contrast, autoclave treatment did not affect the polar surface component of soy flour but increased for all other soy materials compacts. The most appropriate surface properties based on the contact angle analysis for compatibility with hydrophobic polymeric materials appear to be soy flour or insoluble soy subjected to potassium permanganate.

Further work will assess the compatibility of the modified soy materials with polymer and the mechanical properties of these composite materials.

6.6 Acknowledgements

The authors thank Dr. Peldszus at the University of Waterloo for the use of the contact angle instrument, Dr. Boxin Zhao for his time for discussing the results, Priscilla Lai and Steven Zhan for their work on the contact angle analysis, and Bunge and ADM for providing soy materials. Financial support from Grain Farmers of Ontario (formerly Ontario Soybean Growers), NSERC (Natural Sciences and Engineering Research Council of Canada) and Ontario Research Fund (BioCar) are gratefully recognized.

7. Mechanical Properties and Crack Propagation of Soy-Polypropylene Composites

7.1 Outline

Composites from soy flour (SF) and polypropylene (PP) exhibited improved impact and flexural properties when treated with potassium permanganate ($KMnO_4$) or when subjected to autoclave treatment with the addition of the coupling agent maleic anhydride. $KMnO_4$ is known to increase carbonyl and carboxyl groups that lead to a trans-crystalline effect when compounded with polypropylene. The increase in impact strength for the $KMnO_4$ treated SF composites when compared to composites with untreated SF was at least 14 %. The flexural strength increased by at least 13 % and flexural modulus increased at least 23 %. The composites with autoclave treated SF increased their impact strength by at least 18 % when the coupling agent maleic anhydride was present, and flexural properties increased nearly 13 %. These two SF composite materials showed an increase in impact and flexural modulus which differs from most materials where one property is improved but the other property is reduced. Scanning electron micrographs suggested different mechanisms for crack propagation according to soy material treatment and presence and type of coupling agent. Untreated SF showed poor bonding with the matrix whereas SF ($KMnO_4$ treatment) had partial bonding. SF (autoclave treatment) combined with coupling agent (Orevac CA100) revealed a good bonding between SF and matrix.

7.2 Introduction

Composites in automotive applications are used in the exterior and interior parts. The main advantage of agricultural fillers for the preparation of composites is their light weight due to their low density in comparison to mineral fillers (calcium carbonate, talc) or inorganic fibers (glass fiber). Many studies have been conducted on composites with polyolefins containing a range of agricultural fillers [1, 23, 65-67]. Most fillers are selected because of their high cellulose content and structural features. Soy meal represents a different category of filler. This material has negligible structural features and its main constituents are proteins (40-50 %) and carbohydrates (30 %).

When developing composites from agricultural fillers and polyolefins, their incompatibility due to different surface properties remains a major challenge. Fillers derived from agricultural resources are hydrophilic because of their composition (cellulose, hemicellulose, lignin, protein). Polyolefins on the other hand are hydrophobic. Therefore

the two materials are difficult to mix and have little interaction resulting in poor mechanical properties [121, 162, 178]. Surface modification and the addition of coupling agents are known to improve the interaction between surfaces of two materials by creating chemical bonds [43, 46, 90, 121]. Surface modifications that alter the properties of the materials can be chemical or physical and can target the filler or the polymer matrix [43, 46, 179-182]. Combinations of two or more treatments are also possible [75, 121, 130]. Most of the approaches developed for agricultural materials have focussed on high cellulose and/or lignin agricultural materials and have shown to be inefficient when applied to soy flour, milled soy meal [20]. Alternative approaches should be developed that consider the protein content of soy flour and improve their thermal stability as well as the impact properties of the composites. When improving the toughness of a material, often the flexibility needs to be sacrificed because both properties generally will behave as “mutually exclusive” [17]. However, a few materials exist where both properties are mutually inclusive. The most advanced examples of such materials are found in natural materials and contain highly ordered structures, at multiple scales, from nano, to micro and macro scale [17].

Chemical and thermal treatments of natural materials have been considered for the development of high performance materials or biorefineries [193] and the improvement of nutritional characteristics of food products. Oxidation by potassium permanganate is a well-established treatment in the paper industry that increases carbonyl and carboxyl groups [131]. Heat treatment has been extensively studied for the improvement of the nutritional value of soy products, e. g. soy flours, grits and proteins [28].

In this study, the contribution of coupling agents, soy flour treatment and soy flour constituents on the mechanical properties of soy-polypropylene composites was investigated. Correlations between impact strength and flexural modulus were identified. Scanning electron microscopy imaging revealed differences of the interaction between soy materials and polypropylene. Proposed crack propagation mechanisms were developed based on the material imaging.

7.3 Materials and Methods

7.3.1 Materials

Defatted soy meal and soy hulls (SH) were obtained from Bunge Inc. (Hamilton, Canada). Soy protein isolate (SPI (c)) ProFam 974 was obtained from Archer Daniels Midland (ADM) Company (Decatur, USA).

7.3.2 Preparation of Soy Materials

7.3.2.1 Soy Flour Processing

Soy flour (SF) was obtained by milling soy meal, with an ultracentrifugal mill ZM200 (Retsch GmbH, Germany) and 0.08 mm sieve with trapezoid shaped holes (part # 03.647.0231).

Coupling agents listed in

Table 7-1 were used for the first set of composites prepared with 30 % SF (20 % minimum content requirement for bioproducts) and 0.5 % Irganox 1010. These materials were donated by Clariant, Arkema, AddComp and DuPont.

Figure 7-1 shows a diagram of the soy flour processing with the corresponding intermediate products. After milling of the soy meal, an aqueous mixture was prepared with soy flour and milli-Q water and pH adjusted to 9.0 with 1M NaOH. The mixture was heated to 50 °C under stirring on a magnetic stirrer for one hour. The mixture was centrifuged at 10 000 rpm (RCF_{max} = 11 200) for 20 minutes (Sorvall WX 100 with A-621 rotor, Thermo Scientific, USA) and the solid residue (insoluble fraction (IS)) was dried at room temperature in a fume hood (relative humidity (RH)<20 %). The supernatant, containing mostly proteins, sugars and minerals, was adjusted with 1M H_2SO_4 (95-98 %, GR ACS, Fisher Scientific, Canada) to pH 4, just below the isoelectric point of the major soy proteins (glycinin and conglycinin) and centrifuged at 10 000 rpm. The resulting precipitate is referred to as soy protein isolate (SPI (ex)). The remaining liquid solution, containing mostly sugars and minerals, was called soluble sugar extract (SSE).

Table 7-1 Coupling agents used for composites with manufacturer details

Coupling Agent (Manufacturer, Reference)	**Composition**	**Visc./170 °C [mPa*s]**	**Crystallinity**
Licocene 1602 (Clariant, [194])	PP copolymer	700	low
Licocene 1332 TP (Clariant, [194])	PP, MAH grafted	300	low
Licocene 3262Si (Clariant, [194])	PP with high degree of grafted comonomer: Trimethoxy vinyl silane	60	medium
Licocene 6252 (Clariant, [194])	PP, MAH grafted	100	high
Priex 20097 (Addcomp Holland BV, [195])	PP homopolymer, MAH	N/A	N/A
Orevac CA100 (Arkema, [196])	PP with high MAH content	N/A	N/A
Fusabond 353D (DuPont, [197])	PP with very High MAH grafting	N/A	N/A

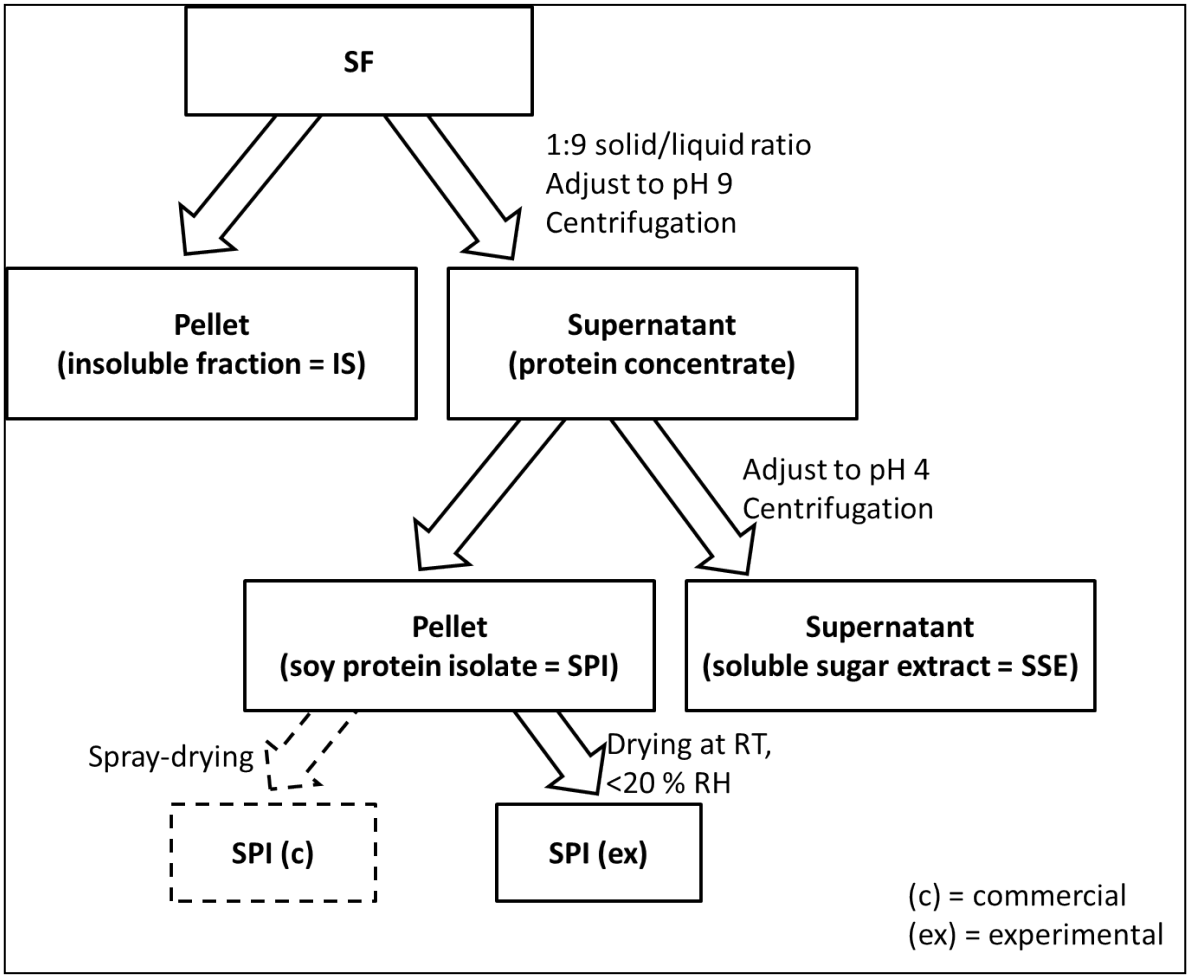

Figure 7-1 Diagram of soy flour (SF) processing for fractionation of the water insoluble fraction (IS), acid precipitated soy protein isolate (SPI) and the water soluble sugars (SSE).

Prior to their use or treatment and after treatment, the soy materials were milled with a ZM 200 ultracentrifugal mill (Retsch GmbH) and sieved with trapezoid shaped 0.08 mm holes (part # 03.647.0231) with the exception of SPI (c) that did not require milling because its particle size was already below 0.08 mm and therefore was used as received. After treatment the soy materials were dried in a fume hood (RH<20 %) at room temperature (RT) until their moisture content was below 5 %.

7.3.2.2 Autoclave Treatment

The soy material (~500 g), placed on a glass tray resulting in a material height less than one centimeter, was put in a direct steam heated sterilizer-autoclave for sterilization of biological materials (Consolidated Stills & Sterilizers, USA) and subjected to 125 °C and steam for 25 minutes. The treated soy material was then dried and milled as described previously.

7.3.2.3 Potassium Permanganate ($KMnO_4$) Chemical Treatment

An aqueous solution containing potassium permanganate ($KMnO_4$, GR ACS, EMD, USA) was prepared with a $KMnO_4$ to soy material 1:2 mass ratio. The volume of water added was adjusted until it was possible to fully mix the water-filler blend. The mass ratios are summarized in Table 7-2. The soy material was soaked at room temperature in the $KMnO_4$ aqueous solution and stirred manually with a spatula until the mixture was homogenous (at least 5 minutes). The mixture was then dried at room temperature and <20 % RH and milled as described previously.

Table 7-2 Mass ratios of water, soy material and $KMnO_4$ for treatment.

Soy material	Parts water	Parts soy material	Parts $KMnO_4$
SF	6	2	1
IS	12	2	1
SPI	20	2	1
SH	6	2	1

7.3.2.4 Chemical Composition

The ash, cellulose, hemicellulose, lignin and fat content analysis of the soy materials were carried out according to AOAC methods and performed by Agri-Food Laboratories, Guelph, Canada. The ash content was determined by the AOAC 942.05 method, lignin by the ANKOM filter bag modified method of AOAC 973.18, protein content by the combustion method AOAC 990.03 and oil content by the AOAC 920.39 method.

Cellulose was obtained by subtracting lignin from acid detergent fiber (ADF). Hemicellulose was obtained by subtracting ADF from neutral detergent fiber (NDF).

Table 7-3 Chemical composition of soy materials before treatment.

Material	**Protein (Nx6.25) [wt-%]**	**Ash [wt-%]**	**Cellulose [wt-%]**	**Hemicellulose [wt-%]**	**Lignin [wt-%]**	**Fat [wt-%]**	**Other* [%]**
SF	47.6	6.2	6.9	1.5	0.03	1.5	36.3
IS	45.9	N/A	10.4	10.2	6.0	N/A	27.5
SPI (c)**	<90.0	<5.0	N/A	N/A	N/A	4.0	1.0
SH	12.6	4.5	32.1	23.7	7.5	N/A	19.7

*Other are mainly sugars other than cellulose and hemicellulose (e.g. pectin, starch)
**reported values obtained from ADM [170]

7.3.2.5 Composite Preparation

EXTRUSION

For the first set of composites with different coupling agents, the polypropylene matrix, a blend of homo- and co-polymer, was pre-extruded with the coupling agent and 0.5 % Irganox 1010 in a Haake MiniLab twin-screw micro compounder (Thermo Electron Corporation, USA) at 190 °C and 40 rpm. For all other composites, the polypropylene blend was extruded with 0.5 % Irganox 1010 at 190 °C and 90 rpm in a Haake Rheomex 252 single-screw extruder with Haake Rheocord 90 Fisons (Thermo Electron Corporation, USA) and pelletized with a Berlyn pelletizer Model HVI (The Berlyn Corporation, USA). For the compounding of the composites, a Haake MiniLab twin-screw micro compounder (Thermo Electron Corporation, USA) was used at 190 °C and 40 rpm. The filler content for all composites was 30 wt-%.

INJECTION MOULDING

The extruded pellets were pressed into bars by using an injection moulding apparatus from Ray-Ran. The barrel temperature was set at 190 °C and the mould temperature 50 °C. The dimensions of the bars were according to ASTM (length 63.5 ±0.2 mm, width 12.7 ±0.2 mm, depth 3.3 ±0.2 mm) [108, 109].

ANNEALING AND CONDITIONING

Before testing, the bars were placed in an oven 5890A GC (Hewlett Packard, USA) with an initial temperature of 31 °C and heated 10 °C/min until the final temperature of 151 °C was reached. The final temperature was kept constant for 10 minutes before cooling to room temperature.

After annealing, the bars were left at least 48 hours in an environmental chamber at 50 % RH and 23 °C (model MLR-351H, Sanyo Electric Co., Ltd., USA).

7.3.2.6 Composite Testing

For the pre-screening of the different materials, two of the most common tests conducted on automotive parts were selected: Three-point bending and Izod impact test. After the identification of the most promising materials, additional tests such as tensile test, water absorption and dynamic mechanical analysis will have to be conducted.

THREE-POINT-BENDING (ASTM D 790)

The testing was performed after annealing and conditioning of the bars as described previously. A flexural property instrument (Actuator model 120Q1000, TestResources,

Inc., USA), was used. For each material, at least five samples were tested and an average was calculated as well as the standard deviation. The reported flexural strength is the maximum point of the stress/strain curve. The flexural modulus represents the slope of the first linear part of the stress/strain curve.

NOTCHED IZOD IMPACT TEST (ASTM D 256)

After notching (for Izod impact), annealing and conditioning the bars were tested for Izod impact strength and flexural properties. For Izod impact testing monitor impact tester model 43-02-01 (TestResources, Inc., USA) was used (50 % RH and 23 °C). The testing was performed after notching with specimen notch cutter XQZ-I (Chengde JinJian Testing Instrument Co., Ltd., China), annealing and conditioning of the bars as described above. For each material at least five samples were tested and an average was calculated as well as the standard deviation.

DIFFERENTIAL SCANNING CALORIMETRY (DSC)

Differential scanning calorimetry (DSC) was used for the analysis of crystallinity in the polymer composites and the melting and crystallization peaks. When DSC is performed in the dynamic mode, the area under the peak represents the energy for the crystallization of the composite which gives a measure of the degree of crystallization of the polymer. The total crystallinity represents the ratio between the crystalline and the amorphous region of the polymer.

DSC was performed with the differential scanning calorimeter Q2000 (TA Instruments – Waters LLC, USA). The materials were placed in aluminum Tzero™ pans and heated in a nitrogen purged chamber from 35 to 200 °C at a rate of 10 °C/min. The analysis of the data (heat flow [W/g] vs. temperature [°C]) was carried out with the software Universal Analysis 2000 4.5A and the linear integration method (TA Instruments – Waters LLC, USA).

7.3.2.7 Field Emission Scanning Electron Microscopy (FESEM)

Samples from Izod impact testing were gold coated in argon with a gold coating unit Desk II (Denton Vacuum, USA). Electron microscopic images were obtained with the Gemini Leo 1550 FESEM (Carl Zeiss AG, Germany) with EDAX Genesis 5.2 (Ametek Inc., USA). The working parameters for the FESEM were 12 kV and the secondary electron signal (SE2).

7.3.2.8 Statistical Analysis

The t-test was used for data analysis of significances between mean values of set of samples. The confidence interval was determined at a significance level of $\alpha = 0.05$.

7.4 Results and Discussion

The independent and combined contribution of coupling agent, and soy treatment on the notched Izod impact and flexural properties for SF composites (30 % soy flour 0.5 % of Irganox 1010) were investigated. The relationship between impact strength and flexural modulus was also evaluated. The contribution of the two major constituents of soy flour, proteins as soy protein isolate (SPI) and carbohydrates as soy hulls (SH), will also be reported. Their mechanical properties will be discussed in the context of composite morphology and crack propagation.

7.4.1 Effect of Coupling Agents on the Mechanical Properties of Soy Flour Composites

The effect of the nature of coupling agents on the mechanical properties of soy flour composites is reported in Table 7-4. All composite materials showed impact strength within a narrow range, between 18.5 and 21.9 J/m. Significantly different impact values of the composites ($\alpha = 0.05$) were observed for Licocene 1602, Licocene 1332, Licocene 3262Si and Orevac CA100. The most significant increase in impact strength (8 % when compared to no coupling agent addition) was observed for the composite material prepared with Orevac CA100 (21.9 J/m) whereas the highest decrease in impact strength (9 % when compared to no coupling agent addition) was observed for the composite material prepared with Licocene 1332 (18.5 J/m). Both coupling agents are maleic anhydride grafted polypropylene but developed for different applications. Licocene 1332 was developed for adhesives and emulsions [194] whereas Orevac CA100 was developed for composites with agricultural fillers [196]. Priex 20097 and Fusabond 353D are also coupling agents developed for improving the compatibility between agricultural fillers and polyolefins. The effect of these two coupling agent was observed for the flexural strength. The increase in flexural strength was between 3.6 % (Licocene 1602) and 16.5 % (Priex 20097, Fusabond 353D) when compared to the composite with no coupling agent. The flexural modulus for the composites with the addition of coupling agents ranged between 1408 MPa (Licocene 1332) and 1607 MPa (Licocene 6252) which is a significant increase (14.6 %).

Based on this analysis, the best and the worst coupling agent, Orevac CA100 and Licocene 1332, were selected for further study when combined with soy flour subjected to autoclave and potassium permanganate treatment.

Table 7-4 Effect of coupling agent on the notched Izod impact strength, flexural strength and flexural modulus of composites (±SD, n≥5) containing 30 % SF, 0.5 % Irganox 1010

Coupling Agent	Notched Izod Impact [J/m]	Change [%]#	Flexural Strength [MPa]	Change [%]#	Flexural Modulus [MPa]	Change [%]#
PP blend (single-screw)	50.0 ±1.8	-	45.4 ±2.5	-	1124.7 ±57.0	-
None (SF (twin-screw))	20.3 ±0.9	0	36.4 ±2.5*	0	1402.8 ±97.9	0
Licocene 1602	19.1 ±0.5*	-5.9	37.7 ± 2.0	3.6	1463.8 ±53.0	4.3
Licocene 1332	18.5 ±3.2*	-8.9	38.1 ±0.6	4.7	1408.1 ±31.9	0.4
Licocene 3262Si	21.6 ±1.4*	6.4	38.0 ±1.3	4.4	1426.4 ±75.3	1.7
Licocene 6252	20.4 ±3.6	0.5	42.0 ±1.3	15.4	1607.1 ±79.1*	14.6
Priex 20097	21.0 ±2.9	3.4	42.4 ±1.4*	16.5	1438.1 ±137.6	2.5
Orevac CA100	21.9 ±0.8*	7.9	41.4 ±1.1	13.7	1420.6 ±42.5	1.3
Fusabond 353D	21.1 ±2.6	3.9	42.4 ±1.3*	16.5	1498.8 ±91.6	6.8

*Significance at $\alpha = 0.05$ when compared to composites with SF and no coupling agent
#Compared to SF with no coupling agent

7.4.2 Effect of Soy Flour Treatment on the Mechanical Properties of Composites

Composites with soy flour subjected to potassium permanganate and autoclave treatment were prepared with no coupling agent (only addition of 0.5 % Irganox 1010 as anti-oxidant). The impact strength, flexural strength and flexural modulus properties are presented in Table 7-5. The impact strength of the composite varied between 18.0 J/m for SF (auto) and 22.6 J/m for SF ($KMnO_4$), thus corresponding to an increase of 14.1 % when compared to the composite with untreated SF. The drop in impact strength for SF (auto) is most likely due to the increased hydrophilicity (increased rate of water absorption, Table 6-5, chapter 1) which results in a higher incompatibility with the hydrophobic matrix. SF ($KMnO_4$), on the other hand, showed a remarkable increase in impact strength which might be due to change of surface properties (rate of water absorption) and decrease polar energy surface composition (Table 6-6, chapter 1) or the formation of a trans-crystalline phase between the soy filler and the polypropylene matrix [16, 166].

The flexural strength and moduli of elasticity increased for all composites with treated SF. The composite with SF (auto) showed an increase flexural modulus by more than 32 % when compared to untreated SF. The composite SF ($KMnO_4$) showed an increase flexural modulus by at least 23 % when compared to untreated SF. The composite with SF

($KMnO_4$) is the only material where all properties tested was improved, suggesting the development of a multi-scale structure.

Table 7-5 Notched Izod impact strength, flexural strength and flexural modulus of composites (±SD, n≥5) containing 30 % of different treated SF

Soy Flour (Treatment)	Notched Izod Impact [J/m]	Change [%]#	Flexural Strength [MPa]	Change [%]#	Flexural Modulus [MPa]	Change [%]#
SF (single-screw)	19.8 ±0.6	0	34.4 ±0.4	0	1173.1 ±24.1*	0
SF (auto)	18.0 ±0.5*	-9.1	38.8 ±4.4*	12.8	1553.4 ±207.0*	32.4
SF ($KMnO_4$)	22.6 ±0.6*	14.1	39.0 ±1.6*	13.4	1445.6 ±73.1*	23.2

#Change to SF

*Statistical significance at $\alpha = 0.05$

7.4.3 Effect of Soy Flour Treatment and Coupling Agent on the Properties of Composites

Composites prepared with SF subjected to autoclave treatment (SF (auto)) and potassium permanganate treatment (SF ($KMnO_4$)) and two selected coupling agents (Orevac CA100 and Licocene 1332) were prepared and tested for Izod impact strength and flexural properties. The effect of individual and combinations of the two treatments, was also investigated, (a) SF (auto) subsequently subjected to $KMnO_4$ treatment (b) SF ($KMnO_4$) subsequently subjected to autoclave treatment, (c) SF in $KMnO_4$ solution subjected to the autoclave (Table 7-6). The addition of coupling agents to SF (auto) increased the impact strength. The highest increase was obtained with the addition of Orevac CA100 (18.3 %). Flexural strength and flexural modulus were improved only for the composite with the addition of Orevac CA100. The addition of coupling agents to composites with SF ($KMnO_4$) decreased the impact strength up to 8.8 %. Similar behaviour as for SF (auto) was obtained for the flexural strength and flexural modulus where the addition of Licocene 1332 decreased the flexural strength while the addition of Orevac CA100 increased the flexural strength. Combining the two treatments resulted in decreased impact and flexural properties, which were more pronounced for the combination SF ($KMnO_4$, auto). The three different combinations of the two treatments resulted in lower impact strength when compared to SF with just one treatment but showed increased flexural properties. The autoclave treatment of SF ($KMnO_4$) and the potassium permanganate treatment of SF (auto) decreased their Izod impacts when compared to SF ($KMnO_4$) and SF (auto) respectively. The combination of the two treatments without an intermediate drying step (SF ($KMnO_4$ &

auto) had a decreased Izod impact when compared to SF ($KMnO_4$) but increased Izod impact when compared to SF (auto).

The improvement in impact properties for the composite with SF (auto) and coupling agent is most likely due to the change in surface chemistry caused by the autoclave treatment. Maleic anhydrides are known to bind to hydrophilic groups on filler surface and the hydrophobic matrix [73]. An increase in mechanical properties is pointing towards an increase in bonding between filler and matrix. Since Orevac CA100 was developed specifically as coupling agent for agricultural materials and polyolefins with high maleic anhydride content it is not surprising that the increase for this formulation was more pronounced [196]. The decrease in mechanical properties by the addition of coupling agents to the composite with SF ($KMnO_4$) may be due to a reduced trans-crystallinity effect, non-specific reactions of the coupling agent or covering the reactive groups on the filler surface with the coupling agent that is suggested by Araújo [166]. Since $KMnO_4$ is an oxidizing reagent that creates carbonyl and carboxyl groups [131], it is possible that these groups reacted with the matrix creating a trans-crystalline interface. When coupling agent was added, specific groups, that were able to chemically bind to the matrix, reacted already with the coupling agent and were not able to react anymore with the polypropylene [16, 166].

Table 7-6 Notched Izod impact strength, flexural strength and flexural modulus of composites (±SD, n=5) containing combinations of treated SF and coupling agents

Composite	Notched Izod Impact [J/m]	Change [%]#	Flexural Strength [MPa]	Change [%]#	Flexural Modulus [MPa]	Change [%]#
SF (single-screw)	19.8 ±0.6	0	34.4 ±0.4	0	1173.1 ±24.1	0
SF (auto) + Licocene 1332	19.7 ±0.6	-0.4	38.7 ±1.0	12.5	1457.9 ±88.1	24.3
SF (auto) + Orevac CA 100	21.3 ±0.6*	7.6	43.8 ±1.1*	27.3	1573.8 ±81.7*	34.2
SF ($KMnO_4$) + Licocene 1332	21.1 ±0.2*	6.7	33.7 ±0.9	-2.0	1237.6 ±76.1*	5.5
SF ($KMnO_4$) + Orevac CA 100	20.6 ±1.0	4.1	42.5 ±0.9*	23.5	1465.9 ±117.4	25.0
SF ($KMnO_4$, auto)	20.7 ±0.6	4.4	31.0 ±0.5*	-9.9	1233.5 ±38.4*	5.1
SF (auto, $KMnO_4$)	17.7 ±1.1*	-10.5	36.3 ±0.7	5.5	1392.4 ±85.6	18.7
SF ($KMnO_4$ & auto)	19.3 ±1.8	-2.3	34.7 ±0.7	0.9	1342.1 ±37.2	14.4

#Change relative to the treated SF with no coupling agent
*Statistical significance at $\alpha = 0.05$

7.4.4 Properties of Composites with Untreated and Treated Soy Materials

Composites were prepared with soy materials representing the major constituents of the soy flour, soy protein isolate (SPI) as protein constituent and soy hulls (SH) as carbohydrate constituent, and subjected to either potassium permanganate treatment or autoclave treatment (Table 7-7). The most significant improvement in impact strength (9.3 %) was obtained for the composite with SPI ($KMnO_4$). In contrast the same treatment on SH resulted in a 4.6 % decrease in impact strength. The autoclave treatment for SPI and SH resulted in slightly improved impact properties (0.5 % and 1.4 % respectively). The flexural properties of the composites with SPI and the two treatments decreased with a more pronounced decrease for SPI (auto) (6.4 % in flexural strength and 20.5 % in flexural modulus). In contrast, the composites with SH and the two treatments and IS ($KMnO_4$) improved flexural properties. The composite with IS ($KMnO_4$) improved its flexural strength up to 16.5 % and its flexural modulus up to 14.9 %. This improvement could be the effect of the combination of the alkaline and $KMnO_4$ treatment because potassium permanganate can have greater oxidation capabilities in alkaline conditions [198].

Table 7-7 Notched Izod impact strength, flexural strength and flexural modulus of composites (±SD, n=5) containing 30 % of untreated, autoclave treated and $KMnO_4$ treated SPI, SH and IS

Material	Notched Izod Impact [J/m]	Change [%]#	Flexural Strength [MPa]	Change [%]#	Flexural Modulus [MPa]	Change [%]#
IS	19.2 ±1.0*	0	32.1 ±0.8*	0	1155.2 ±39.7*	0
IS ($KMnO_4$)	20.0 ±0.8	4.2	37.4 ±0.6*	16.5	1327.1 ±48.8	14.9
SPI (c)	19.4 ±0.3*	0	34.4 ±0.9	0	1452.1 ±48.1*	0
SPI (auto)	19.5 ±1.0	0.5	32.2 ±0.6*	-6.4	1154.2 ±24.1*	-20.5
SPI ($KMnO_4$)	21.2 ±1.6	9.3	33.6 ±0.3*	-2.3	1193.5 ±18.4*	-17.8
SH	21.7 ±0.6*	0	34.3 ±0.8	0	1188.1 ±18.7*	0
SH (auto)	22.0 ±0.5*	1.4	37.4 ±0.6*	9.0	1327.1 ±48.8	11.7
SH ($KMnO_4$)	20.7 ±0.7	-4.6	36.2 ±0.5	5.5	1276.9 ±35.4	7.5

#Change relative to the given soy material with no treatment
*Statistical significance $\alpha = 0.05$

7.4.5 Melting Behaviour and Crystallinity

The crystallization and melting behaviour of the composite materials was studied by DSC analysis (Table 7-8). The melting peak of the polypropylene blend was at 163 °C and its degree of crystallinity was at 58 %. The melting peak of the composite materials ranged between 159.0 (SF) and 163.1 °C (SPI (auto)). The crystallization peak ranged from 116.8 °C (IS) and 121.3 °C (SPI ($KMnO_4$)). The degree of crystallinity of the composite materials ranged between 45.0 (SF (Orevac CA100)) and 49.9 % (for SPI ($KMnO_4$)).

Table 7-8 Melting and crystallization properties of composite materials

Material	Melting		Crystallization		Degree of Crystallinity [%]
	Peak [°C]	ΔH_m [J/g]	Peak [°C]	ΔH_c [J/g]	
PP blend	*163.1*	*119.4*	*119.5*	*120.8*	*57.8*
SF (Fusabond 353D)	159.9	70.9	119.3	72.5	49.5*
SF (Orevac CA100)	159.6	65.8	118.2	65.9	45.0*
SF (Priex 20097)	160.3	70.5	119.7	71.5	48.9*
SF (Licocene 1332)	160.6	82.1	117.8	70.5	48.2
SF (single-screw)	159.0	69.5	117.1	68.4	46.7*
SF (auto)	159.3	72.4	117.8	71.9	49.2*
SF ($KMnO_4$)	159.3	70.8	117.5	70.1	47.9
SF ($KMnO_4$) + Orevac CA100	160.9	73.3	120.0	70.9	48.4
SF (auto) + Orevac CA100	159.7	72.7	118.9	71.1	48.6
IS	160.0	72.5	116.8	69.6	47.6
IS ($KMnO_4$)	161.8	71.4	117.6	69.7	47.6
SPI	160.9	70.0	120.3	69.3	47.4
SPI (auto)	163.1	76.3	120.8	71.0	48.5
SPI ($KMnO_4$)	160.6	73.5	121.3	72.9	49.9*
SH	159.4	72.0	117.3	69.1	47.2*
SH (auto)	160.6	71.9	118.0	70.0	47.9
SH ($KMnO_4$)	160.9	67.7	117.2	69.1	47.2*

*Statistical significance $\alpha = 0.05$

7.4.6 Correlations between Toughness, Strength, Stiffness and Soy Surface Properties

The Izod impact strength is presented according to flexural modulus (Figure 7-2), protein content (Figure 7-3), initial water contact angle (Figure 7-4) and polar surface energy (Figure 7-5) for the composite materials. Generally composite materials will show an opposite relationship between impact and flexural properties, which means that by increasing one property, the other property will decrease and vice versa [24, 199]. This opposite effect is the consequence of the correlation of toughness and strength as well as stiffness which is considered contradictory [17]. Such a correlation has also been observed for polyesters and PTE [199, 200]. Therefore a trade-off must be made between toughness and elasticity to obtain the best suitable material for a specific application. An inversely proportional correlation was observed between the Izod impact strength and the flexural modulus, for most soy composites with the exception of SF ($KMnO_4$) and SF (auto) with Orevac CA100 (Figure 7-2). These two SF composite materials showed improved Izod impact strength with increased flexural moduli which could be due to a multi-level

structural organization of the soy filler [17]. No correlation was observed between the Izod impact strength and protein content (Figure 7-3) or soy material surface properties (Figure 7-4, Figure 7-5). Figure 7-6 shows the correlation between flexural modulus and contact angle. With the exception of SF and SPI (auto), there is a linear relationship between these two properties, suggesting that with increasing contact angle the flexural modulus decreases. The composite materials with the lowest flexural modulus have relatively high Izod impact properties and high contact angle values.

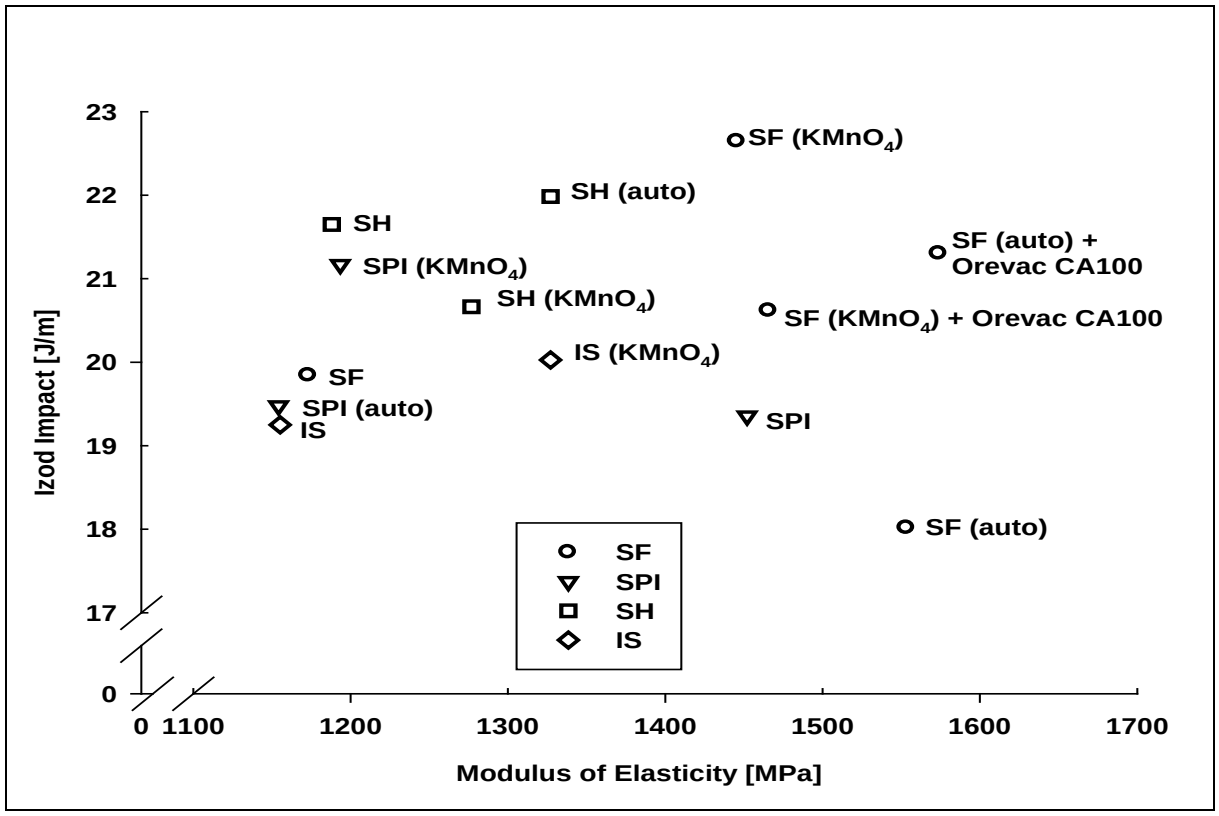

Figure 7-2 Correlation between Izod impact and flexural modulus of untreated and $KMnO_4$ and autoclave treated SF, SPI, SH and IS.

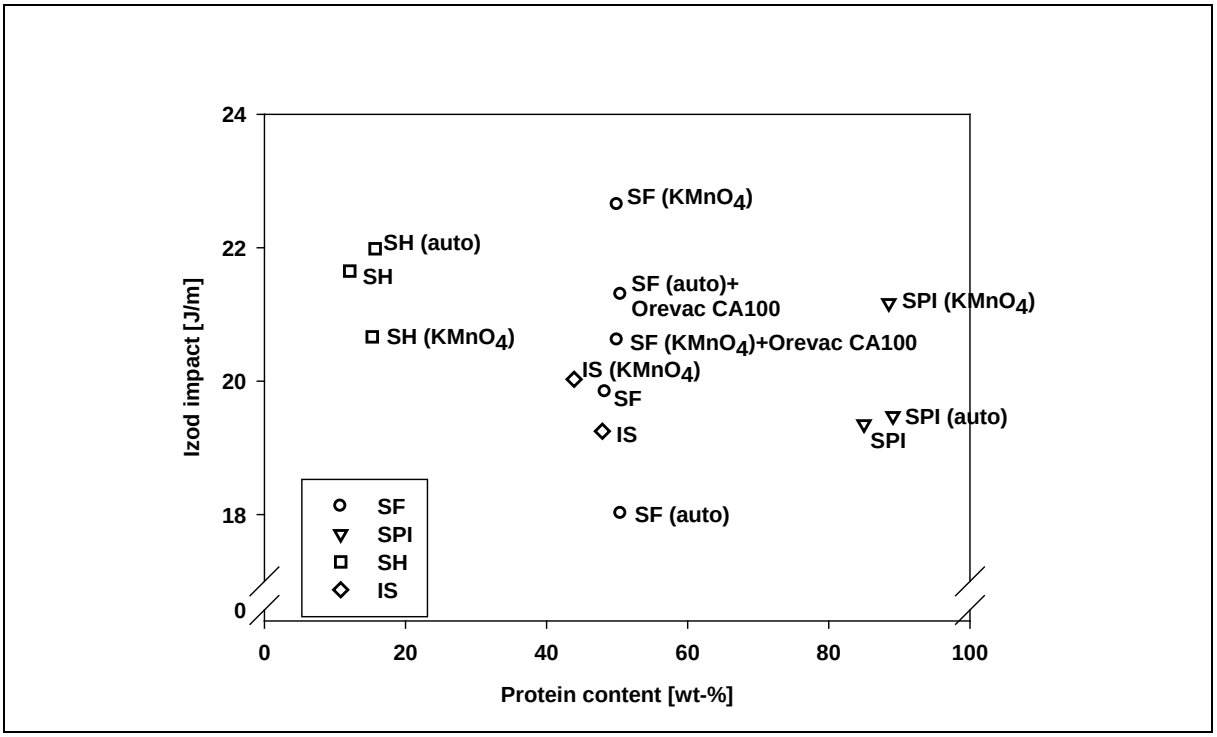

Figure 7-3 Izod impact vs. protein content

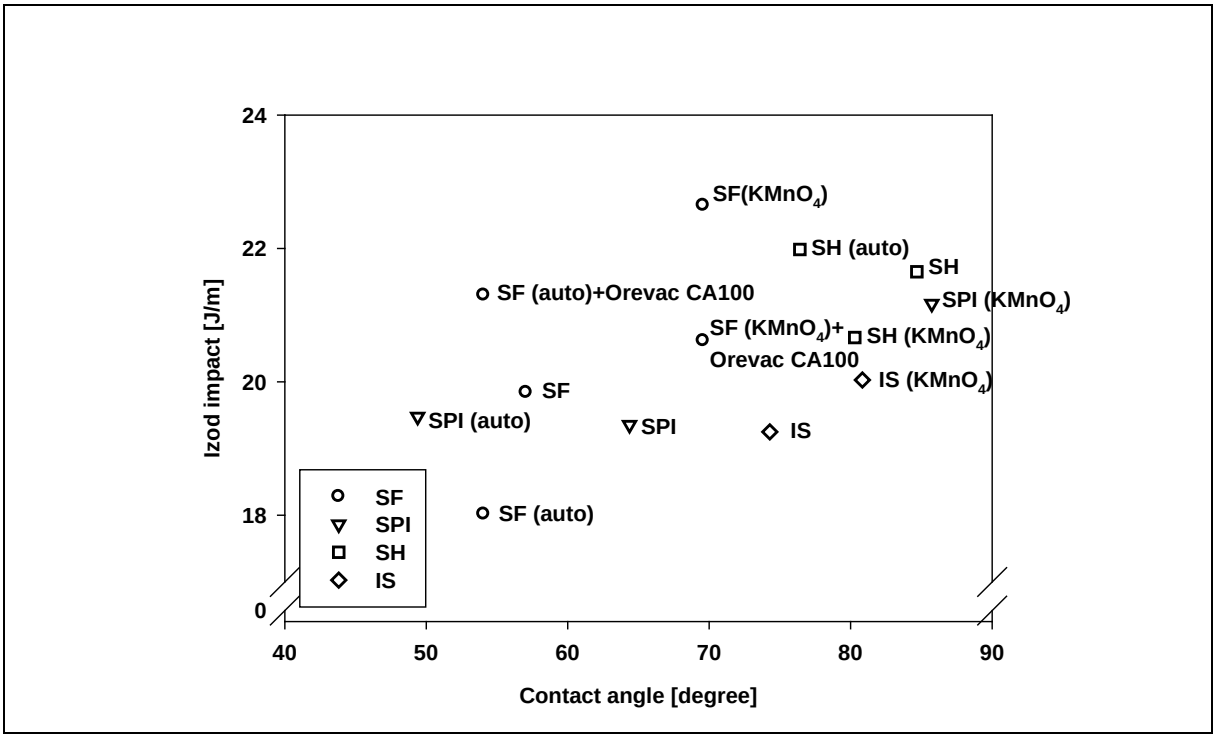

Figure 7-4 Izod impact vs. initial water contact angle

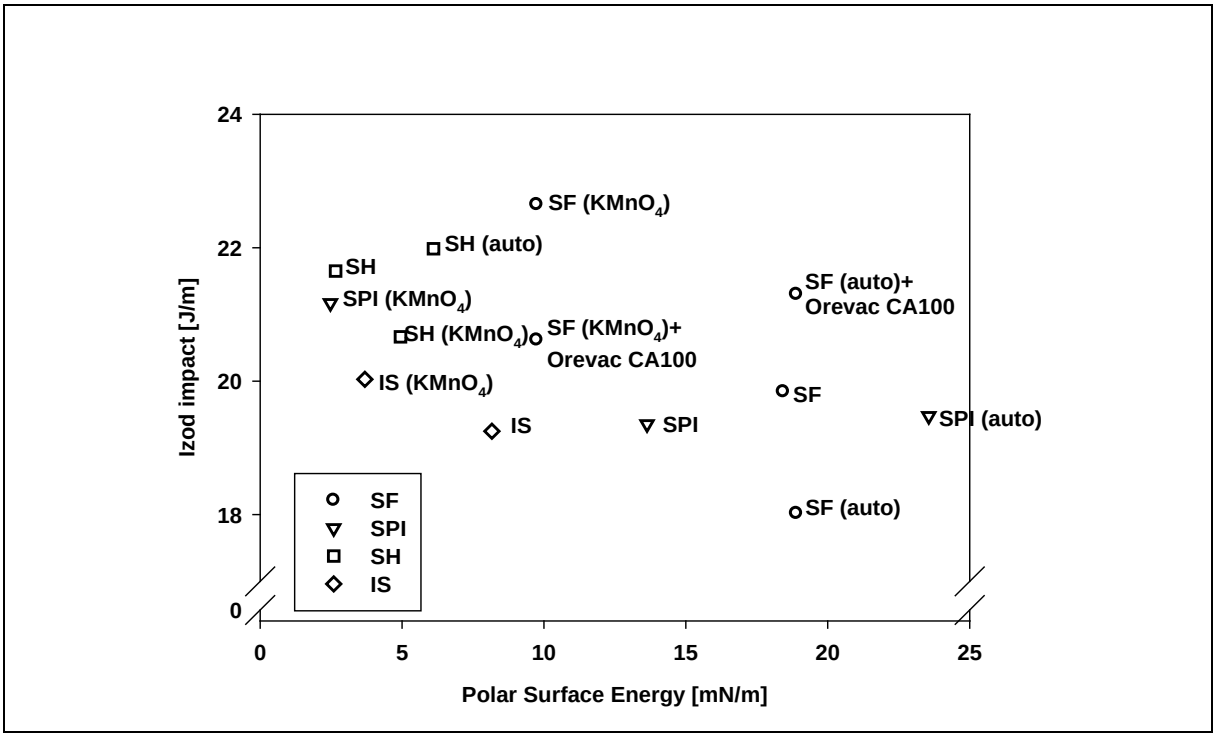

Figure 7-5 Izod impact vs. polar surface energy

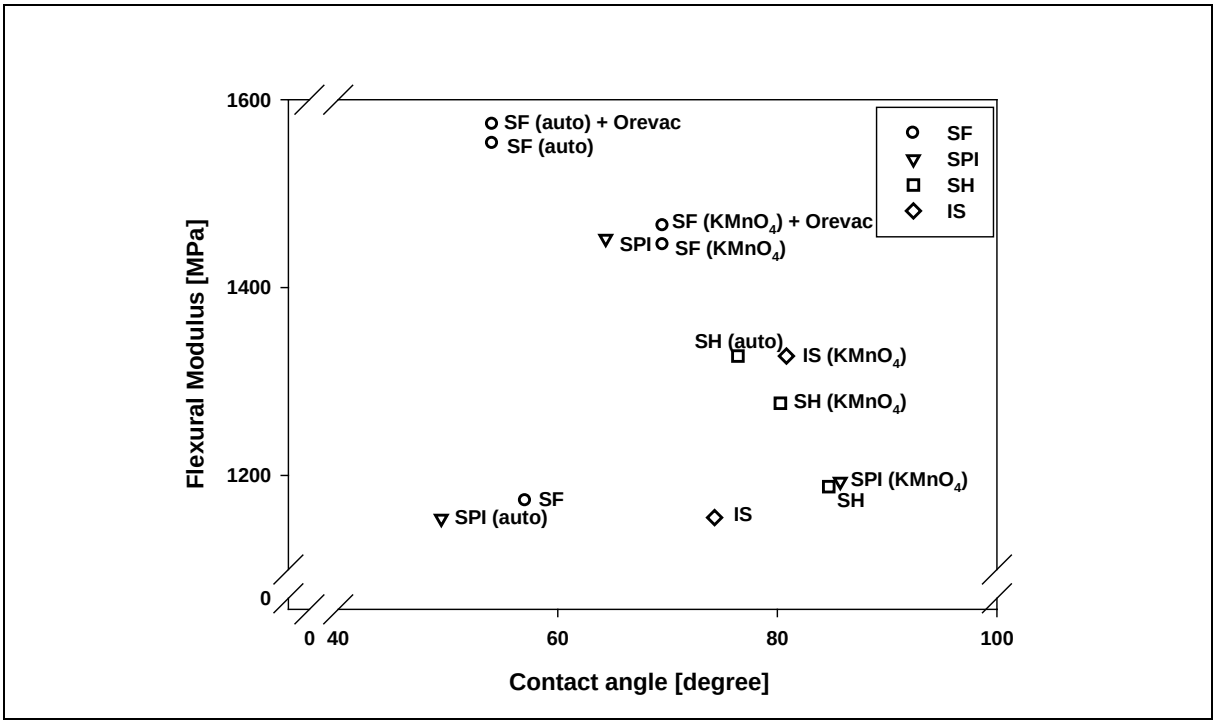

Figure 7-6 Flexural modulus vs. contact angle

7.4.7 Morphology of the Composites after Impact Testing

Field Emission Scanning Electron Microscopy (FESEM) of the fractured surface produced after impact testing is shown for general appearance (Figure 7-7). The surface of SF and SF (auto) (Figure 7-7 c and Figure 7-7 d) showed clear gaps between the soy materials and matrix with many of the soy flour largely separated from the surrounding polymer. The surface of SF ($KMnO_4$) (Figure 7-8 b and Figure 7-8 d) showed soy flour partially attached to the matrix but cracks between the soy flour and the polymer were also visible. The surface of the soy flour (especially the palisade layer which has a fibrous structure) had a smoother appearance when compared to the soy material surfaces of SF, SF (auto). A comparison of SF (auto) and Orevac CA100 (Figure 7-8 f) to the other materials revealed a much smoother surface with most of the soy flour fully embedded in the matrix.

No crystals were observed for the composites prepared with soy material and the $KMnO_4$. This indicates negligible residual $KMnO_4$.

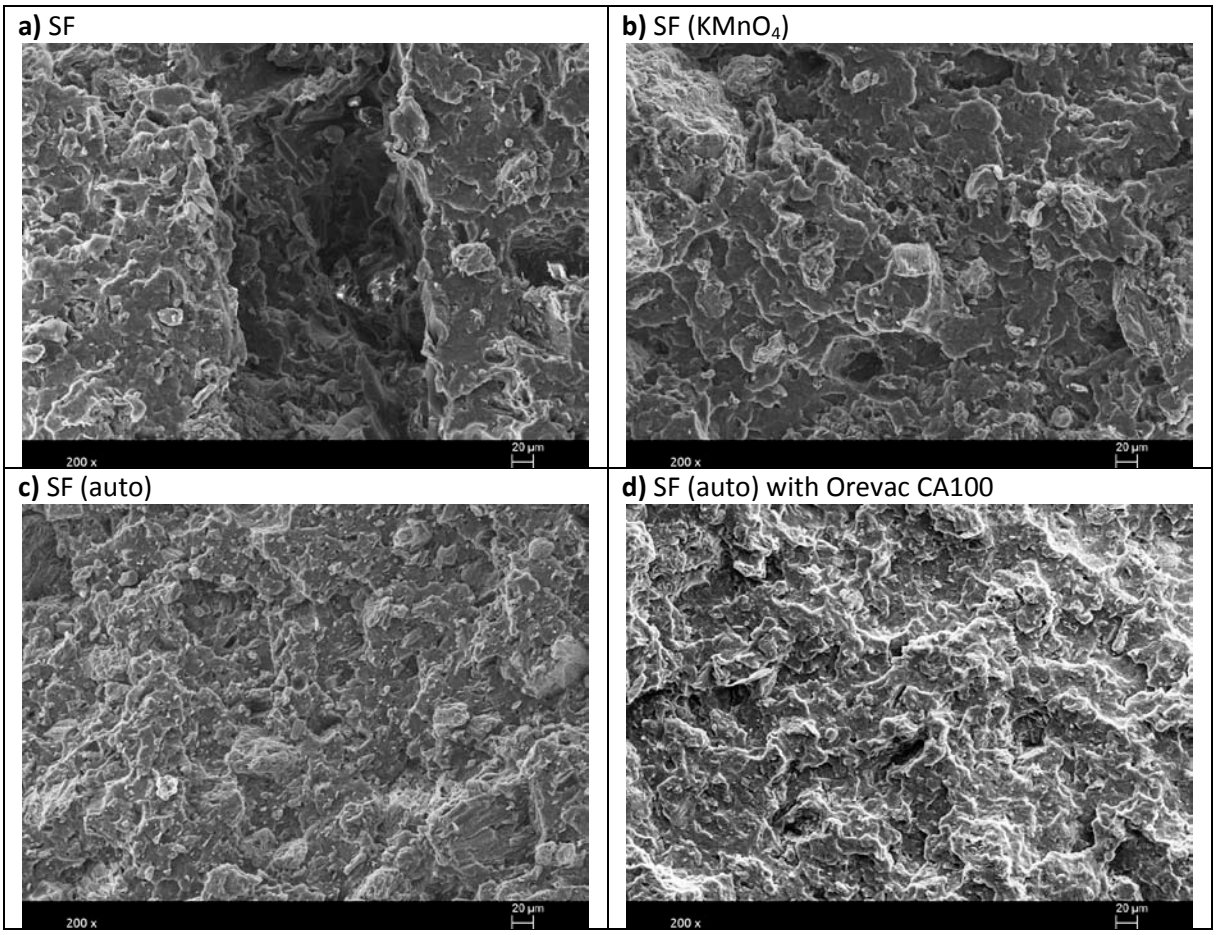

Figure 7-7 FESEM images (200x magnification) of the fractured surface produced after impact testing of composites formulated with a) 30 % SF, b) 30 % SF (KMnO4) c) 30 % SF (auto), d) 30 % SF (auto) with 2.25 % Orevac CA100

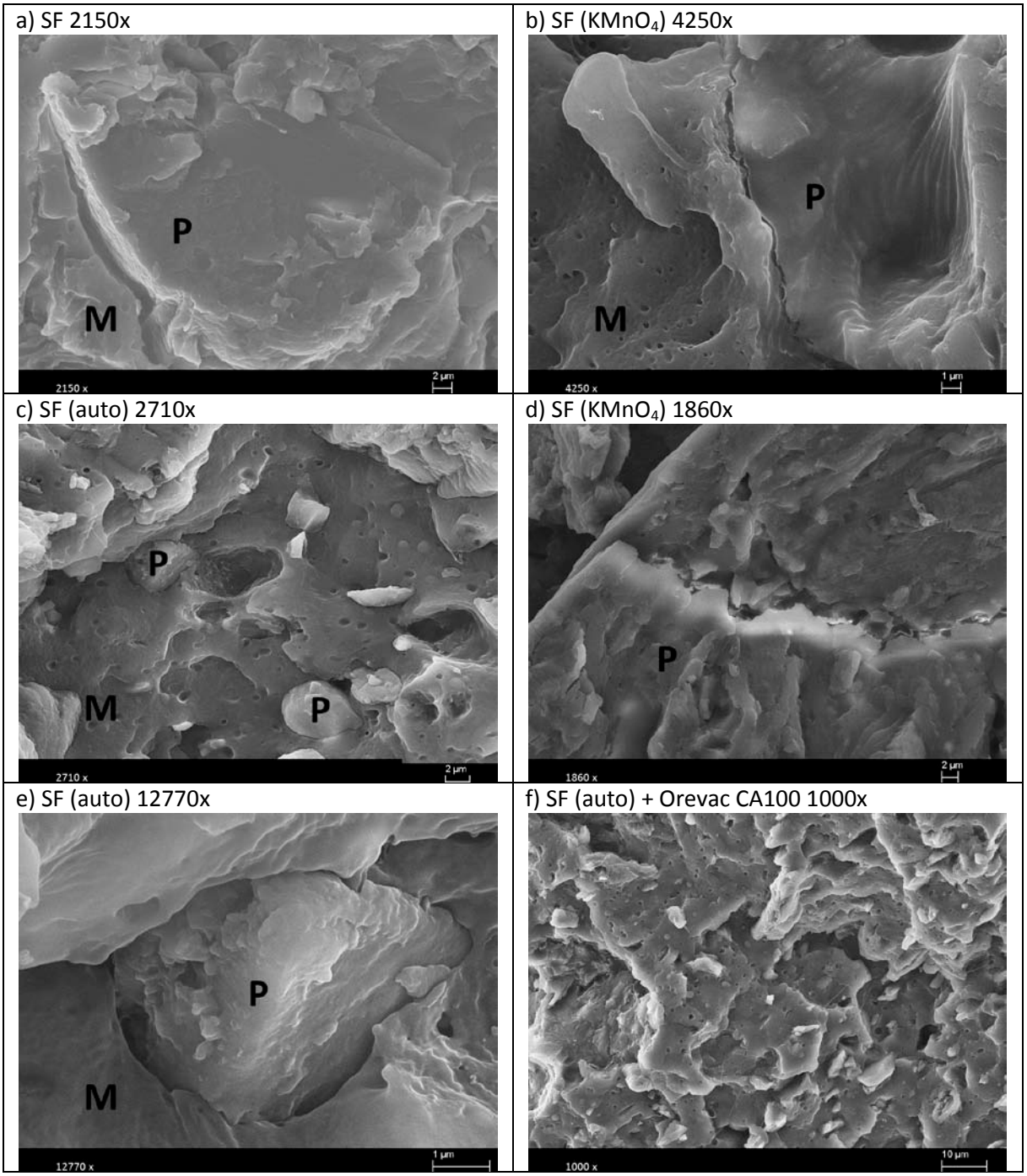

Figure 7-8 FESEM images of the fractured surface produced after impact testing of composites formulated with a) 30 % SF (2150x), b) 30 % SF ($KMnO_4$) (4250x), c) 30 % SF (auto) (2710x) d) 30 % SF ($KMnO_4$) (1860x), e) 30 % SF (auto) (12770x), f) 30 % SF (auto) with 2.25 % Orevac CA100 (1000x)

7.5 Proposed Crack Propagation

Cracks in a material will appear in response to mechanical stresses. In the context of composite materials, cracks will develop in the least resistant domain of the material. Accordingly, three cases for cracks propagation through a particulate filled polymer have been recognized and are shown in Figure 7-9: a) through the matrix, b) through the dispersed phase and c) through the interface. The mechanical properties change according to the interfacial bond strength between the dispersed phase and the continuous polymer phase [34]. The interface can be modified by chemical or mechanical treatments resulting in changes in mechanical properties. For example, the impact strength depends in the matrix-interface characteristic and may increase according to the type of dispersed phase (filler or fiber), its loading, orientation and simply its nature [34]. When the dispersed phase-matrix interface is very strong, the matrix becomes the weakest region of the composite and cracks will propagate through this region leaving the dispersed phase and the interface intact (case a). When the bonding between the dispersed phase and matrix is strong, the dispersed phase will break before detaching from the matrix (case b). If the bonding between the dispersed phase and matrix is poor, the dispersed phase will detach from the matrix when stress is applied (case c). Qualitative effects of interfacial shear strength on the properties of composites are shown in Table 7-9.

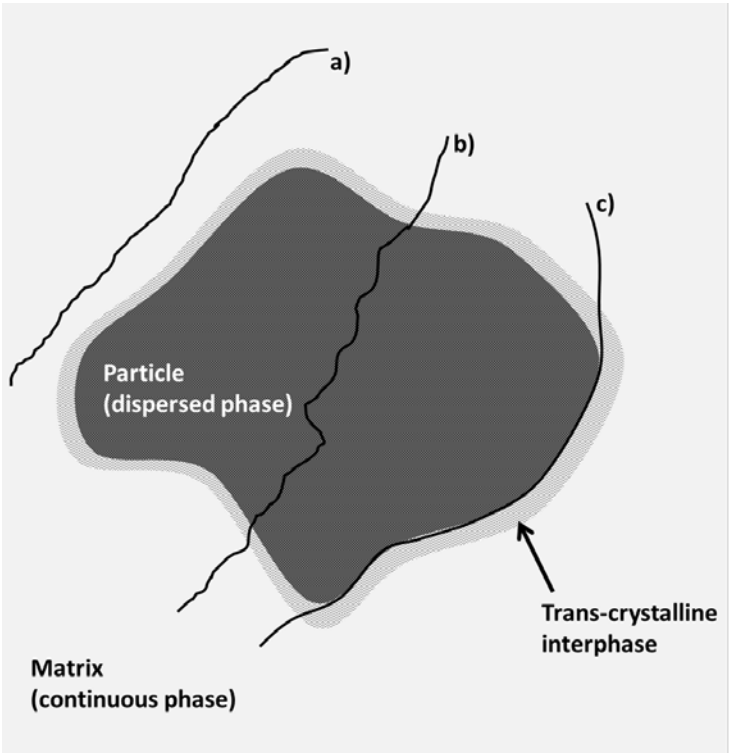

Figure 7-9 Schematic of different crack propagation theories: a) through matrix, b) through dispersed phase, c) through interface

Table 7-9 Qualitative effects of interfacial shear strength on composite properties [34]

	Low	**Intermediate**	**High**
Crack propagation	At interface or under fiber surface	Slightly above interface	Through matrix or transverse to dispersed phase
Weatherability	Poor	Good	Good
Longitudinal strength	Good	Good	Excellent
Transverse strength	Poor	Good	Excellent
Fracture toughness	Good	Good	Poor

Comparing the FESEM images presented in Figure 7-7 and Figure 7-8, different mechanisms of crack propagation occurred in a given soy composite material. The SF composites showed mostly detachment between the soy material and matrix (case c) whereas the SF ($KMnO_4$) composite contained partial soy material-matrix bonding that was associated with improved impact strength. The SF ($KMnO_4$) composite material showed also some cracks through the soy material (case b). An example for good interfacial bonding was SF (auto) + Orevac CA100 which shows a crack propagation through the matrix (case a).

Yang and his colleagues studied rice husk in polypropylene with and without coupling agent [201]. They found that without coupling agent there was no good bonding between the dispersed phase and the matrix resulting in cracks at the interface. When 3 % coupling agent was added, the cracks were located in the dispersed phase.

Sailaja et al. studied composites from 20 % soy flour and polypropylene [154]. Without coupling agent, detachment between dispersed phase and matrix was also observed. After the addition of 6 % coupling agent, a better dispersion and interlocking of soy flour and matrix were obtained.

A summary of the composites materials with observed crack propagation mechanisms and polar surface energies of the respective soy materials is given in Table 7-10. No correlation could be identified in terms of soy surface properties and crack propagation mechanism.

Table 7-10 Summary of observed crack propagation mechanisms and soy material with the polar surface energy of the soy material

Composite	Crack propagation mechanism	Polar Surface Energy [mN/m]
SF	Case c)	18.4
SF ($KMnO_4$)	Case a) and b)	9.8
SF (auto)	Case c)	18.9
SF (auto) + Orevac CA100	Case a)	18.9

7.6 Conclusions

Soy flour (SF) obtained after milling to a particle size below 80 µm was subjected to potassium permanganate and autoclave treatments. The treated soy flour was compounded with polypropylene with and without the addition of coupling agents. Two treatments and two coupling agents (most and least suitable according to impact strength) were selected for composite formulation. Impact strength for the composites and the combination of SF (auto) with coupling agent improved but decreased for the combination of SF ($KMnO_4$) with coupling agent. The increased hydrophilicity of SF (auto) may have enhanced its reactivity with maleic anhydride but reduced trans-crystallinity effect due to the addition of coupling agent and its non-specific reactions with the initial reactive groups on the soy flour surface. Scanning electron microscopic imaging of the fractured surface produced during impact testing revealed different crack propagation mechanisms depending on the type of treatment and/or coupling agent. Even though the surface of SF (auto) + Orevac CA100 showed crack propagation through the matrix, indicating a very good dispersed phase-matrix bonding, the impact strength of SF ($KMnO_4$) was the highest. Nevertheless, both materials present good mechanical properties with increased impact strength and flexural modulus. Since the treated SPI showed higher changes in impact strength then the

treated SH, one can assume that the main effect of the two treatments in SF occurred in the protein fraction.

Overall, both $KMnO_4$ and autoclave treatments, changed the soy materials where their compatibility with the polypropylene matrix (SF ($KMnO_4$)) improved or their reactivity with a MAPP coupling agent (SF (auto)) improved resulting in improved toughness and strength.

7.7 Acknowledgements

The authors would like to thank Bunge Inc. (Hamilton, Canada) for providing soy materials, Archer Daniels Midland Company (ADM, USA) and esp. Russ Egbert for kindly providing soy materials and productive discussions, A. Schulman for providing polypropylene and AddComp, Arkema, Clariant, and DuPont for providing coupling agents. Special thanks to Dr. Costas Tzoganakis (University of Waterloo) for access of Haake Rheomex 252 single-screw extruder and pelletizer and Dr. Shuihan Zhu for his assistance with the operation. Financial support from Grain Farmers of Ontario (formerly Ontario Soybean Growers), NSERC (Natural Sciences and Engineering Research Council of Canada) and Ontario Research Fund (BioCar) are gratefully recognized.

8. Acid treated Soy Materials for Compatibilization with Polypropylene

8.1 Synopsis

In the previous chapters soy flour and its components were investigated. In this chapter the focus was only on the effect of sulfuric acid as a pre-treatment method. In this context only soy flour was investigated. During the characterization of this soy material lower thermal stability was observed. Therefore, the sulfuric acid treatment is discussed separately with a focus on the thermal behaviour and composite properties.

8.2 Outline

The treatment of soy flour with sulfuric acid was carried out to alter protein conformation or charge. An aqueous soy flour solution was prepared, pH adjusted to pH 3 with sulfuric acid and dried at room temperature. The surface chemistry of soy flour was obtained by Fourier transform infrared spectroscopy (FTIR). The thermal behaviour during isothermal conditions at 200 °C in air environment and dynamic heating from 40 to 800 °C in nitrogen environment was investigated by thermogravimetric analysis (TGA). FTIR showed increased relative contributions of the hydroxyl and amide functional groups. The thermal degradation after sulfuric acid treatment decreased significantly with the appearance of components degrading in the 100 to 200 °C temperature range and suspected to be sugars and sugar-derivatives from the hydrolysis of the soy saccharide fraction. Isothermal TGA showed good stability (6 wt-% mass loss over 60 minutes at 200 °C) after the removal of the volatile fraction (100 and 200 °C). Contact angle analysis revealed a minor decrease (6 %) which may be caused by the increased surface roughness (1.86 µm). The total surface energy increased slightly (5.6 %) and predominantly its polar component (9.4 %). Mechanical properties showed constant impact strength with improved flexural strength (18.6 %) and flexural modulus (31.7 %). Field Emission Scanning Electron Microscopy images of the fractured composite revealed some cracks through the dispersed phase but also good partial bonding between the dispersed and the continuous phase.

8.3 Introduction

A number of studies of agricultural fillers in composites have been conducted over the past decades [1, 23, 65-67]. The main benefit of agricultural fillers over mineral filler, such as calcium carbonate and talc, is their light weight associated with the low density of

agricultural fillers. Most of the agricultural fillers contain significant amount of cellulose, one of the major constituents responsible for structural features in plants. Soy meal represents a different category of filler with its main constituents being protein (40-50 %) and carbohydrates (30 %) that have negligible structural features.

Due to their composition (cellulose, hemicellulose, lignin, protein) and surface properties, agricultural fillers are hydrophilic leading to their incompatibility with hydrophobic polymers such as polypropylene. Therefore, the two materials are difficult to mix and have little interaction resulting in poor mechanical properties [121, 162, 178]. To overcome this incompatibility, surface modification and the addition of coupling agents can improve their interaction by creating chemical bonds between the surfaces of the filler and the polymer matrix [43, 46, 90, 121].

Soybean meal is the largest source of vegetable oil and proteins worldwide with over 40 % of the soybean production in 2009 grown and harvested in North America [52]. The two major proteins in soybeans are glycinin and conglycinin with isoelectric points (pI) around pH 4 [202]. Below the isoelectric point (pI), proteins have a positive net charge and above their pI a negative net charge.

When acid is added to a protein solution, the conformation of the protein will change due to their change in charge. The degree of change depends on the proteins amino acid composition and sequence which will also affect properties such as solubility or interactions with other molecules [202, 203].

Acid treatments of wood and cellulose materials are common pre-treatment methods to improve sugar accessibility for enzymatic hydrolysis [204] or pre-hydrolyze them to break down chemical structures for further applications for example in the paper industry to achieve better interaction between the cellulose fibers [205, 206].

The objective of this work was to evaluate the effect of acid treatment on soy flour as a means to improve the adhesion of soy flour to polypropylene and ultimately the mechanical properties of soy flour composite materials. Thermal stability of the soy flour after acid treatment was also considered. Visualization by field emission scanning microscopy provided information on the morphology of the materials and where cracks occurred during the impact testing.

8.4 Materials and Methods

8.4.1 Materials

Defatted soy meal was obtained from Bunge Inc. (Hamilton, Canada). D-glucose was obtained from Invitrogen (anhydrous, USP grade, Gibco, Invitrogen Corporation, Canada) and D-fructose from Baker (Baker Analyzed'® Biochemical, J.T. Baker, USA).

8.4.1.1 Soy flour processing

Soy flour (SF) was obtained by milling soy meal as described previously, with an ultracentrifugal mill ZM200 (Retsch GmbH, Germany) and 0.08 mm sieve with trapezoid shaped holes (part # 03.647.0231).

8.4.1.2 Acid Treatment

The soy flour was soaked in deionized (DI) water with a soy material/liquid mass ratio of 1/9 and the pH of the solution was adjusted under stirring to pH 3 with 1 M H_2SO_4 (95-98 %, GR ACS, Fisher Scientific, Canada). The adjusted solution was then dried in a fume hood (relative humidity (RH<20 %) and RT) and milled as described previously.

The H_2SO_4 was not removed due to cost reasons for the process upscale and possible changes of the protein fraction in the soy flour. At this point, consequences of this decision were possible since interaction with the coupling agent could occur but remained to be tested.

8.4.1.3 Autoclave Treatment

The soy material (~500 g), placed on a glass tray resulting in a material height less than one centimeter, was put in a direct steam heated sterilizer-autoclave for sterilization of biological materials (Consolidated Stills & Sterilizers, USA) and subjected to 125 °C and steam for 25 minutes. The treated soy material was then dried and milled as described previously.

8.4.1.4 Thermal Characterization

All thermogravimetric analysis (TGA) was conducted with thermogravimetric analyzer (TGA Q500, TA Instruments, USA). Two modes were considered: (1) dynamic TGA mode in a nitrogen environment with temperature increase from 40 to 800 °C and heating rate of 10 °C/min; (2) isothermal TGA in air, to simulate processing conditions of biocomposites manufacture as described previously for flax and wood [64, 78]. These conditions were air at 110 °C for 5 minutes followed with 60 minutes at 200 °C.

The analysis of the dynamic TGA in nitrogen was obtained by plotting the temperature against the relative mass. Due to different exposure times of the samples in the air prior to TGA, the relative mass of the sample was adjusted to the mass recorded at 110 °C. It is assumed that at 110 °C, all water is evaporated and changes in mass can only be due to the degradation of the material [167].

The isothermal TGA data were plotted as the mass change over time. The reported values are the residual mass after 60 minutes exposure to 200 °C in an air environment.

8.4.1.5 Fourier Transform Infrared Spectroscopy (FTIR)

The soy materials were prepared with potassium bromide (KBr, IR grade CAS 7758-02-3, Fisher Scientific) and pressed into pellets with an evacuable KBr pellet die (International Crystal Laboratories, USA) in a press (model #3925, Carver, Inc., USA). The FTIR measurements were performed with a Tensor27 (Bruker Optik GmbH, Germany) and the spectra were analyzed with the software OPUS Version 4.2 (Bruker Optik GmbH, Germany). The background spectrum was recorded and 32 scans were performed per sample in a range between 4000 and 400 cm^{-1} with a resolution of 4 cm^{-1}.

Since the spectra consist of numerous overlapping peaks associated with the many constituents of the soy materials, the analysis of the spectra was performed by integrating the area under the spectra for regions of wavenumber (Table 8-1). The changes in the ratio of specific area were also investigated. An example of a FTIR absorbance spectrum and its analyzed wavelength regions is presented in Figure 8-1. The analysis was conducted with OPUS 4.2 software (Bruker Optik GmbH, Germany) using the integration method A.

Table 8-1 Wavenumber regions with corresponding vibration and functional groups [33].

Area	Wavenumber region [cm^{-1}]	Vibration	Functional Groups
1	3800-3000	O-H stretch N-H stretch	Alcohols, phenols Amines Carboxylic acids
2	3000-2850	C-H stretch	Alkanes Carboxylic acids
3	1900-1482	C=O, C=C double bonds	Alkenes, ketones, aldehydes, ester, carboxylic acids
4	1195-875	N-H wag C-N stretch C-O stretch O-H bend	Amines, amides, carboxylic acids

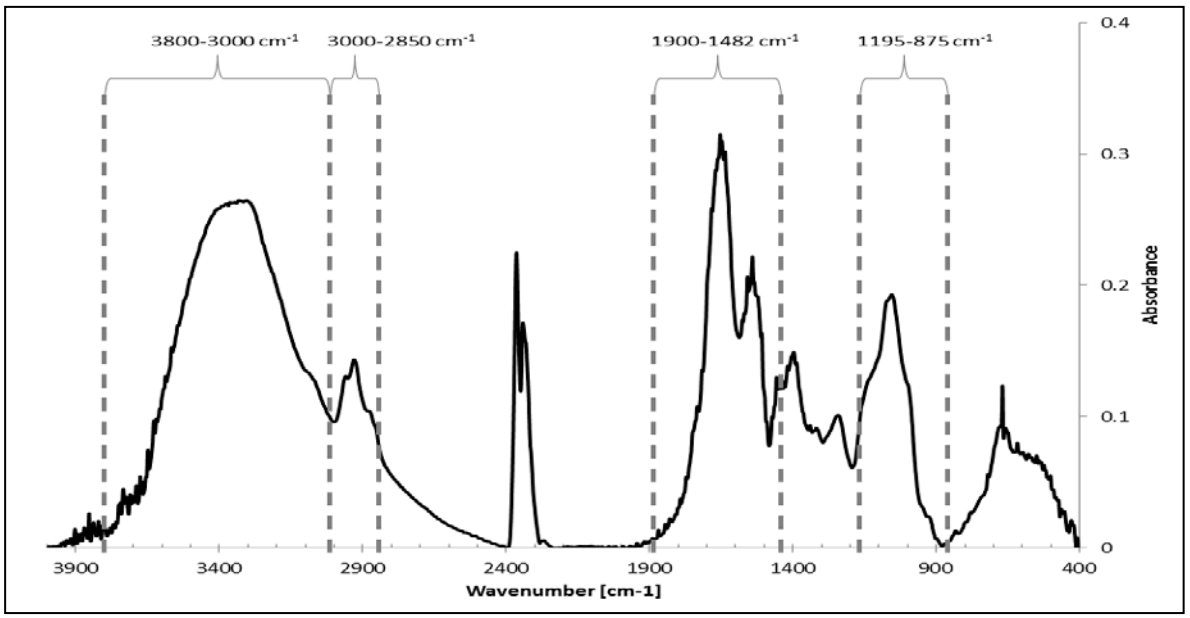

Figure 8-1 Example of FTIR spectra of SF with analyzed wavelength regions

8.4.1.6 Chemical Composition

The composition of SF is presented in Table 8-2 (before treatment). The ash, cellulose, hemicellulose, lignin and fat content analysis of the soy materials was carried out according to AOAC methods and performed by Agri-Food Laboratories, Guelph, Canada. The ash content was determined by the AOAC 942.05 method, lignin by the ANKOM filter bag modified method of AOAC 973.18, protein content by the combustion method AOAC 990.03 and oil content by the AOAC 920.39 method.

Cellulose was obtained by subtracting lignin from acid detergent fiber (ADF). Hemicellulose was obtained by subtracting ADF from neutral detergent fiber (NDF).

Table 8-2 Chemical composition of soy flour before treatment.

Material	Protein (Nx6.25) [wt-%]	Ash [wt-%]	Cellulose [wt-%]	Hemicellulose [wt-%]	Lignin [wt-%]	Fat [wt-%]	Other* [%]
SF	47.6	6.2	6.9	1.5	0.03	1.5	36.3

*Other are mainly sugars other than cellulose and hemicellulose (e.g. pectin, starch)

8.4.1.7 Sample Preparation for Contact Angle Analysis

For contact angle analysis, soy materials were pressed in compacts with evacuable KBr pellet die (International Crystal Laboratories, USA) at room temperature as suggested for pigment specimens in ASTM D7490 – 08 [189]. The KBr mould was 13 mm in diameter and a 7 t (7000 kg/132.73 mm^2 = 517.19 MPa) load applied during at least 60 seconds in a

press Model #3925 (Carver Inc., USA). The pellets were then fixed onto a microscope object slide (Pearl 7101,T & Q Industries, China) with double sided tape (137-2C, Scotch, Canada (part of 3M)) and stored in a desiccator (Nalgene, Sybron Corporation, USA) until testing.

8.4.1.8 Surface Roughness Measurement

For measurements of the surface roughness, the soy materials were prepared as for the contact angle analysis. The optical profiler WYKO NT100 (Veeco Instruments Inc., Plainview, NY, USA) was used in VSI mode with a magnification of 5.1x (set-up parameter: size 736 x 480; sampling 1.65 µm). Each material sample was measured at least three times and the average surface roughness (R_a) and peak-to-valley difference (R_t) over the entire profile was calculated by the software Wyko Vision® analysis software (Veeco Instruments Inc., Plainview, NY, USA) based on Equation 8-1 and Equation 8-2.

$$R_a = \frac{1}{N}\sum_{i=1}^{N}|Z_i| \qquad \textit{Equation 8-1}$$

Z_i = height of each pixel after the zero mean is removed

$$R_t = R_p - R_v \qquad \textit{Equation 8-2}$$

R_p = maximum peak hight
R_v = minimum valley height

8.4.2 Contact Angle Measurement

Contact angle analysis was conducted with the Drop shape analyzer DSA100 (Krüss GmbH, Germany) at room temperature in a static mode with at least six liquid drops per specimen. The measurement was digitally recorded and the videos were analyzed with the software DSA1 V1.9-03 9 (Krüss GmbH, Germany). Two analysis methods were considered for low contact angle values: Tangent method 1 and Young-Laplace method (sessile drop) [12]. The initial contact angle and the change over time (at least ten seconds) were recorded for a drop of liquid deposited on a compact of a given soy material. The apparent absorption rate of the liquid drop was calculated by linear regression as the slope of contact angle measurements versus time curves during the first five seconds [85, 87].

8.4.3 Surface Energy

The total surface energy, the dispersive surface energy and the polar surface energy were estimated according to the method of Owens, Wendt, Rabel and Kaelble (OWRK)[12].

Milli Q water and diiodomethane (99 % CAS# 75-11-6, Alfa Aesar, USA) were selected as liquids with surface energy properties presented in Table 8-3.

Table 8-3 Reported surface energy components of water and diiodomethane [12].

Liquid	Total Surface Energy [σ_{Total}, mN/m]	Dispersive Surface Energy Component [σ^D, mN/m]	Polar Surface Energy Component [σ^P, mN/m]
Water (W)	72.8	21.8	51.0
Diiodomethane (D)	50.8	50.8	0.0

8.4.4 Composite Preparation

EXTRUSION

The polypropylene blend was extruded first with 0.5 % Irganox 1010 at 190 °C and 90 rpm in a Haake Rheomex 252 single-screw extruder with Haake Rheocord 90 Fisons (Thermo Electron Corporation, USA) and pelletized with a Berlyn pelletizer Model HVI (The Berlyn Corporation, USA). For the compounding of the composites a Haake MiniLab twin-screw micro compounder (Thermo Electron Corporation, USA) was used at 190 °C and 40 rpm.

INJECTION MOULDING

The extruded pellets were pressed into bars by using an injection moulding apparatus from Ray-Ran. The barrel temperature set at 190 °C and the mould temperature 50 °C. The dimensions of the bars were according to ASTM (length 63.5 ±0.2 mm, width 12.7 ±0.2 mm, depth 3.3 ±0.2 mm) [108, 109].

ANNEALING AND CONDITIONING

Before testing the bars they were put into an oven 5890A GC (Hewlett Packard, USA) with an initial temperature of 31 °C and heated 10 °C/min until the final temperature of 151 °C was reached. The final temperature was kept isothermal for 10 minutes before cooling down to room temperature.

After annealing the bars were put for at least 48 hours in an environmental chamber model MLR-351H (Sanyo Electric Co., Ltd., USA) (50 % RH and 23 °C).

8.4.4.1 Composite Testing

THREE-POINT-BENDING (ASTM D 790)

The injection moulded bars were annealed and conditioned before testing. For testing flexural properties Actuator model 120Q1000 (TestResources, Inc., USA) was used at 50 % RH and 23 °C. The testing was performed after annealing and conditioning of the bars as

described. For each material at least five samples were tested and an average was calculated as well as the standard deviation. The reported flexural strength is the maximum point of the stress/strain curve. The flexural modulus represents the slope of first linear part of the stress/strain curve.

NOTCHED IZOD IMPACT TEST (ASTM D 256)

After notching (for Izod impact), annealing and conditioning the bars were tested for Izod impact strength and flexural properties. For Izod impact testing monitor impact tester model 43-02-01 (TestResources, Inc., USA) was used (50 % RH and 23 °C). The testing was performed after notching with specimen notch cutter XQZ-I (Chengde JinJian Testing Instrument Co., Ltd., China), annealing and conditioning of the bars as described above. For each material at least five samples were tested and an average was calculated as well as the standard deviation.

DIFFERENTIAL SCANNING CALORIMETRY (DSC)

Differential scanning calorimetry (DSC) was used for the analysis of crystallinity in the polymer composites and the melting and crystallization peaks. When DSC is performed in the dynamic mode, the area under the peak represents the energy for the crystallization of the composite which gives a measure of the degree of crystallization of the polymer. The total crystallinity represents the ratio between the crystalline and the amorphous region of the polymer.

The DSC was performed with the differential scanning calorimeter Q2000 (TA Instruments – Waters LLC, USA). The materials were placed in aluminum Tzero™ pans and heated in a nitrogen purged chamber from 35 to 200 °C at a rate of 10 °C/min. The analysis of the obtained graphs (heat flow [W/g] vs. temperature [°C]) was carried out with the software Universal Analysis 2000 4.5A using the linear integration method (TA Instruments – Waters LLC, USA).

8.4.4.2 Field Emission Scanning Electron Microscopy (FESEM)

Samples from Izod impact testing were gold coated in argon with a gold coating unit Desk II (Denton Vacuum, USA). Electron microscopic images were taken by using the Gemini Leo 1550 (Carl Zeiss AG, Germany) with EDAX Genesis 5.2 (Ametek Inc., USA). The working parameters for the FESEM were 12 kV and the secondary electron signal (SE2).

8.4.4.3 Statistical Analysis

The t-test was used for data analysis of significances between mean values of set of samples. The confidence interval was determined at a significance level of $\alpha = 0.05$.

8.5 Results and Discussion

8.5.1 FTIR

A large number of functional groups were expected from the FTIR analysis of the soy materials as a result of their complex composition and the overlap between chemical spectra (appendix I., Table 10-1 and Table 10-2). Cellulose and hemicellulose have relatively well defined FTIR spectra [171, 172]. Lignin, on the other hand, has a very complex structure not yet fully elucidated [173]. Proteins present a different challenge since they can take on many conformations. Therefore, wavenumber regions of the spectrum shown in Figure 8-2 were identified, normalized and compared to each other by building ratios (Table 8-4 and Table 8-5). The changes in relative contribution of each wavenumber region are very small but increase could be observed for the region 3800-3000 cm^{-1} that represents hydroxyl groups. The relative contribution of the wavenumber region between 1900 and 1482 cm^{-1} also increased. This region is specific for amide I and II groups in proteins. Due to these changes, the area ratio 1/3 increased by nearly 10 % whereas the area ratio 3/4 decreased by nearly 10 %.

Additional peaks in the FTIR spectra of SF (H_2SO_4) suggest the presence of furan (1560, 1384, 1040, 613 cm^{-1}), formic acid (1445, 1454, 1387, 1105 cm^{-1}) and acetonitrile (1448, 1385, 1041 cm^{-1}) [33]. The presence of these species could represent degradation products of the carbohydrates initially present in soy flour [139, 140, 204].

Table 8-4 Normalized area for wavenumber region of soy flour before and after sulfuric acid treatment

	Normalized Area [%]			
Soy Material	**3800-3000 cm^{-1} (1)**	**3000-2850 cm^{-1} (2)**	**1900-1482 cm^{-1} (3)**	**1195-875 cm^{-1} (4)**
SF	56.0	2.5	26.5	15.0
SF (H_2SO_4)	57.4	2.4	24.8	15.5

Table 8-5 Ratio of normalized FTIR spectra areas of soy flour before and after sulfuric acid treatment for wavenumber regions reported in Table 5-2 and relativet change when compared to untreated soy flour.

	Normalized Area Ratio					
Soy Material (Treatment)	**1/3**	**Change [%]#**	**1/4**	**Change [%]#**	**3/4**	**Change [%]#**
SF	2.11	0	3.73	0	1.77	0
SF (H_2SO_4)	2.32	9.95	3.71	-0.54	1.60	-9.60

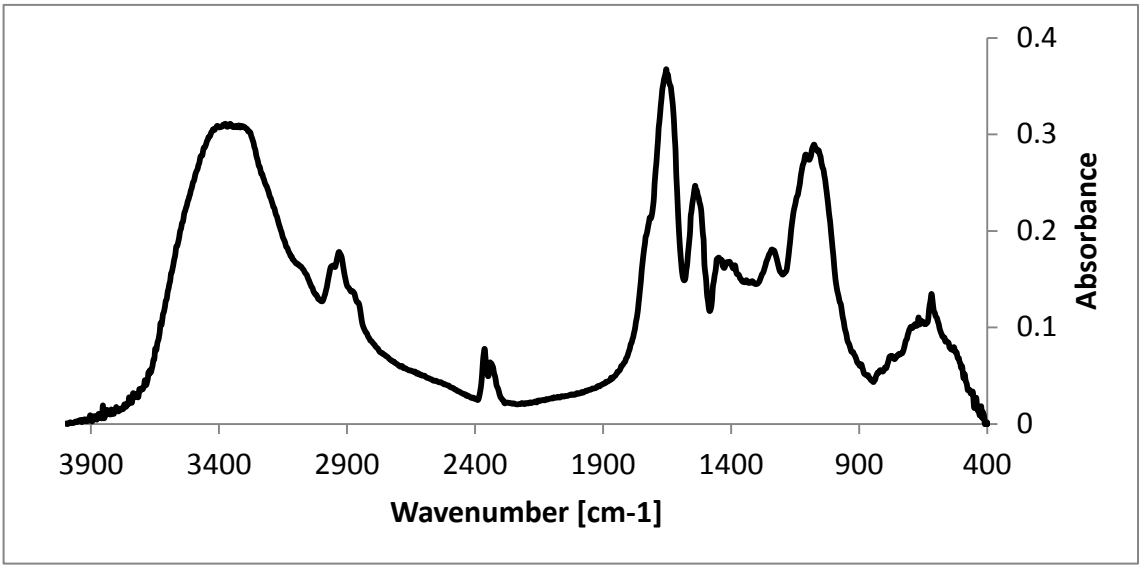

Figure 8-2 FTIR spectra of SF (H_2SO_4)

8.5.2 TGA at Dynamic Conditions

The thermogravimetric analysis in nitrogen environment was conducted between 40 and 800 °C (Figure 8-3). The temperature at 1 wt-% and 5 wt-% mass loss and the residual mass at the end of the TGA experiment are reported in Table 5-3. The temperatures at 1 wt-% and 5 wt-% mass loss decreased dramatically which is due to the degradation of components in the temperature range of 100 and 200 °C. When comparing the D-TGA curve of SF (H_2SO_4) and SSE (discussed previously in section 5.4.3), the first peaks for SF (H_2SO_4) and SSE appear in a similar temperature range, 100 and 200 °C. The TGA analysis of pure D-glucose and D-fructose, monomers of many polysaccharides present in the soy flour carbohydrates (Figure 8-4) indicate lower thermal stability for both sugars. D-fructose shows a shoulder in its D-TGA curve that overlays with the second peak of the D-TGA curve of SSE. Since soy flour contains a complex mixture of sugars, the treatment with acid may have produced sugar derivatives, such as furfural with a boiling point at 161 °C, that degrade at lower temperature [33, 140]. When SF (H_2SO_4) was autoclaved (presented previously, chapter 5.3.2.2, Figure 8-5), the first peak in the D-TGA curve decreased but a new peak appeared in a higher temperature range (200-300 °C).The drop in residual mass at the end of the run could be also explained by these sugar derivatives with low thermal stability.

Table 8-6 Degradation temperatures at 1 wt-% and 5 wt-% mass loss and residual mass at 793 °C of SF before and after sulphuric acid treatment obtained during dynamic TGA in N_2 environment.

Soy material	Temperature at 1 wt-% mass loss [°C]	Change [%]#	Temperature at 5 wt-% mass loss [°C]	Change [%]#	Residual mass at 793 °C [%]	Change [%]#
SF	177	0	213	0	24	0
SF (H_2SO_4)	137	-22.8	180	-15.8	29	21.1

#Compared to untreated SF

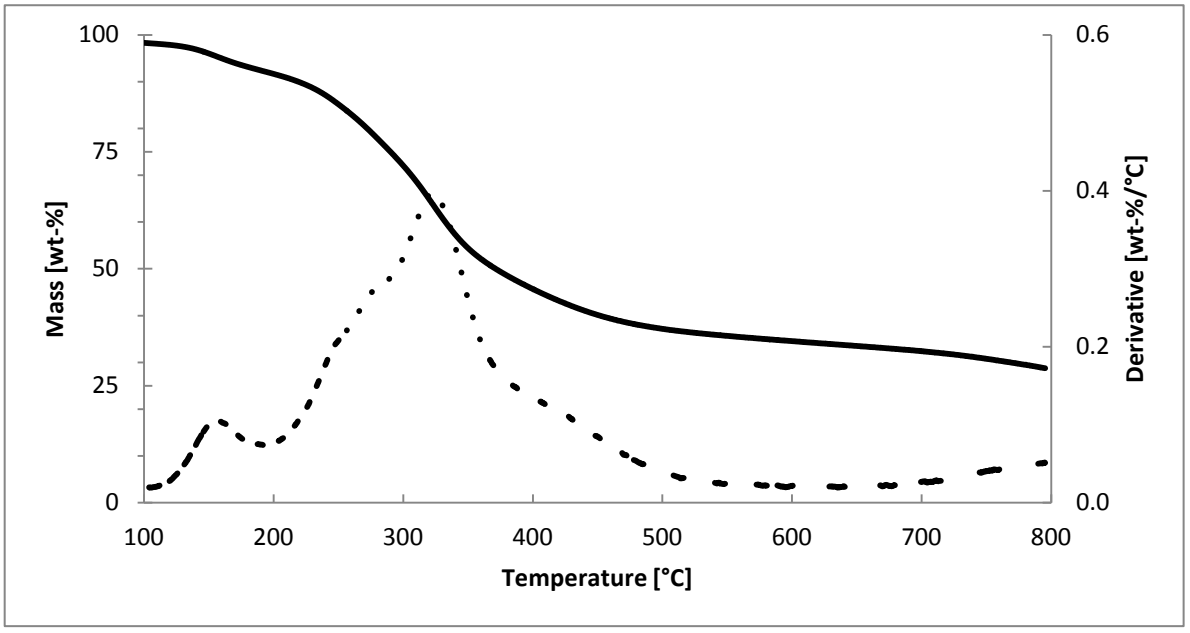

Figure 8-3 Dynamic TGA in N_2 environment for SF (H_2SO_4). Continuous lines represent mass change over temperature. Dashed lines are the first derivatives of the respective straight line (D-TGA) which represent the fraction of weight loss over temperature

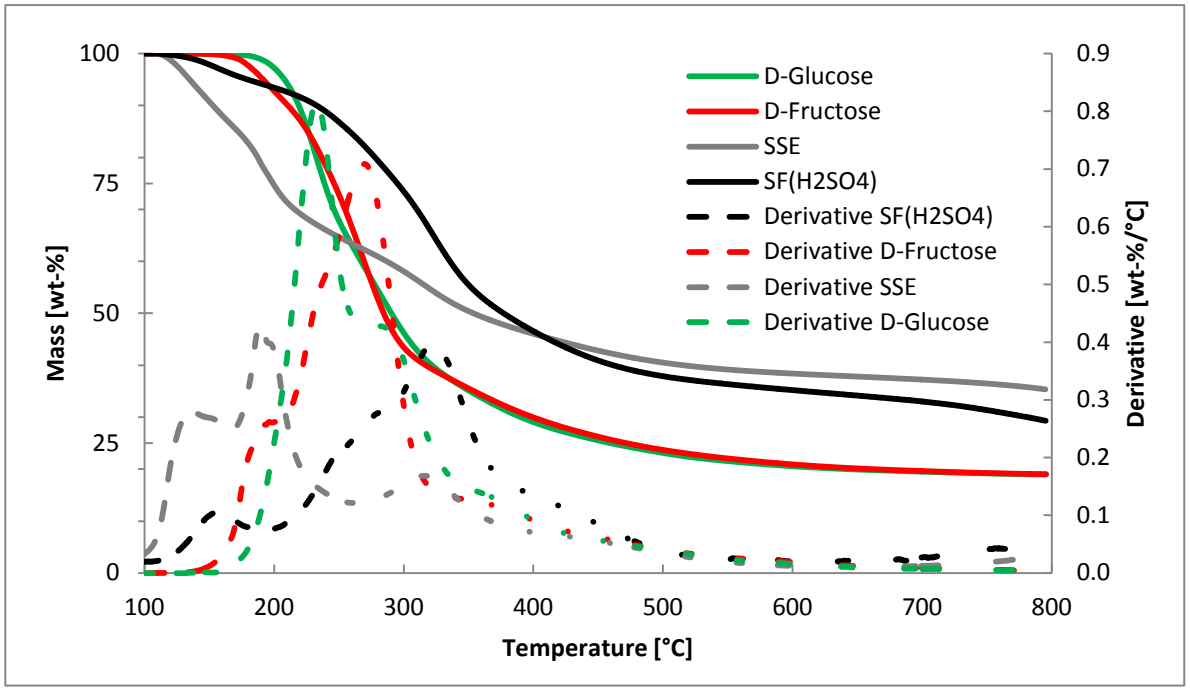

Figure 8-4 Dynamic TGA in N_2 environment for SSE, SF (H_2SO_4), D-glucose and D-fructose. Continuous lines represent mass change over temperature. Dashed lines are the first derivatives of the respective straight line (D-TGA) which represent the fraction of weight loss over temperature

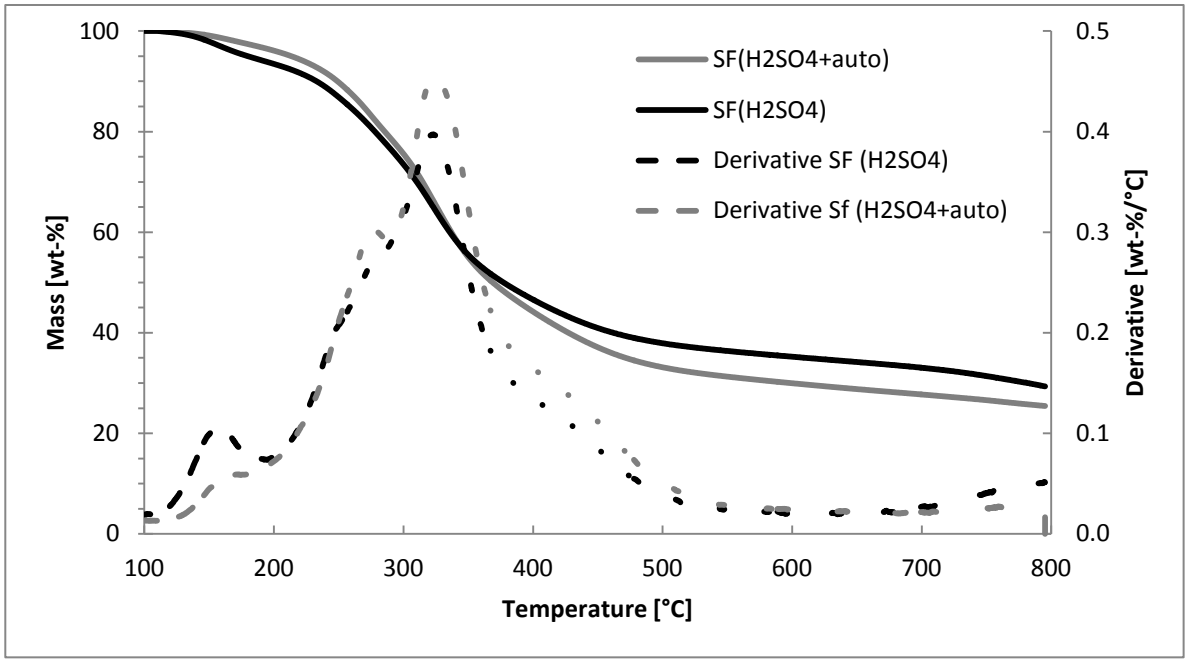

Figure 8-5 Dynamic TGA in N_2 environment for SF (H_2SO_4) and autoclaved SF (H_2SO_4). Continuous lines represent mass change over temperature. Dashed lines are the derivatives of the respective straight line (D-TGA) which represent the rate of weight loss over temperature

8.5.3 TGA at Isothermal Conditions

The thermogravimetric analysis of SF (H_2SO_4) showed good thermal stability at isothermal conditions at 200 °C in air environment (Figure 8-6). Its residual mass after 60 minutes was 94 wt-% representing a 9% increase when compared to untreated SF.

It has to be pointed out again that a three minute period of isothermal conditions at 110 °C for water removal was present prior to the actual isothermal TGA at 200 °C. Therefore, the mass loss between 100 and 200 °C, observed during the dynamic TGA (8.5.2), is not presented in the isothermal TGA curve. This approach explains the higher residual mass measured after the exposure of SF (H_2SO_4) at 200 °C for 60 minutes in air.

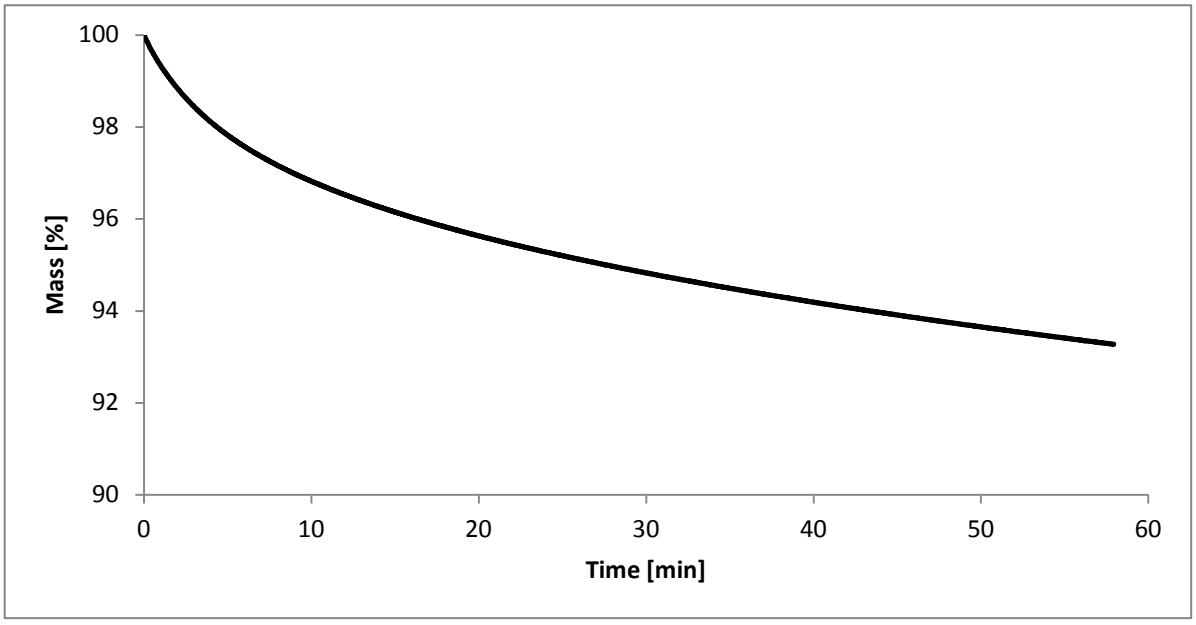

Figure 8-6 Isothermal TGA of SF (H_2SO_4) at 200 °C in air environment. Samples were subjected to three minute isothermal conditions at 110 °C for water removal prior to the at 200 °C isothermal conditions.
Contact Angle and Surface Energy

After acid treatment of the soy flour, the contact angle of SF (H_2SO_4) decreased slightly (about 6 %) whereas the apparent rate of water absorption remained constant (Table 8-7). This could be due to the change in surface roughness (R_a) from 1.32 µm ±0.11 (SF) to 1.86 µm ±0.15 with a peak-to-valley difference of R_t = 68.10 µm ±7.73. The surface energy for SF (H_2SO_4) remained relatively constant when compared to SF. The total surface energy increased by 5.6 %, with minor increase of the dispersive (3.2 %) and polar (9.4 %) surface energy (Table 8-8).

Table 8-7 Contact angle (W) and apparent rate of water absorption (±SD, n≥6)

Soy material	Initial contact angle [°]	Apparent rate of water absorption [°/s]
SF	57.06 ±2.24	-1.04 ±0.08
SF (H_2SO_4)	53.57 ±2.12	-1.07 ±0.86

Table 8-8 Surface energy (±SD, n≥6)

Soy material	Dispersive surface energy [mN/m]	Polar surface energy [mN/m]	Total surface energy [mN/m]
SF	29.91	18.43	48.34
SF (H_2SO_4)	30.88	20.16	51.05

8.5.4 Soy Flour Composites

8.5.4.1 Impact and Flexural Properties

The composites prepared from SF (H_2SO_4) were tested for notched Izod impact, flexural strength and flexural modulus (Table 8-9) according to the ASTM methods explained in section 8.4.4.1. Even though the impact properties remained constant, the flexural strength and flexural modulus increased up to almost 19 % and 32 % respectively. The increase in flexural properties could be due to the development of weak chemical bonds between the dispersed and the continuous phase that impart the composite material with higher elasticity but no increased toughness for the force applied during impact testing.

Table 8-9 Notched Izod impact, flexural strength and flexural modulus (±SD, n≥5) of polypropylene composites with soy flour before and after sulfuric acid treatment

SF (treatment)	**Notched Izod Impact [J/m]**	**Change [%]#**	**Flexural Strength [MPa]**	**Change [%]#**	**Flexural Modulus [MPa]**	**Change [%]#**
SF	19.8 ±1.0	0	34.4	0	1173.1	0
SF (H_2SO_4)	19.4 ±1.1	-2.0	40.8	18.6	1545.5	31.7

8.5.4.2 DSC

The composite materials were tested with differential scanning calorimetry (DSC) regarding their melting and crystallization behaviour (Table 8-10). The melting peak for pure polypropylene was at 163 °C and the crystallization peak at 119 °C. Composites made with SF had a lower melting and crystallization peak at 159 °C and 117 °C. Composites made with SF (H_2SO_4) had slightly higher melting and crystallization peaks when compared to SF. The degree of crystallinity of composites with SF (H_2SO_4) increased by 8 % when compared to composite materials with SF. The increase could be due to changes

in the particle size of the soy flour which can lead to increased nucleation of polypropylene and subsequently increase the crystallinity of the composite. But also changes of the charge at the protein surface may induce nucleation. Overall the increase in crystallinity was not sufficiently high to increase the impact behaviour of the SF (H_2SO_4) composite.

Table 8-10 Melting and crystallization peaks and energy and degree of crystallinity of polypropylene and soy flour composites

	Melting		Crystallization		
Sample	Peak [°C]	H_m [J/g]	Peak [°C]	H_c [J/g]	Degree of Crystallinity [%]
PP blend	163.06	119.4	119.46	120.8	57.80
SF (single)	159.04	69.53	117.05	68.38	46.74
SF (H_2SO_4)	159.96	75.71	117.75	73.99	50.57

8.5.4.3 Field Scanning Electron Microscopy (FESEM)

Field Scanning Electron Microscopy was performed on the fractured surface produced during the impact testing of the composite materials. The soy flour in the composite with SF (H_2SO_4) had a very porous and brittle appearance (Figure 8-7 a)). Many soy flour components had cracks (Figure 8-7 c), d) and f)) and others seemed to be broken off from larger soy flour (Figure 8-7 b)). The holes in the composite material seemed to be the result of soy flour that had detached completely from the matrix during the impact test and fell out, similar as a "fiber-pull-out" (Figure 8-7 b)) [207]. Some soy flour components displayed poor interphase with the polypropylene matrix (Figure 8-7 e)). Other soy flour components showed partial bonding with the matrix (Figure 8-7 c) and g)). No crystals were observed for the composites prepared with soy material and the H_2SO_4. This indicates negligible residual H_2SO_4 treatment were found as seen in previous work [20].

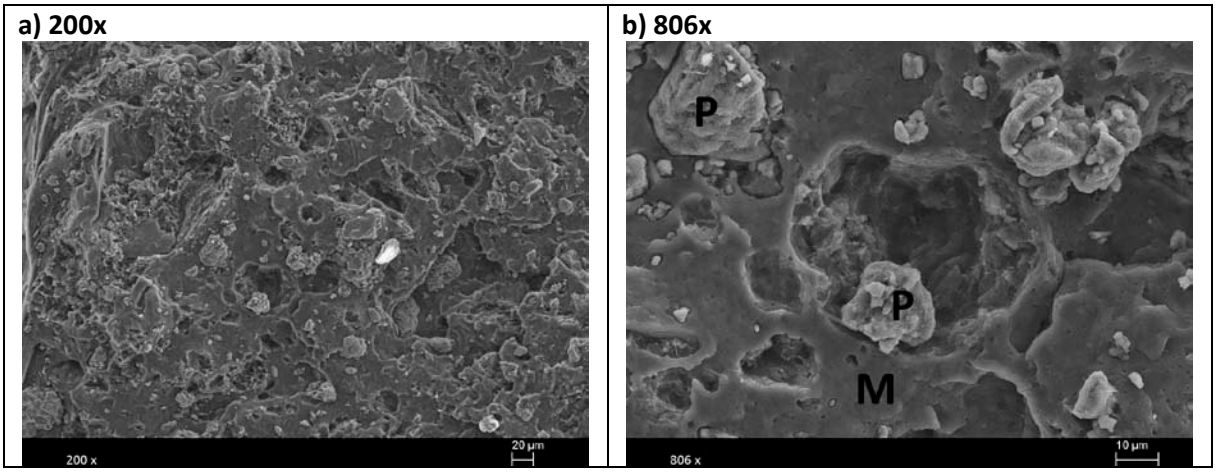

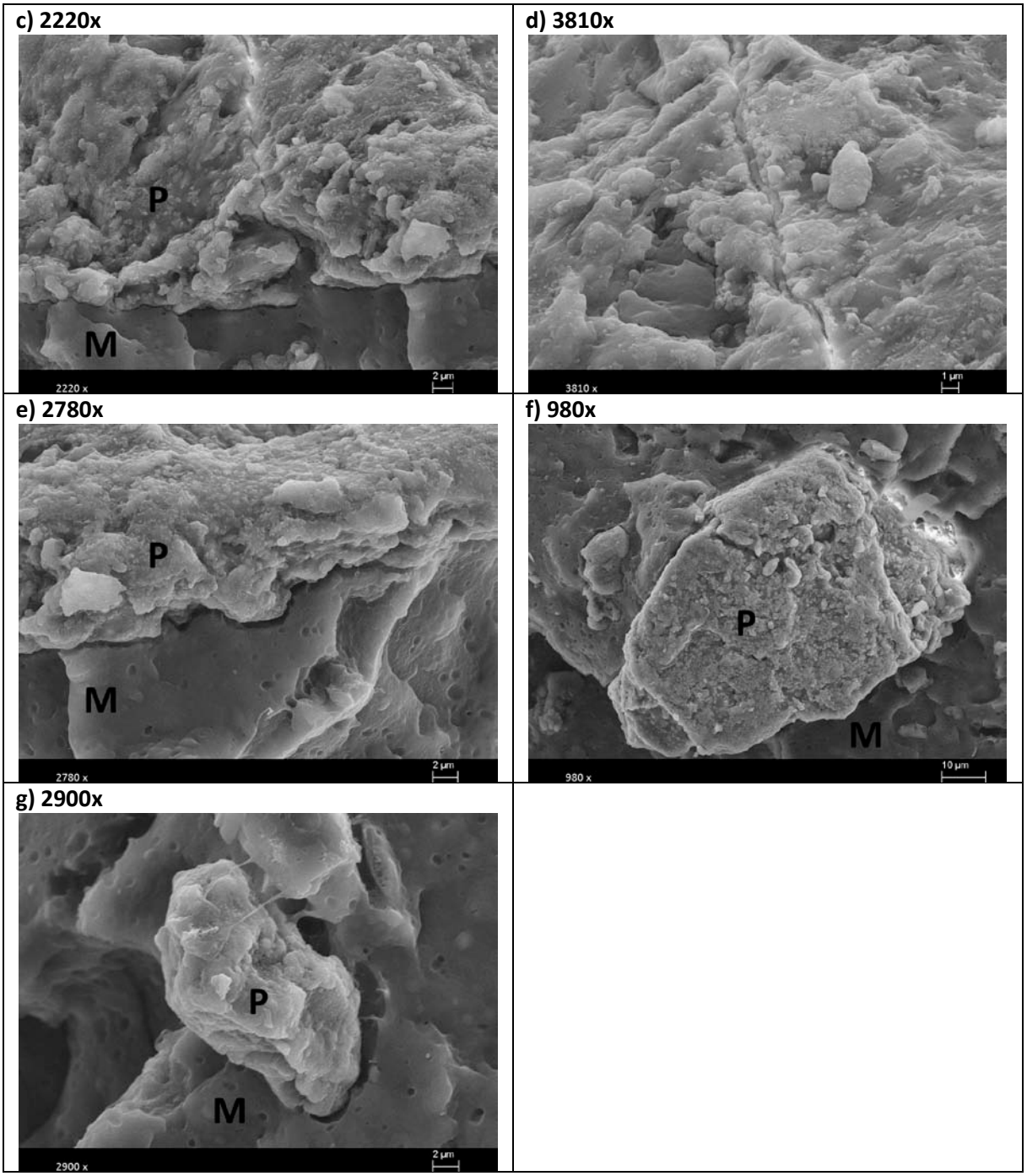

Figure 8-7 Scanning electron microscopy images of SF (H_2SO_4) polypropylene composites at different magnifications

8.6 Conclusions

Soy flour (SF) was treated with sulfuric acid (H_2SO_4) by adjusting the pH of aqueous water-SF slurry to pH 3 and with subsequent drying at room temperature.

FTIR spectra of SF (H_2SO_4) showed an increase of the wavenumber region 3800-3000 cm^{-1}, specific for hydroxyl groups, and an increase for the wavenumber region 1900-1482 cm^{-1}, specific for amide I and II groups present in proteins. Additional peaks were observed and suggest the presence of furan, formic acid and acetonitrile which are known derivatives or by-products of sugars [204].

The dynamic TGA, performed in nitrogen in a temperature range of 40 to 800 °C, revealed a very early onset of degradation due to components degrading in the temperature range between 100 and 200 °C. These components could be sugars or sugar derivatives with low boiling points. Isothermal TGA revealed a good thermal stability with 6% mass loss after 60 minutes at 200 °C in air. This mass loss is probably due to the removal of the sugar derivatives identified during the dynamic TGA before 200 °C.

Contact angle and surface energy of the SF (H_2SO_4) showed slight increases. The increase in total surface energy was predominantly in the polar component.

Composites made with SF (H_2SO_4) showed no change in Izod impact strength but increased in flexural strength and flexural modulus when compared to composites with untreated SF. This behaviour could be due to weak bonds between the soy material and the polypropylene matrix that enhance elasticity but not impact strength. The degree of crystallization was increased up to 8 % which could be due to a decrease in the size of the soy material or changes of the soy flour surface that created nucleation points resulting in higher crystallinity. The increase was minor and its effect did not improve the impact properties of the composites.

FESEM imaging revealed different mechanisms of crack propagation when compared to the other types of soy material investigated in this work. Many soy flour components were broken or cracked. Some soy material had good bonding with the polymer matrix while others showed poor bonding. This is thought to be due to the heterogeneity in composition of the soy material dispersed phase. The treatment of soy flour with sulfuric acid shows promising results in thermal behaviour of the soy flour as well as partial bonding with the polypropylene matrix. Further studies should include the combination of the acid treatment with heat treatment in order to remove the thermally unstable fraction before 200 °C of SF (H_2SO_4) which might result in improved mechanical properties due to removal of some of the volatile components.

8.7 Acknowledgements

The authors would like to thank Bunge Inc. (Hamilton, Canada) for providing soy materials, Archer Daniels Midland Company (ADM, Decatur, USA) and especially Russ Egbert for kindly providing soy materials and productive discussions and A. Schulman for providing polypropylene. Special thanks to Dr. Peldszus at the University of Waterloo for the use of the contact angle instrument. Special thanks to Dr. C. Tzoganakis (University of Waterloo) for access of Haake Rheomex 252 single-screw extruder and pelletizer and Dr. S. Zhu for his assistance with the operation. Thanks to Jacob Drouillard for his help with the preparation and testing of the composite materials. Financial support from Grain Farmers of Ontario (formerly Ontario Soybean Growers), NSERC (Natural Sciences and Engineering Research Council of Canada) and Ontario Research Fund (BioCar) are gratefully recognized.

9. Conclusions and Recommendations

The research presented in this PhD project focused on the development of soy polypropylene composite materials with improved mechanical properties when compared to untreated soy materials. The emphasis was on soy flour in polypropylene composites and their impact properties. A number of soy materials were investigated in addition to soy flour, soy reference materials (soy protein isolate (SPI), soy hulls (SH)) and soy flour by-product materials (insoluble soy (IS), soluble sugar extract (SSE)). The discussion, to follow, will emphasize the knowledge acquired during the characterization of the soy materials and the major developments achieved in producing soy-polypropylene composites with improved mechanical properties by manipulation of the soy polypropylene interface properties. The first phase of the work consisted of extensive soy material characterization and served as the basis for the subsequent formulation and production of composite materials.

Studies of the thermal behaviour of the soy materials indicated that SSE had the lowest thermal stability while SPI had the highest thermal stability according to their 1 and 5 wt-% onset of degradation temperature. These results suggest that SSE, present in SF, should be the first fraction to degrade when exposed to high temperatures such as the processing conditions of SF polypropylene composites. By removing SSE from SF, which can be achieved by alkaline extraction and will generate a solid residue, (IS), one would expect higher thermal stability of the composites and lower release of volatile components during composite manufacturing. Treatment by potassium permanganate or autoclave of the soy flour and reference soy materials showed no significant changes in the thermal stability of soy flour but minor improvement was observed for autoclaved SPI, SH and IS.

Studies of the chemical surface composition by FTIR analysis revealed differences between the reference materials for the specific wavenumber regions: 1900 to 1482 cm^{-1} and 1195 to 875 cm^{-1}. Treatments with potassium permanganate resulted in a decreased relative contribution in the wavenumber region between 1900 and 1482 cm^{-1} for SPI but an increased relative contribution in the same wavelength region for SH. The relative contribution for these regions of SF and IS remained constant which indicates that the effects of the potassium permanganate treatment on protein and carbohydrates might balance out.

Contact angle analysis proved to be a powerful tool for the investigation of the surface properties of the soy materials and the effect of treatment. Potassium permanganate

treatment increased the water contact angle for all soy materials, except SPI. In contrast, the autoclave treatment decreased the water contact angle. Potassium permanganate treatment was more efficient in reducing the difference of the water contact angle between the soy material and polypropylene. The change of the water contact angle over time due to absorption was also investigated. The water absorption rates of the untreated soy materials were, with exception of SH, lower than their values after autoclave treatment but higher than their water absorption rates after potassium permanganate treatment. The water absorption rates for SH decreased after both treatments. Autoclaved SPI and IS had the fastest water absorption rate and potassium permanganate treated SF and SPI had the lowest water absorption rate.

The surface energy analysis of the soy materials revealed significant differences of the polar surface energy component according to the protein content of the soy materials. Increased protein content of the soy material was associated with increasing polar surface energy. The increase was more pronounced when the high protein containing soy materials (SPI, SF and IS) were autoclaved. Potassium permanganate treatment, on the other hand, decreased the polar surface energy of the high protein containing soy materials (SPI, SF and IS).

The impact and flexural properties of the soy flour polypropylene composites were improved when soy flour was treated when compared to untreated soy flour polypropylene composites. The autoclave treatment of soy flour decreased the impact properties while improving the flexural properties of the composites. However, when the autoclave treated soy flour was combined with maleic anhydride coupling agent, the impact and flexural properties improved when compared to untreated soy flour composites. Composites with SF ($KMnO_4$) showed increase impact and flexural properties but when SF ($KMnO_4$) was compounded with maleic anhydride coupling agents its properties decreased. The binding mechanisms of SF (auto) and SF ($KMnO_4$) are different because of their different performance with and without coupling agent. SF (auto) showed poor interfaces when investigated with FESEM whereas SF (auto) with coupling agent had a much smoother surface with well-embedded dispersed phase. The propagation of the cracks clearly changed after the addition of coupling agent from “through the interface” to “through the matrix” indicating a good chemical bonding between dispersed and continuous phase. When SF ($KMnO_4$) was investigated with FESEM, partial good bonding between dispersed and continuous phase was visible but not all areas of the dispersed phase bonded to the polymer. Both composite materials showed improvements in impact and flexural properties which is an unusual behaviour. Often toughness and strength behave in opposite directions. Similar toughness-strength behaviour is known for natural materials and is explained by

their multi-scale structure that can create different bonding mechanisms in every layer making it tough and strong at the same time. Therefore, the most promising materials from this study are the composites from SF (auto) with Orevac CA100 and the composite SF ($KMnO_4$).

The most important contribution of this research was the development of the contact angle analysis method by creating soy material disks as well as the investigation of the effects of the $KMnO_4$ and autoclave and H_2SO_4 treatments on the soy flour fractions when producing soy-polypropylene composite materials. This work has never been presented in literature. The impact of the findings presented in this thesis can serve in the development of characterization methods for natural materials when used as filler in polymer composite materials.

The results presented in this study have led to the formulation of the following recommendations for future work. These recommendations are made along two avenues of work, soy material characterization, and formulation and composite production.

1. **Chemical Surface Composition**

   Partial surface composition was obtained by FTIR. It is proposed to obtain elemental and functional surface composition with a second characterization method, X-ray photoelectron spectroscopy (XPS).

2. **Contact angle analysis**

   Since the contact angle analysis is known to be very sensitive to the specimen morphology (roughness and homogeneity), the preparation of the soy material discs for the contact angle analysis should be optimized to improve the reproducibility. The effect of the pressure during pellet preparation should be investigated and quantified so that variations during preparation of the samples as well as during the measurement can be assigned to the source of error.

3. **Composite Formulation: Coupling agents**

   Other types of coupling agents should be investigated: (1) Coupling agents with acrylic or isocyanate functional groups, employed previously in similar applications and showing improvements in mechanical properties [130, 179, 181, 208-210].

   (2) Multifunctional coupling agents that may have the ability to bind to protein groups and cellulose groups on the soy material surface [124, 126, 127].

4. Composite manufacture

Since the composites were manufactured in a lab-scale mini-extruder, the findings of this work should be evaluated with an industrial scale extruder. Different extrusion conditions, e.g. feeding position of soy material could also be investigated and optimized [211].

5. Composite properties

A number of properties remain to be evaluated before the materials can be used in commercial applications. Those properties were not the scope of this work but can be used when developing automotive interior parts. Additional properties include dynamic mechanical analysis, water absorption behaviour and tensile properties, biodegradability, odour, scratch resistance, hardness and long term performance.

References

[1] Krenkel W (2008) Verbundwerkstoffe - 17. Symposium Verbundwerkstoffe und Werkstoffverbunde. Wiley VCH GmbH & Co. KGaA, Weinheim

[2] Trabi: Die Karosserie. (2012) . http://www.jhk1.de/trabi/karosserie.htm. Accessed 02/03 2010

[3] Ersatzteile und Sportzubehör für den Trabant 601. (2009) LDM-tuning.de, Plauen. http://www.ldm-tuning.de/trabant_601/. Accessed 08/02 2010

[4] Branchenführer Innovative Biowerkstoffe (BIB 2010). (2010) nova-Institut GmbH. http://www.biowerkstoff.info/. Accessed 02/03 2010

[5] Süss T (2009)

[6] Informationen zur Fachagentur Nachwachsende Rohstoffe e.V. (2010) Fachagentur Nachwachsende Rohstoffe e.V. (FNR). http://www.nachwachsenderohstoffe.de/. Accessed 02/03 2010

[7] Sathe SN, Rao GSS, Devi S (1994) J Appl Polym Sci 53:239

[8] Determination of Secondary Structure in Proteins by Fourier Transform Infrared Spectroscopy (FTIR). Leibniz Institute for Age Research - Fritz Lipmann Institute (FLI), Jena, Germany. www.fli-leibniz.de/IMAGE.html. Accessed 01/20 2012

[9] Hühne R, Koch F, Suhnel J (2007) Briefings in functional genomics & proteomics 6:220

[10] Reichert J, Suhnel J (2002) Nucleic Acids Res 30:253

[11] Mansfeldt T, Leyer H, Barmettler K et al (2004) Vadose Zone Journal 3:471

[12] Krüss GmbH (2004) DSA1 v 1.9 Drop Shape Analysis for DSA100.

[13] Fekete E, Hornsby PR, Jancar J et al (1999) Mineral Fillers in Thermoplastics I - Raw Materials and Processing. Springer-Verlag, Germany

[14] McCrum NG, Buckley CP, Bucknall CB (1990) Principles of Polymer Engineering. Oxford University Press, Oxford

[15] Wimmer R (2009) Angewandte Anatomie und Struktur der Holzwerkstoffe (presentation) Teil 4.

[16] Pompe G, Mader E (2000) Composites Science and Technology 60:2159

[17] Ritchie RO (2011) Nature Materials 10:817

[18] Murphy J (2001) Additives for Plastics Handbook, Second Edition. Elsevier Science

[19] Mohanty AK, Misra M, Drzal LT (2002) Journal of Polymers and the Environment 10:19

[20] Güttler BE (2009) Soy-Polypropylene Biocomposites for Automotive Applications. University of Waterloo, Waterloo, Ontario, Canada

[21] Alter H (1965) J Appl Polym Sci 9:1525

[22] Fu S, Feng X, Lauke B et al (2008) Composites Pt B: Eng 39:933

[23] Bledzki AK, Sperber VE, Faruk O (2002) Natural and Wood Fibre Reinforcement in Polymers (Report 152). Rapra Technology Inc.

[24] Maier C (1998) Polypropylene : the definitive user's guide and databook. Norwich, NY : Plastics Design Library, Norwich, NY

[25] Seymour RB (1971) Introduction to Polymer Chemistry. McGraw-Hill Book Company, University of Michigan

[26] Solid surface energy data (SFE) for common polymers. (2007) www.surface-tension.de, www.surface-tension.de. http://www.surface-tension.de/solid-surface-energy.htm. Accessed 03/01 2012

[27] Eustathopoulos N, Nicholas MG, Drevet B (1999) Wettability at High Temperatures. Elsevier Science, UK

[28] Endres JG (2001) Soy Protein Products Characteristics, Nutritional Aspects, and Utilization. AOCS Press, USA

[29] Eldridge A, Black L, Wolf W (1979) J Agric Food Chem 27:799

[30] Karr-Lilienthal LK, Grieshop CM, Spears JK et al (2005) J Agric Food Chem 53:2146

[31] Amino Acid Properties. (2009) University of California. http://www.mcb.ucdavis.edu/courses/bis102/AAProp.html. Accessed 03/03 2010

[32] Renner K, Moczo J, Suba P et al (2010) Composites Sci Technol 70:1141

[33] (2011) U.S. Department of Commerce, National Institute of Standards and Technology (NIST). http://www.nist.gov/index.html. Accessed 11/30 2011

[34] Stokes RJ, Evans DF (1997) Fundamentals of Interfacial Engineering. Wiley-VCH, New York ; Chichester, England

[35] Kacurakova M, Capek P, Sasinkova V et al (2000) Carbohydr Polym 43:195

[36] Mann D (1999) Automotive Plastics and Composites - Worldwide Markets and Trends to 2007. ELSEVIER

[37] Nicolais L, Meo M, Milella E (2011) Composite Materials - A Vision for the Future. Springer-Verlag, London

[38] Mallick PK (2010) Materials, design and manufacturing for lightweight vehicles. Woodhead Publishing Limited

[39] Stauber R (2006) Werkstoffe im Automobilbau – Anforderungen und Trends. Cluster „Neue Werkstoffe“ in Bayern München-Perlach

[40] Bratzel S, Tellermann R, Lehmann L et al (2010) Center of Automotive Management 2010-05:1

[41] Markarian J (2006) Automotive drives mineral modifier developments. Plastics, Additives and Compounding 8

[42] Rouilly A, Rigal L (2002) Journal of Macromolecular Science-Polymer Reviews C42:441

[43] Saheb DN, Jog JP (1999) Adv Polym Technol 18:351

[44] Bledzki AK, Faruk O, Sperber VE (2006) Macromolecular Materials and Engineering 291:449

[45] Gassan J, Reihmane S, Bledzki AK (1996) Journal of Applied Polymer Science (USA) 59:1329

[46] Bledzki AK, Gassan J (1999) Progress in Polymer Science 24:221

[47] Monteiro SN, Lopes FPD, Ferreira AS et al (2009) JOM 61:17

[48] John MJ, Thomas S (2008) Carbohydr Polym 71:343

[49] Sgriccia N, Hawley MC, Misra M (2008) Composites Part A-Applied Science and Manufacturing 39:1632

[50] Holbery J, Houston D (2006) JOM 58:80

[51] Mohanty AK, Misra M, Hinrichsen G (2000) Macromolecular Materials and Engineering 276:1

[52] Soy Stats 2011. (2011) . http://www.soystats.com/2010/Default-frames.htm. Accessed 9/22 2011

[53] Composition of Soy. (2011) American Soybean Association, USA. www.wishh.org/aboutsoy/composition.html. Accessed 12/28 2011

[54] Garcia M, Torre M, Marina M et al (1997) Critical Reviews in Food Science and Nutrition 37:361

[55] Biowerkstoff-Report 2009. (2010) nova-Institut GmbH. www.nachwachsende-rohstoffe.info. Accessed 2/03 2010

[56] Fowler PA, Hughes JM, Elias RM (2006) J Sci Food Agric 86:1781

[57] American Society for Testing and Materials (2008) Standard Practice for Evaluating and Reporting Environmental Performance of Biobased Products [ASTM D 7075 - 04].

[58] Naturfaserverstärkter Kunststoff . (2010) . http://de.academic.ru/dic.nsf/dewiki/1004732. Accessed 02/03 2010

[59] Kapustan Krüger P (2007) Wheat Straw-Polypropylene Composites. University of Waterloo, Waterloo, Ontario, Canada

[60] Sardashti A (2009) Wheat straw-clay-polypropylene hybrid composites. University of Waterloo, Waterloo, Ontario, Canada

[61] Ford teams up to develop wheat straw-reinforced plastic; New biomaterial debuts in 2010 Ford Flex. (2010) Ford Motor Company. http://media.fordvehicles.com/article_display.cfm?article_id=31391. Accessed 02/22 2010

[62] Callister WDJ, Rethwisch DG (2008) Fundamentals of Material Science and Engineering: An Integrated Approach. John Wiley and Sons, Inc.

[63] Davies G (2004) Materials for Automobile Bodies, 1st edn. Butterworth-Heinemann

[64] Nwabunma D, Kyu T (2007) Polyolefin composites. Hoboken, N.J., Wiley-Interscience, John Wiley & Sons

[65] Lewin M (2006) Handbook of Fiber Chemistry, 3rd edn. CRC Press

[66] Wool R, Sun XS (2005) Bio-Based Polymers and Composites, 1st edn. Elsevier, Academic Press

[67] Wypych G (1999) Handbook of Fillers, 2nd edn. Elsevier Science

[68] Albano C, Lavadi M, González J et al (2009) Macromolecular Symposia 286:70

[69] Steckel V, Clemons CM, Thoemen H (2007) J Appl Polym Sci 103:752

[70] Marcovich NE, Reboredo MM, Aranguren MI (1998) J Appl Polym Sci 68:2069

[71] Yang H, Kim H, Park H et al (2007) Composite Structures 77:45

[72] Marti-Ferrer F, Vilaplana F, Ribes-Greus A et al (2006) J Appl Polym Sci 99:1823

[73] Kim H, Lee B, Choi S et al (2007) Composites Part A: Applied Science and Manufacturing 38:1473

[74] Wang B, Sain M (2007) Polym Int 56:538

[75] Rothon RN (2003) Particulate-filled polymer composites. Smithers Rapra Press

[76] Majer Z, Hutar P, Knesl Z (2011) Materials Structure & Micromechanics of Fracture 465:564

[77] Kalia S, Kaith BS, Kaur I (2011) Cellulose Fibers: Bio- and Nano-Polymer Composites - Green Chemistry and Technology. Springer-Verlag, Berlin, Heidelberg

[78] Wielage B, Lampke T, Marx G et al (1999) Thermochimica Acta 337:169

[79] Mohan S, Durairaj KSP, Jose SP (2003) Spectrochimica Acta Part A-Molecular and Biomolecular Spectroscopy 59:1697

[80] Herrebout W, Clou K, Desseyn H et al (2003) Spectroc Acta Pt A-Molec Biomolec Spectr 59:47

[81] Doerr S, Schade U, Hellwig P (2008) Vib Spectrosc 47:59

[82] MacRitchie F (1990) Chemistry at interfaces. Academic Press, San Diego ; Toronto; San Diego

[83] Xanthos M (2005) Functional Fillers for Plastics. Wiley-VCH Verlag GmbH & Co. KGaA, Weinheim

[84] Owens DK, Wendt RC (1969) J Appl Polym Sci 13:1741

[85] Dankovich TA, Gray DG (2011) J Adhes Sci Technol 25:699

[86] Buckton G (1990) Powder Technol 61:237

[87] Roman-Gutierrez A, Sabathier J, Guilbert S et al (2003) Powder Technol 129:37

[88] Heng JYY, Pearse DF, Thielmann F et al (2007) Composite Interfaces 14:581

[89] Lampke T (2001) Beitrag zur Charakterisierung naturfaserverstaerkter Verbundswerkstoffe mit hochpolymerer Matrix.

[90] Jacob M, Joseph S, Pothan LA et al (2005) Composite Interfaces 12:95

[91] Butt H (2010) Surface and interfacial forces. Wiley-VCH, Weinheim

[92] Israelachvili JN (1991) Intermolecular and surface forces. Academic Press, London ; Toronto; London

[93] Zenkiewicz M (2007) Methods for the calculation of surface free energy of solids. 24

[94] Mittal KL (2006) Contact Angle, Wettability and Adhesion Volume 4. VSP, The Netherlands

[95] Recum AF, Shannon CE, Cannon CE et al (1996) Tissue Eng 2:241

[96] Adamson AW (1997) Physical Chemistry of Surfaces, 6.th edn. John Wiley & Sons, Inc., USA

[97] Butt H-, Graf K, Kappl M (2004) Physics and Chemistry of Interfaces. Wiley-VCH Verlag GmbH & Co. KGaA, Weinheim

[98] Wenzel RN (1949) The Journal of Physical Chemistry 53:1466

[99] Jahanmir J, Wyant JC (1992) Comparison of Surface-Roughness Measured with an Optical Profiler and a Scanning Probe Microscope. SPIE 1720. DOI:10.1117/12.132117

[100] Ayrilmis N (2011) Bioresources 6:3178

[101] Tan PL, Sharif S, Sudin I (2012) Wood Sci Technol 46:129

[102] Moutinho I, Figueiredo M, Ferreira P (2007) Tappi J 6:26

[103] Johnson LA, White PJ, Galloway R (2008) Soybeans: Chemistry, Production, Processing, and Utilization. AOCS Press, USA

[104] Ozaki Y, McClure WF, Christy AA (2007) Near-Infrared Spectroscopy in Food Science and Technology. John Wiley & Sons, Inc., USA

[105] Jong L (2007) Composites Part A-Applied Science and Manufacturing 38:252

[106] Tucker N, Lindsey K (2002) An Introduction to Automotive Composites, first edn. iSmithers Rapra Publishing, United Kingdom

[107] Progelhof RC, Throne JL (1993) Polymer Engineering Principles Properties, Processes, and Tests for Design. Hanser/Gardner Publications, Inc.

[108] American Society for Testing and Materials (2008) Standard Test Method for Flexural Properties of Unreinforced and Reinforced Plastics and Electrical Insulating Materials [ASTM D 790 - 07].

[109] American Society for Testing and Materials (2008) Standard Test Methods for Determining the Izod Pendulum Impact Resistance of Plastics [ASTM D 256 - 06a].

[110] Degischer HP, Lüftl S (2009) Leichtbau - Prinzipien, Werkstoffauswahl und Fertigungsvarianten. Wiley-VCH Verlag GmbH & Co. KGaA, Germany

[111] Lakes R (1993) Nature 361:511

[112] Arencon D, Ignacio Velasco J (2009) Materials 2:2046

[113] Mallakpour S, Hajipour A, Zadhoush A et al (2001) Journal of Applied Polymer Science 79:1317

[114] Le Digabel F, Boquillon N, Dole P et al (2004) J Appl Polym Sci 93:428

[115] Tabtiang A, Venables R (2000) European Polymer Journal 36:137

[116] Arbelaiz A, Fernández B, Ramos JA et al (2005) Composites Science and Technology 65:1582

[117] Espert A, Vilaplana F, Karlsson S (2004) Composites Part A: Applied Science and Manufacturing 35:1267

[118] Rana AK, Mandal A, Mitra BC et al (1998) J Appl Polym Sci 69:329

[119] Ton-That TM, Jungnickel BJ (1999) J Appl Polym Sci 74:3275

[120] Qiu WL, Zhang FR, Endo T et al (2005) Polymer Composites 26:448

[121] Dekker M (1999) Handbook of polypropylene and polypropylene composites. Eastern Hemisphere Distribution Marcel Dekker AG

[122] Fuad MYA, Ismail Z, Ishak ZAM et al European Polymer Journal 31:885

[123] Ishida H, Chiang Ch, Koenig JL (1982) Polymer 23:251

[124] Boehme F, Jakisch L, Komber H et al (2007) Polym Degrad Stab 92:2270

[125] Jakisch L, Komber H, Bohme F (2003) Journal of Polymer Science Part A: Polymer Chemistry 41:655

[126] Jakisch L, Komber H, Wursche R et al (2004) Journal of Applied Polymer Science 94:2170

[127] Taylor-made Polymer Modificators and Coupling Agents. (2010) Leibniz Institute für Polymerforschung Dresden e.V., Dresden, Germany. http://www.ipfdd.de/Tailor-made-Polymer-Modificators-and-Cou.750.0.html?&L=0. Accessed 3/23 2010

[128] Brechet Y, Cavaille JYY, Chabert E et al (2001) Advanced Engineering Materials 3:571

[129] Takemoto T, Yasuda K, Ley S (2001) Synlett:1555

[130] Li X, Tabil LG, Panigrahi S (2007) Journal of Polymers and the Environment 15:25

[131] Garves K (1997) Holzforschung 51:526

[132] Paul A, Joseph K, Thomas S (1997) Composites Sci Technol 57:67

[133] De Rosa IM, Kenny JM, Maniruzzaman M et al (2011) Composites Sci Technol 71:246

[134] Han YH, Han SO, Cho D et al (2007) Composite Interfaces 14:559

[135] Kalia S, Kaith BS, Kaur I (2009) Polym Eng Sci 49:1253

[136] Kalapathy U, Hettiarachchy NS, Rhee KC (1997) Journal of the American Oil Chemists Society 74:195

[137] Hettiarachchy NS, Kalapathy U, Myers DJ (1995) Journal of the American Oil Chemists Society 72:1461

[138] Su J, Huang Z, Yuan X et al (2010) Carbohydr Polym 79:145

[139] Perez Locas C, Yaylayan VA (2008) J Agric Food Chem 56:6717

[140] Zeitsch KJ (2000) The Chemistry and Technology of Furfural and its many by-products (Sugar Series, 13), 1st edn. Elsevier Science B.V., Netherlands

[141] Swain SN, Rao KK, Nayak PL (2004) J Appl Polym Sci 93:2590

[142] Das SN, Routray M, Nayak PL (2008) Polym Plast Technol Eng 47:576

[143] Gaceva G, Avella M, Malinconico M et al (2007) Polymer Composites 28:98

[144] Drzal LT, Mohanty AK, Misra M (2000) :21

[145] Bernland K, Tervoort T, Smith P (2009) Polymer 50:2460

[146] Roy S, Scionti V, Jana SC et al (2011) Macromolecules 44:8064

[147] Su J, Yang G, Geng C et al (2011) Chin J Polym Sci 29:732

[148] Subirade M, Kelly I, Gueguen J et al (1998) Int J Biol Macromol 23:241

[149] Cho SY, Rhee C (2002) Lebensmittel-Wissenschaft Und-Technologie-Food Science and Technology 35:151

[150] Denavi G, Tapia-Blacido DR, Anon MC et al (2009) J Food Eng 90:341

[151] Yin S, Tang C, Wen Q et al (2007) J Agric Food Chem 55:7399

[152] Ogale AA, Cunningham P, Dawson PL et al (2000) J Food Sci 65:672

[153] Juskey VP(, Chaffey CE((1982) Can J Chem Eng 60:334

[154] Sailaja RRN, Girija BG, Madras G et al (2008) J Mater Sci 43:64

[155] Choi HY, Han SO, Lee JS (2009) Composite Interfaces 16:359

[156] Kumar L, Chandra R, Chung PA et al (2010) Bioresour Technol 101:7827

[157] Kaboorani A (2009) J Composite Mater 43:2599

[158] Morales FJ, van Boekel MAJS (1998) Int Dairy J 8:907

[159] van Boekel MAJS (1999) Int Dairy J 9:237

[160] Metwalli AAM, van Boekel MAJS (1998) Food Chem 61:53

[161] Rong M, Zhang M, Liu Y et al (2002) Polym Compos 23:182

[162] Pietak A, Korte S, Tan E et al (2007) Appl Surf Sci 253:3627

[163] Prinyawiwatkul W, Beuchat L, McWatters K (1993) J Food Sci 58:1318

[164] Braskem and Novozymes to make green plastic. (2009) . http://www.braskem.com.br/site/portal_braskem/en/sala_de_imprensa/sala_de_imprensa_detalhes_9529.aspx. Accessed 4/04 2010

[165] Braskem & Toyota Tsusho start joint marketing activities for green polyethylene from sugar cane in Asia. (2009) Braskem. http://www.braskem.com.br/site/portal_braskem/en/sala_de_imprensa/sala_de_imprensa_detalhes_7983.aspx. Accessed 03/04 2010

[166] Araujo JR, Waldman WR, De Paoli MA (2008) Polym Degrad Stab 93:October

[167] Park S, Venditti RA, Jameel H et al (2006) Cellulose 13:23

[168] Lang CA (1958) Anal Chem 30:1692

[169] Jung S, Rickert DA, Deak NA et al (2003) Journal of the American Oil Chemists Society 80:1169

[170] Archer Daniels Midland Company (2010) ADM Food Ingredient Catalog 2010-11. SB0510

[171] Carrillo A, Colom X, Sunol J et al (2004) European Polymer Journal 40:2229

[172] Pandey K (1999) J Appl Polym Sci 71:1969

[173] Agarwal UP, Ralph SA, Atalla RH (1997) FT Raman spectroscopic study of softwood lignin

[174] Surewuz WK, Mantsch HH, Chapman D (1993) Biochemistry (N Y) 32:389

[175] Proniewicz L, Paluszkiewicz C, Weselucha-Birczynska A et al (2002) J Mol Struct 614:345

[176] Tian K, Porter D, Yao J et al (2010) Polymer 51:2410

[177] Schmidt V, Giacomelli C, Soldi V (2005) Polym Degrad Stab 87:25

[178] Christophe B, Frederic B, Yves G et al (2006) Composites Part A: Applied Science and Manufacturing 37A:128

[179] Zhang J, Yao Y, Wang X et al (2006) J Appl Polym Sci 101:436

[180] Domka L (1994) Colloid Polym Sci 272:1190

[181] Ashori A, Nourbakhsh A (2009) J Appl Polym Sci 111:1684

[182] Angles MN, Salvado J, Dufresne A (1999) J Appl Polym Sci 74:1962

[183] Novák I, Borsig E, Hrčková L et al (2007) Polym Eng Sci 47:1207

[184] Tian H, Zhang L, Wu Q et al (2010) Macromol Mater Eng 295:451

[185] Buckton G, Newton JM (1986) Powder Technol 46:201

[186] Buckton G (1992) Drug Dev Ind Pharm 18:1149

[187] Surface Energy Data for PP: Polypropylene, CAS #s 9003-08-0 (atactic) and 25085-53-4 (isotactic). (2009) .
http://www.accudynetest.com/polymer_surface_data/polypropylene.pdf 2011

[188] Shen Q, Nylund J, Rosenholm JB (1998) Holzforschung 52:521

[189] American Society for Testing and Materials (2008) ASTM D7490-08 Standard Test Method for Measurement of the Surface Tension of Solid Coatings, Substrates and Pigments using Contact Angle Measurements.

[190] Tang C, Choi S, Ma C (2007) Int J Biol Macromol 40:96

[191] Fahmy TYA, Mobarak F, Kassem N et al (2008) Carbohydr Polym 74:892

[192] Zaman HU, Khan MA, Khan RA et al (2010) Fibers and Polymers 11:455

[193] Martin-Sampedro R, Antonio Martin J, Eugenio ME et al (2011) BioResources 6:4922

[194] Clariant International Ltd. Pigments & Additives Division (2006)

[195] Priex Maleic Anhydride Grafted. . http://www.addcomp.nl/priex/priex-grafted.php 2012

[196] Arkema (2004)

[197] E.I. du Pont de Nemours and Company, Inc. (2010)

[198] Office of Water (1999) In: Anonymous
EPA Guidance Manual - Alternative Disinfectants and Oxidants. Office of Water, United States Environmental Protection Agency

[199] Lu MS, Manning K, Nelsen S et al (1998) High impact strength reinforced polyester engineering resins for automotive applications

[200] Yu ZZ, Yang MS, Dai SC et al (2004) J Appl Polym Sci 93:1462

[201] Yang H, Kim H, Park H et al (2007) Composite Structures 77:45

[202] Yuan YJ, Velev OD, Chen K et al (2002) Effect of pH and Ca2+ - Induced Associations of Soybean Proteins. 50

[203] Renkema JMS, Gruppen H, van Vliet T (2002) J Agric Food Chem 50:6064

[204] Söderström J, Pilcher L, Galbe M et al (2003) Biomass & Bioenergy 24:475

[205] Zhao B, Kwon HJ (2011) J Adhes Sci Technol 25:557

[206] Gütsch JS, Nousiainen T, Sixta H (2012) Bioresour Technol 109:77

[207] Mallick PK (2008) Fiber-Reinforced Composites - Materials, Manufacturing, and Design, 3rd edn. CRC Press, Taylor & Francis Group, USA

[208] Nourbakhsh A, Kokta B, Ashori A et al (2008) Journal of Reinforced Plastics and Composites 27:1679

[209] Van de Velde K, Kiekens P (2001) J Thermoplast Compos Mater 14:244

[210] Lee S, Wang S (2006) Composites Part A: Applied Science and Manufacturing.Vol.37 37:80

[211] Ruch J, Fritz H-, Bürkle E et al (2002) Kunststoffe Aufbereitung:28

[212] Istguro T, Ono T, Nakasato K et al (2005) J Food Sci 70:C63

[213] Wang Guang-Heng, Zhou An-Ning, Hu Mao-Bing (2006) J Appl Polym Sci 102:3134

[214] Schmidt V, Soldi V (2006) Polym Degrad Stab 91:3124

[215] Yang H, Yan R, Chen H et al Fuel 86:1781

[216] Chen H, Ferrari C, Angiuli M et al (2010) Carbohydr Polym 82:772

Appendix I. (Chapter 5): Filler Characterization

FTIR

Table 10-1 Overview of FTIR values for soy proteins, soy saccharides and other soybean constituents previously published

Compound	Vibration	Wavelength [cm^{-1}]	Reference
Soy saccharides		900-1200	[212]
Potassium phytate	-PO3	970	[212]
Aromatic groups	Out-of-plane C-H bending	1060	[138]
Potassium phytate	C-O-P	1070	[212]
SPI-SDS	Out-of-plane C-H bending (from aromatic structures), PO2-, P-OH stretching from phosphate esters	1100	[177]
Potassium phytate	C-C	1124	[212]
Potassium phytate	P=O	1170	[212]
Proteins (SPI-SDS)	C(O)-O and C-N stretching, N-H bending (amide III)	1220	[177]
Proteins	C-N stretching and N-H bending (amide III)	1241-1472	[138, 213]
Proteins (soy)	N-H in-plane bending, C-N stretching of backbone, C=O in-plane bending, C-C and C-N stretching(Amide II)	1500-1600	[176]
Proteins (soy)	Tyr side chains	1515	[176]
SPI-SDS	N-H bending (amide II)	1530	[177]
Proteins	-NH (amide I and II)	1533-1559	[138]
Defatted soy flour	N-H (amide II)	1542	[213]
Proteins (soy)	Overlapped band of the amide II mode from random coil structures	1550	[176]
Proteins (soy)	C=O stretching of amide I group (coupled to the in-phase bending of the N-H bond and the stretching of the C-N bond)	1600-1700	[174, 176]
Proteins (SPI-SDS)	Amide I	1630	[177]
Proteins	-NH (amide I and II)	1636-1680	[138]
Proteins (soy)	Random coils and α-helix structures in the silk fibroin	1640-1660	[176]
Defatted soy flour	C=O (amide I)	1654	[213]
Proteins (soy)	ß-sheet vibrations (maybe better to ß-turns)	1690-1700	[176]
SPI-SDS	C=O stretching	1740	[177]
SPI-SDS	C-H stretching of CH_2 and CH_3	2850-2980	[177]
Defatted soy flour	Free bounded –OH and -NH	3000-3600	[213, 214]
Proteins (soy)	Hydrogen bonding between	3294	[176]

	protein chains and moisture in proteins		

Table 10-2 Overview of FTIR values for cellulose, hemicellulose, lignin, saccharides previously published

Compound	**Vibration**	**Wavelength [cm^{-1}]**	**Reference**
Cellulose, hemicellulose, lignin	C-C stretching	400-700	[215]
(Okra)	C-OH bending	598	[133]
Aromatic hydrogen (cellulose, hemicellulose, lignin)	C-H	700-900	[215]
Monosaccharides	ß-glycosidic linkage between monosaccharides	894	[133]
Cellulose I and II	Group C_1 frequency	895 and 893	[171]
Softwood/Hardwood	Character of cellulose P-chains, C-H stretching out of plane of aromatic ring	896	[216]
Cellulose	Glucose ring stretch, C_1-H deformation	897	[172]
Softwood/Hardwood	C-O deformation in primary alcohols, plus C=O stretch unconj., plus aromatic C-H in-plane deformation	1030	[216]
Cellulose	C-O stretch	1033	[172]
Polysaccharides	C-O and O-H stretching in polysaccharides from cellulose	1035	[133, 171]
Cellulose I and II	C-O stretching	1055	[171]
Cellulose	C-O stretch	1059	[172]
C-OH (ethanol)	C-O stretching and C-O deformation	1060	[215]
C-OH	OH association	1108	[215]
Cel I/Cell II	Antisymmetric in-phase ring stretching	1111/1007	[171, 216]
Cellulose	Glucose ring stretch (asymmetric)	1112	[172]
Cellulose I and II	C-O-C asymmetric stretching	1155 and 1162	[171]
Softwood/Hardwood	C-O-C stretching in pyranose rings, C=O stretching in aliphatic groups	1160	[216]
Cellulose	C-O-C asymmetric vibration	1163	[172]
Pyranose ring skeletal	C-O-C stretching	1170, 1082	[215]
Cellulose	O-H deformation	1201	[172]
Cellulose I and II	-OH in plane bending	1205 and 1200	[171]
Phenol	C-O stretching	1215	[215]
Hardwood	C-C plus C-O plus C=O stretching	1230	[216]
Aryl-alkyl ether linkage	C-O-C stretching	1232	[215]
Lignin and hemicellulose	C-O stretching of acetyl group in lignin and hemicellulose	1243, 1384	[133]
Softwood	Guaiacyl ring breathing plus C=O	1270	[216]

	stretching		
Cellulose I and II	CH bending	1282 and 1278	[171]
Cellulose I and II	CH_2 wagging	1317 and 1315	[171]
Softwood/Hardwood	Condensation of guaiacyl unit and syringyl unit, syringyl unit and CH_2 bending stretching	1317/1321	[216]
Cellulose	CH_2 wagging	1318	[172]
Polysaccharides	C-H and C-O bending of aromatic ring in polysaccharides	1320, 1370	[133]
Cellulose	O-H in-plane deformation	1336 and 1335	[171, 172]
Cellulose	C-H deformation (symmetric)	1372	[172]
Softwood/Hardwood	Aliphatic C-H stretching in methyl and phenol OH	1375	[216]
Cellulose I and II	CH bending	1375	[171]
	CH bending	1402	[215]
Softwood/Hardwood	Aromatic skeletal combined with C-H in-plane deforming and stretching	1425	[216]
Cellulose	CH_2 symmetric bending in cellulose	1430	[133]
Cellulose	C-H deformation (asymmetric)	1430	[172]
Cellulose I and II	CH_2 symmetric bending	1430 and 1420	[171]
Methoxyl-O-CH_3	O-CH_3	1430-1470	[215]
Acid	OH bending	1440-1400	[215]
Cellulose I and II	-OH in plane bending	1455 and 1470	[171]
Softwood/Hardwood	CH_2 deformation stretching in lignin and xylan	1463	[216]
Softwood/Hardwood	Aromatic skeletal stretching	1510/1507	[216]
Ketone and carbonyl	C=O stretching	1510-1560	[215]
Lignin	C=C stretching of aromatic ring in lignin	1517	[133]
Hardwood	C=O stretching conjugated to aromatic ring	1595	[216]
Aromatic skeletal mode	C=C stretching	1613, 1450	[215]
Benzene stretching ring	C=C	1632	[215]
Cellulose I and II	OH of water absorbed from cellulose	1635	[171]
Cellulose	Adsorbed O-H, conjugated C=O	1640	[172]
Softwood/Hardwood	C=O stretching conjugated to aromatic ring	1640	[216]
Alkyl, aliphatic, aromatic	C-H_n stretching	1700-1730	[215]
Softwood/Hardwood	C=O stretching in unconjugated ketone, carbonyl and aliphatic groups xylan	1739	[216]
Lignin and hemicellulose	Carbonyl C=O stretching of carboxylic acid in lignin or ester	1743	[133]

	group in hemicellulose		
Cellulose I and II Cellulose I and II	CH_2 asymmetric stretching	2853	[171]
Cellulose and hemicellulose	C-H stretching from CH and CH2	2854, 2925	[133]
Alkyl, aliphatic, aromatic	C-H_n stretching	2860-2970	[215]
Cellulose I and II	CH stretching	2900	[171]
Cellulose	C-H stretching	2902	[172]
Cellulose I and II	CH stretching	2945 and 2955	[171]
Cellulose I and II	CH stretching	2970	[171]
Acid, methanol	OH stretching	3000-3600	[215]
Cellulose and hemicellulose	O-H stretching, hydrogen bond of hydroxyl groups	3100-3600	[133]
Cellulose II	-OH stretching intramolecular hydrogen bonds	3175	[171]
Cellulose	O-H stretch (hydrogen-bonded)	3348	[172]
Cellulose I and II	-OH stretching intramolecular hydrogen bonds	3350	[171]
Cellulose I	-OH stretching intramolecular hydrogen bonds	3405	[171]
Cellulose II	-OH stretching intramolecular hydrogen bonds	3447	[171]
Cellulose II	-OH stretching intramolecular hydrogen bonds	3488	[171]

Table 10-3 FTIR wavelengths of plant cell wall polysaccharides [35].

Compound	**(C-OH), (C-O-C), (C-C), Ring**					**(Cl-H), Ring**			
Pectin	1144	1100		1047, 1017	953	896		857	835
Rhamnogalacturonan	1150	1122	1070	1043, 989	951, 916	902		846	823
Galactan	1155	1134	1072	1038		893	883		
Arabinan	1141	1097	1070	1039	918	895			807
Arabinogalactan			1074	1045		897	868		808
Arabinogalactan	1139		1078	1043, 985			880	842	
Arabinogalactan (type II)	1156		1078	1040	916	892	879		
Arabinogalactan (type II) + Glucomannan	1146		1066	1034		896	872		809
Arabinogalactorhamnoglycan				1049	914			837	810
Xyloglucan	1153	1118	1078	1041	945	897			
Glucan	1151	1104	1076	1041, 1026	916			840	
Glucomannan	1150		1092,	1034	941	898	872		814

			1064						
Galactoglucomannan	1149		1064	1034, 960	934	897	872		813
Arabinoglucuronoxylan + Galactoglucomannan	1161, 1151	1109	1070	1038		898	881		809
Pectin	1152	1004	1082, 1051	1022, 972		891		834	
GX	1147		1084	1047, 985		897			
Starch	1155	1110	1082	1026	931			850	

Table 10-4 Example of calculation for FTIR analysis

3800-3000	**3000-2850**	**1900-1482**	**1195-875**	**Peak-to-Peak-Ratio**					
1	**2**	**3**	**4**	**1/2**	**1/3**	**1/4**	**2/3**	**2/4**	**3/4**
80.92	3.66	38.27	21.67	22.12	2.11	3.73	0.10	0.17	1.77

Peak-to-Peak-Ratio 1/2: $\frac{Peak\ 1}{Peak\ 2} = \frac{80.92}{3.66} = 22.1$

FTIR Spectra

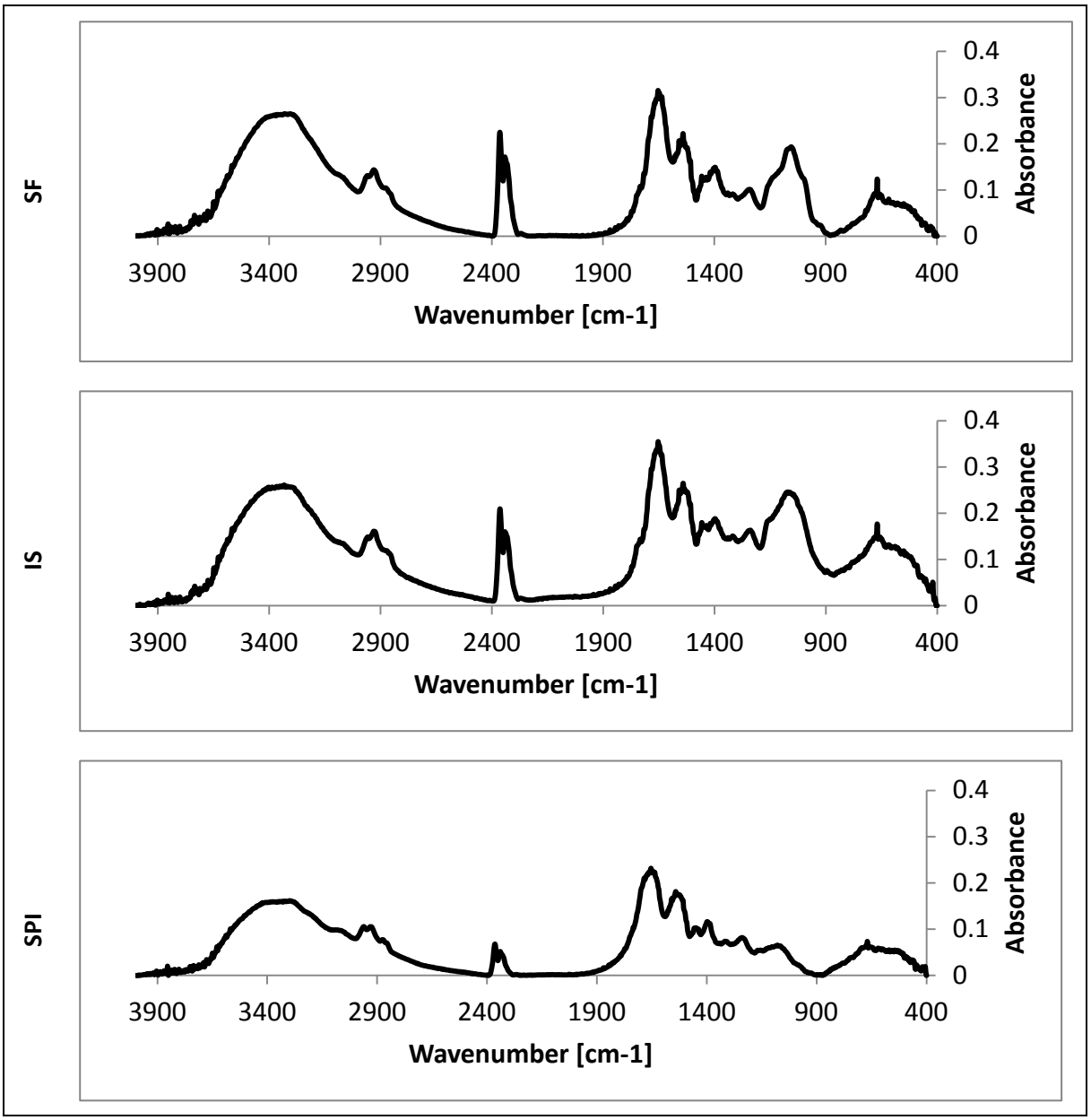

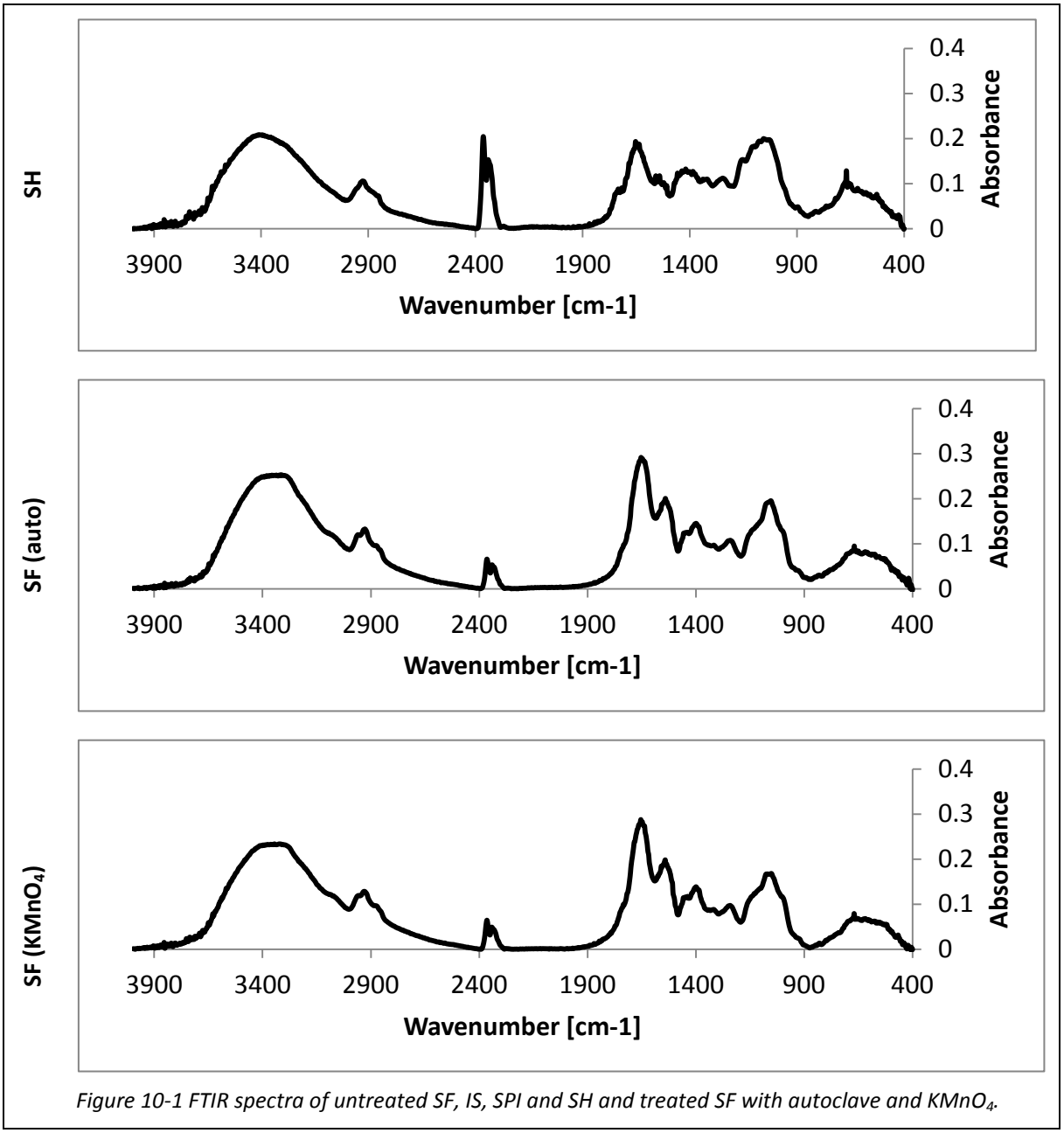

Figure 10-1 FTIR spectra of untreated SF, IS, SPI and SH and treated SF with autoclave and $KMnO_4$.

Appendix II. (Chapter 7): Composites

Energy Dispersive X-ray Spectroscopy (EDX)

The identification of the soy particles in the FESEM images was conducted by EDX and obtained by chemical mapping of the surface and detecting carbon (C), nitrogen (N) and oxygen (O). High amounts of nitrogen indicated soy particles since the polypropylene matrix has no nitrogen bonded. Figure 10-2 to Figure 10-5 present the EDX images for the composite fractures of SF, SF (auto), SF ($KMnO_4$) and SF (auto) + Orevac CA100.

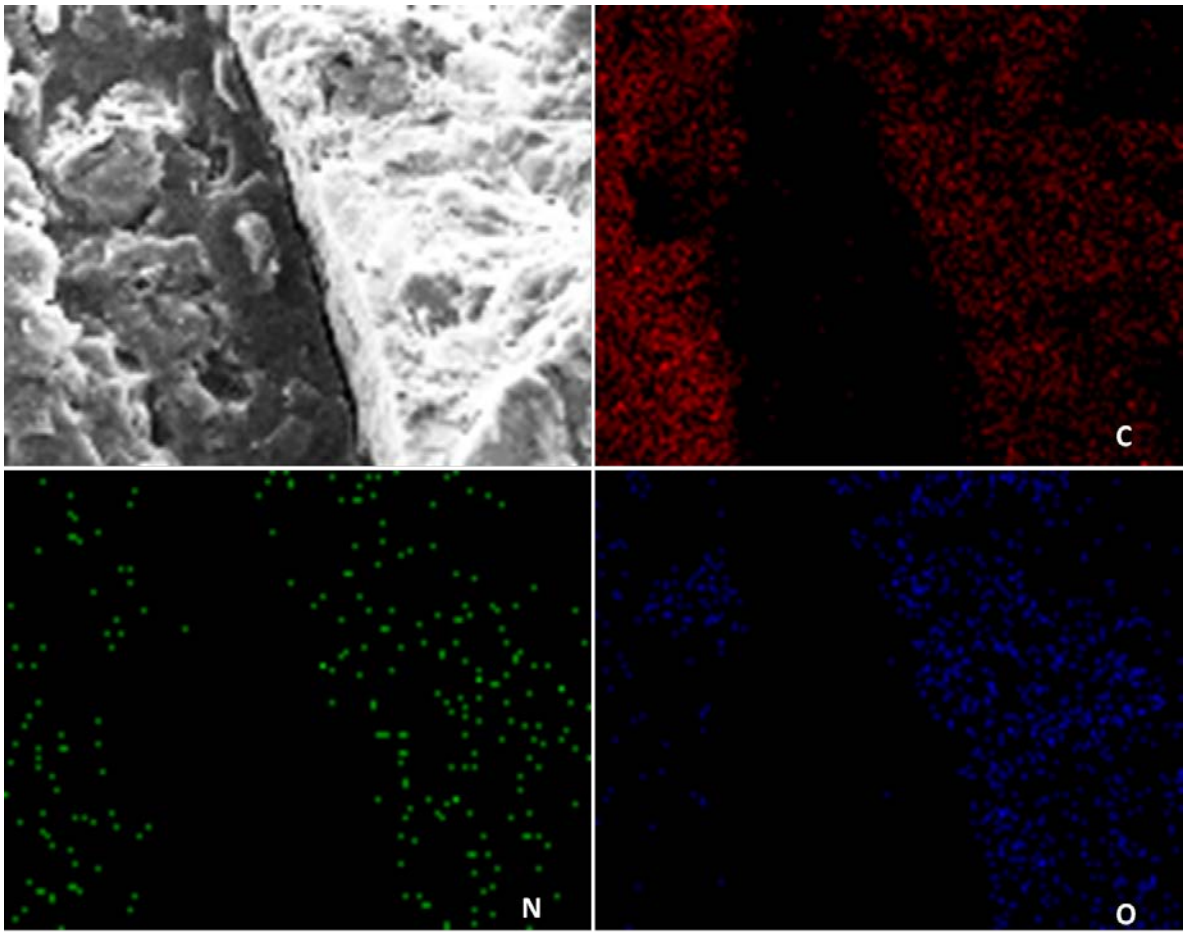

Figure 10-2 EDX of SF composite surface (C = carbon, N = nitrogen, O = oxygen)

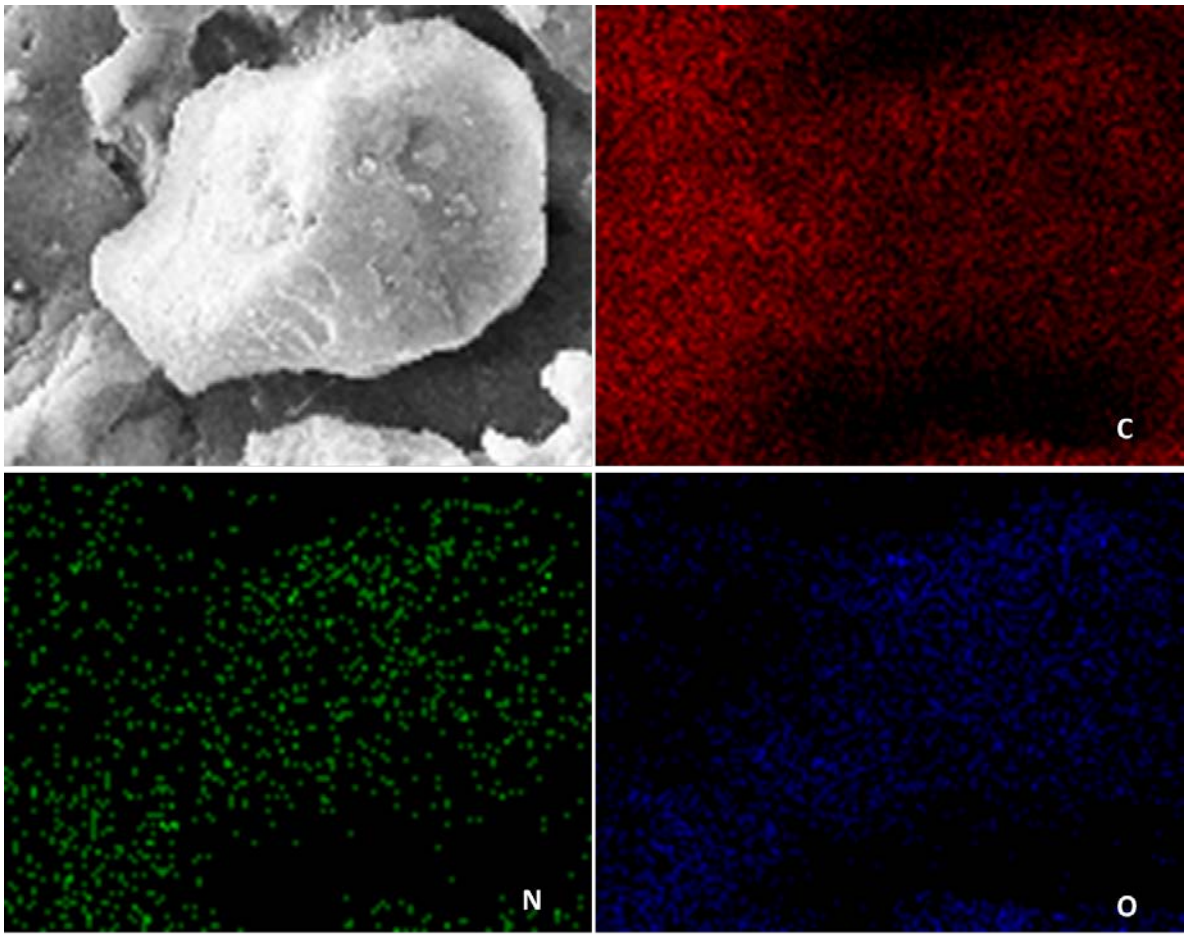

Figure 10-3 EDX of SF (auto) composite surface (C = carbon, N = nitrogen, O = oxygen)

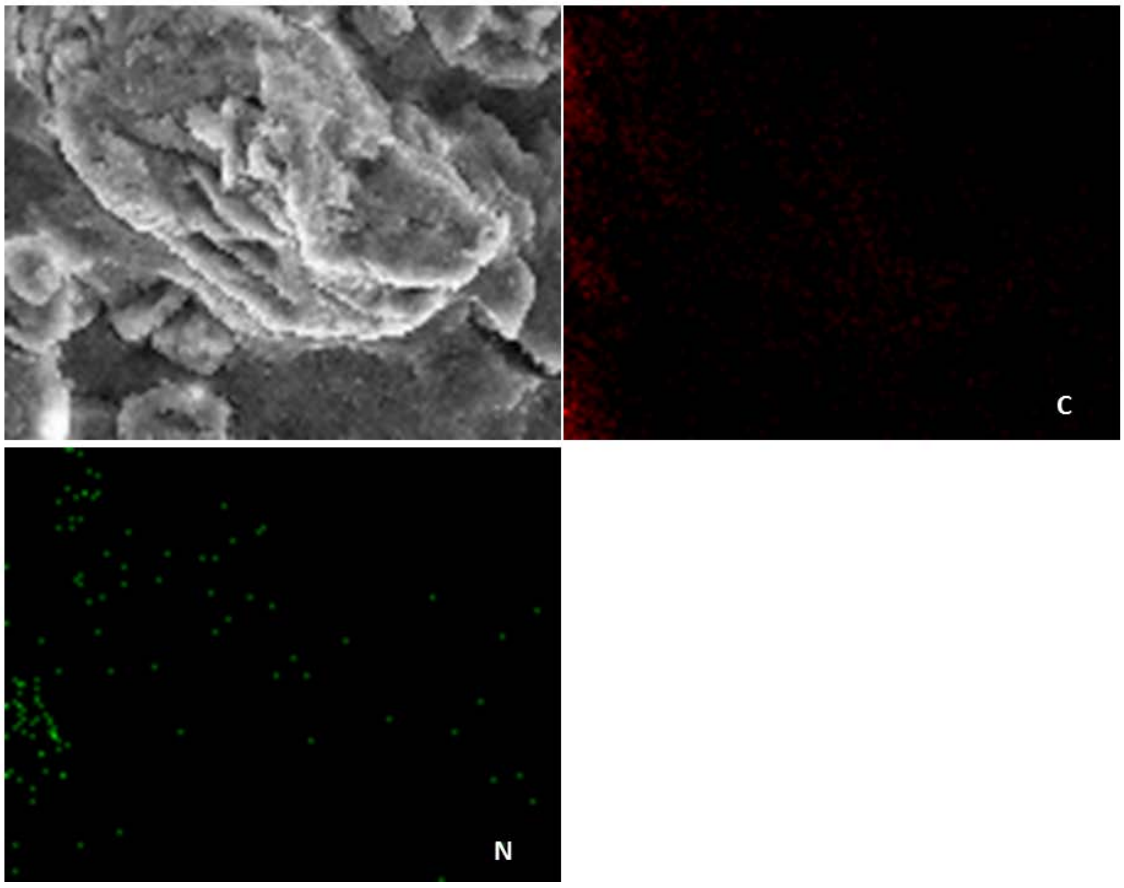

Figure 10-4 EDX of SF ($KMnO_4$) composite surface (C = carbon, N = nitrogen)

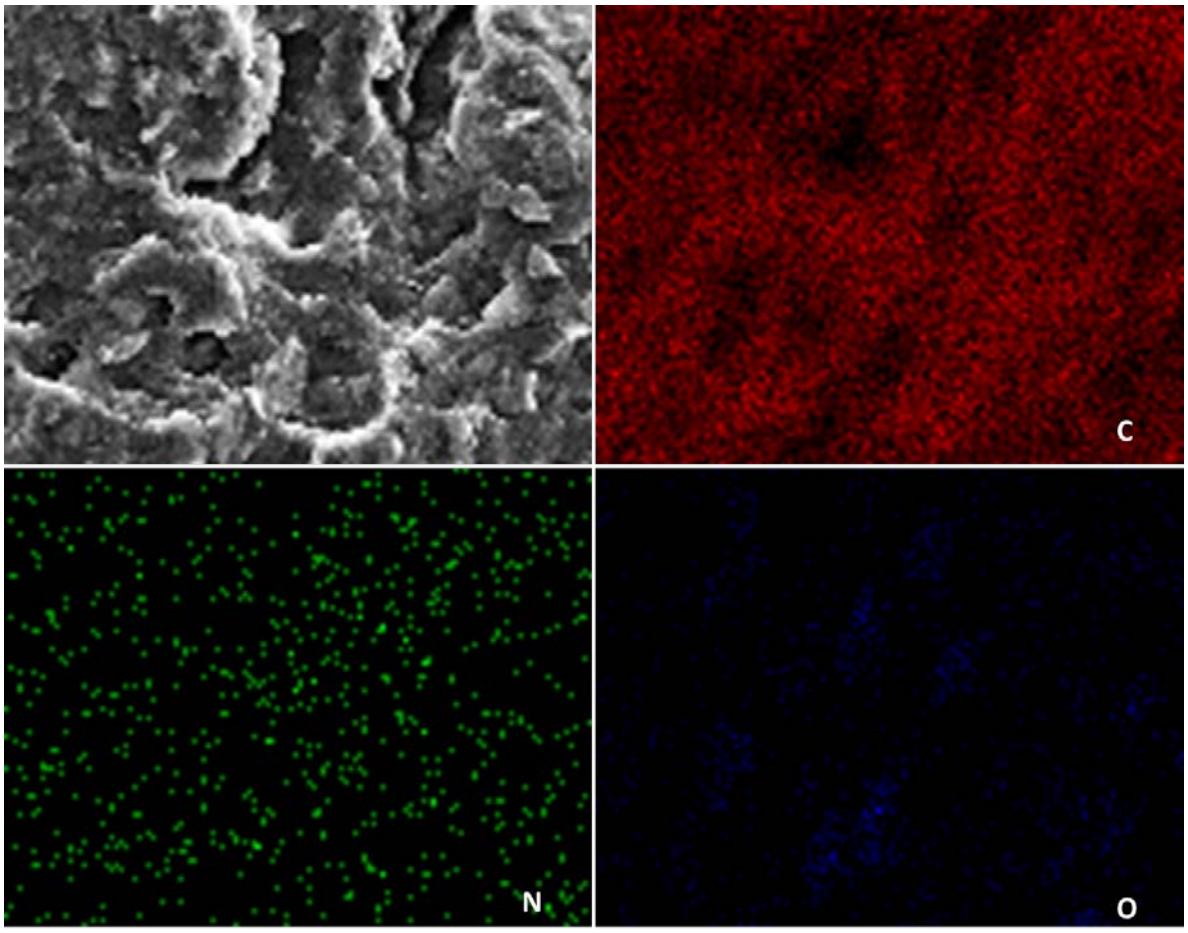

Figure 10-5 EDX of SF (auto) + Orevac CA100 composite surface (C = carbon, N = nitrogen, O = oxygen)